

**MODELING & SIMULATION OF THE EFFECT OF COOLING
PHOTOVOLTAIC PANELS**

by

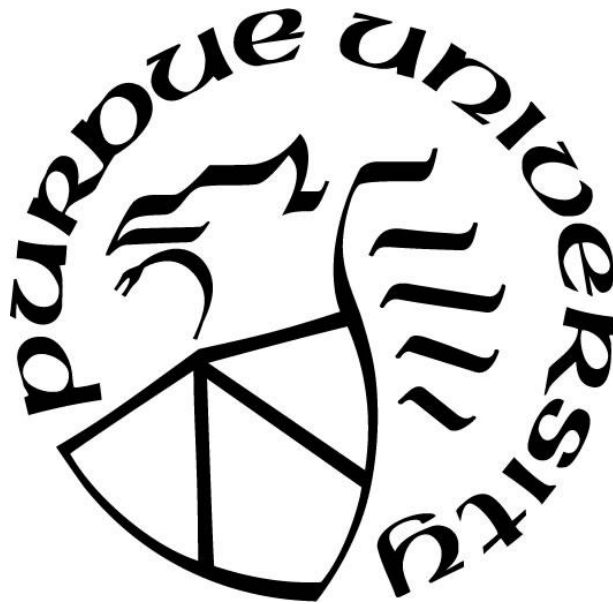
Qasim Abumohammad

A Thesis

Submitted to the Faculty of Purdue University

In Partial Fulfillment of the Requirements for the degree of

Master of Science in Engineering



Civil & Mechanical Engineering (CME)

Fort Wayne, Indiana

December 2021

THE PURDUE UNIVERSITY GRADUATE SCHOOL
STATEMENT OF COMMITTEE APPROVAL

Dr. Hosni Abu-Mulaweh, co-chair

Department of Civil and Mechanical Engineering

Dr. Donald Mueller, co-chair

Department of Civil and Mechanical Engineering

Dr. Zhuming Bi

Department of Civil and Mechanical Engineering

Approved by:

Dr. Hosni Abu-Mulaweh

This study is dedicated to my beloved father Amin Salem, in loving memory. His encouragement to do good, to better the environment, the community, the society and tomorrow pushed me to completion of my thesis, who has been my source of inspiration when I thought of giving up, who continually provided moral, emotional, and spiritual support.

To our brothers, sisters, mentors, relatives, friends, and classmates who shared their words of advice and encouragement to finish this study.

To the environment and for a better future, to a green solution for poverty & electrical scarcity where there is a lot of Sun!

And most importantly, I dedicate this study to the Almighty God, thank you for the guidance, strength, power of mind, and for giving us a healthy life.

ACKNOWLEDGMENTS

I would like to express my sincere gratitude to Purdue University, Fort Wayne for letting me fulfill my dream of being a student here.

To my committee chairman, Dr. Donald Mueller, I am extremely thankful for your assistance, advice, helpfulness, and suggestions throughout my project.

To the department head, Dr. Nash Younis, thank you for always listening and giving me words of encouragement, you have resembled a father figure to me, during my stay in Indiana.

To my teammates, David Ruiz & Jackson Jaworski, thank you for your assistance, and words of encouragement during late night work.

To the staff at the CME department, Nancy, and Maurice for helping me get equipment for my project.

To all my friends and family for helping me survive all the stress from this year and not letting me give up.

Most of all, I am indebted to Dr. Hosni Abu-Mulaweh, my advisor and director, for his wisdom, understanding, enthusiasm, patience, and motivation for pushing me farther than I thought I will go, despite all the hardships from this year.

TABLE OF CONTENTS

LIST OF TABLES	7
LIST OF FIGURES	8
NOMENCLATURE	11
ABSTRACT.....	13
1. INTRODUCTION	14
1.1 Photovoltaic Technology	14
1.2 Description of Solar Panel Cooling Methods	18
1.2.1 Heat Sinks	19
1.2.2 Fins	20
1.2.3 Photovoltaic/Thermal (PVT) Systems.....	21
1.2.4 Hybrid Thermoelectric Generation Systems (TEG).....	22
1.2.5 Water Spraying	23
1.3 Thesis Objectives and Scope of Work	24
1.4 Thesis Organization	25
2. MODELING AND SIMULATION OVERVIEW	27
2.1 Model Parameters	28
2.2 Model Inputs	30
2.3 Intermediate Calculations	33
2.4 Model Output	34
3. THERMAL MODEL.....	36
3.1 Cell Temperature Calculation	34
3.1.1 Ross Thermal Model.....	36
3.1.2 Faiman Thermal Mode	36
3.1.3 Sandia Laboratory Temperature Model.....	37
3.1.4 Fuentes PVWatts Model	38
3.1.5 Thermal Capacitance Model with McAdams's Relation.....	38
3.2 Comparison of Thermal Models	39
4. ELECTRIC MODEL	40
4.1 Mathematical Model	40

4.2	I-V & P-V Characteristics with Constant Temperature	42
4.3	I-V & P-V Characteristics with Constant Radiation	44
4.4	I-V & P-V Characteristics with Weather Data	45
5.	MODEL VERIFICATION	47
5.1	Verification of Thermal Model	47
5.1.1	Comparison of Thermal Models	47
5.1.2	Behavior of the Thermal Model	47
5.1.3	Thermal Model Parameter Sensitivity	50
5.2	Verification of Electrical Model	51
6.	MODEL VALIDATION	55
6.1	Temperature and Solar Irradiance Measurements	56
6.2	Array Maximum Power Point Measurements	57
6.3	Description of Input Data Collected	58
6.4	Simulation Results	60
6.5	Discussion of Simulation Results	64
6.6	Relationship between Efficiency and Cell Temperature	65
7.	EFFECT OF COOLING ON PHOTOVOLTAIC PERFORMANCE.....	67
7.1	Use of Measured Data to Simulate Cooling Effects	67
7.2	Using TMY3 Data to Simulate Cooling Effects	70
7.3	Effect of Increasing Wind Speed during Peak Hours	71
7.4	Effect of Geographical Location.....	74
7.4.1	Effect of Wind Speed on Annual Energy Production and Costs – Fort Wayne, IN..	74
7.4.2	Effect of Wind Speed on Annual Energy Production and Costs – San Diego, CA...	77
7.5	Return on Investment for Cooling Solar Arrays	80
8.	CONCLUSIONS	82
8.1	Recommendations.....	83
	APPENDIX A. MANUFACTURER’S DATA SHEETS	84
	APPENDIX B. ANNUAL HOURLY DATA	86
	APPENDIX C. PVWATTS CALCULATOR	90
	REFERENCES	97

LIST OF TABLES

Table 1.1: Water spraying cooling results.....	24
Table 2.1: Model parameters to the MATLAB Simulation.....	29
Table 5.1: PVWatts annual energy results and annual energy simulation results compared. Input data TMY3.....	54
Table 6.1: RMSE values for temperature measurement compared to simulation on 5 Oct. – 06 Oct. 2020.....	64
Table 7.1: Summary of Annual Energy savings due to cooling.	80
Table C.1: Sample of PVWatts calculator results of 7.6 kWp roof mounted PV array at Purdue University, Fort Wayne campus. Input data TMY3.	95

LIST OF FIGURES

Figure 1.1: Estimated share of renewable energy compared to total energy consumption.....	14
Figure 1.2: Cumulative U.S. solar installations.....	15
Figure 1.3: Photovoltaic power potential	15
Figure 1.4: P-N migration explained	16
Figure 1.5: Solar panel layers	17
Figure 1.6: Research cell efficiencies	18
Figure 1.7: Schematic of modeling heat sinks to cool photovoltaics.....	19
Figure 1.8: Schematic of fin array mounted to the back of a PV panel to enhance cooling.	21
Figure 1.9: Schematic of passive cooling of PV/T.....	21
Figure 1.10: TEG with fins mounted to the back of a PV panel to enhance cooling.....	22
Figure 1.11: Schematic of automated water spraying to cool PV systems.....	23
Figure 2.1: Simplified modeling and simulation process.....	27
Figure 2.2: PV model flow chart.....	28
Figure 2.3: Solar Irradiance data collected for the month of June (a) diffuse (b) beam. Data collected June TMY3.....	31
Figure 2.4: Input data (a) ambient temperature, (b) solar irradiance, and wind speed. Data collected 5 June TMY3.....	32
Figure 2.5: Intermediate calculation - cell temperature. Data collected 5 June TMY3.....	33
Figure 3.1 Comparison of thermal models for cell temperature calculation. Input data from 16 June TMY3.....	9
Figure 4.1 The equivalent circuit of a solar cell and a PV device.....	40
Figure 4.2: Variation of plane of array irradiance with constant temperature, (a) I-V & P-V curves, (b) predicted maximum power point.....	43

Figure 4.3: I-V & P-V curves for variation of cell temperature with constant plane of array irradiance.....	44
Figure 4.4: Variation of plane of array irradiance and constant temperature, (a) I-V & P-V curves, (b) predicted maximum power point for 16 June TMY3.....	45
Figure 5.1: Cell and ambient temperatures compared. Input data from 16 June TMY.....	48
Figure 5.2: Effect of different thermal models on cell temperature calculation. Input data from 16 June TMY3.....	49
Figure 5.3: Cell and ambient temperatures compared. Input data from 16 June TMY3.....	50
Figure 5.4: Parameter variability sensibility analysis.....	51
Figure 5.5: Predicted power simulation results and PVWatts power results compared. Input data from 20 June TMY3.....	52
Figure 5.6: PV-Watts annual energy results and annual energy simulation results compared. Input data TMY3.....	53
Figure 6.1: Schematic of PV array that is used for data collection. The PV array is roof mounted at Kettler’s Hall in Purdue University, Fort Wayne campus.....	55
Figure 6.2: Solar Survey 100 temperature and solar irradiance data logger.....	56
Figure 6.3: 7.6 kWp roof ballast PV array mounted at Kettler Hall rooftop, Purdue University, Fort Wayne campus.....	57
Figure 6.4: Input data. (a) irradiance, (b) ambient temperature. Data recorded 5 October – 8 October 2020.....	58
Figure 6.5: Input data (a) wind speed, (b) ambient temperature, (c) irradiance. Data recorded on 5 October 2020.....	59
Figure 6.6: Comparison between the cell temperature experimental data and MATLAB predictions. Results obtained for 5 October 2020. (a) cell Temperature, (b) power.....	61
Figure 6.7: Comparison between the cell temperature experimental data and MATLAB predictions. Results obtained for 6 October 2020. (a) cell Temperature, (b) Power.....	62
Figure 6.8: Comparison between the power experimental data and MATLAB predictions. Results obtained for (a) 7 October 2020, (b) 8 October 2020.....	63
Figure 6.9: Relationship between efficiency and rise in temperature. Results obtained for 5. Oct. 2020.....	66

Figure 7.1: Effect of varying wind speed on cell temperature. Input data from 5 October 2020.	68
Figure 7.2: Effects of varying wind speed on the power output of the array by varying wind speed. Input data from (a) 5 Oct. 2020 and (b) 6 Oct. 2020.	69
Figure 7.3: Experimental data measured for the array from Jun. 16 - Jun. 23, 2020.	70
Figure 7.4: Cooling effects on DC power output. Input and recorded data from 17 June TMY3.	71
Figure 7.5: Effects of varying wind speed during peak hours on (a) cell temperature (b) power output. Data obtained for 5 June TMY3.	73
Figure 7.6: kWh energy produced in a day in different regions across the US.	74
Figure 7.7: Simulation of increase in energy production due to increasing wind speed, based on a 7.6 kWp roof mounted PV array in Fort Wayne, IN. Input data TMY3.	75
Figure 7.8: Savings from cooling the photovoltaic array, based on a 7.6 kWp roof mounted PV array in Fort Wayne, IN. Input data TMY3.	76
Figure 7.9: Annual energy simulation results by varying wind speed in San Diego, California. Input hourly data from TMY3.	77
Figure 7.10: Simulation of increase in energy production due to increasing wind speed, based on a 7.6 kWp roof mounted PV array in San Diego, CA. Input data TMY3.	78
Figure 7.11: Savings from cooling the photovoltaic array, based on a 7.6 kWp roof mounted PV array in San Diego, CA. Input data TMY3.	79

NOMENCLATURE

AC	Alternative Current
a	Ideality constant
DC	Direct current
EVA	Ethylene-vinyl acetate
E_g	Band gap of silicon
E_{poa}	Plane of array irradiance
G	Solar irradiance
G_n	Nominal solar irradiance
h	Heat transfer coefficient
h_{conv}	Heat transfer coefficient due to convection
h_{exp}	Experimental heat transfer coefficient
I_{ph}	Photogenerated current
I_{pv}	Nominal photogenerated current
I_d	Diode current
I_o	Saturation current
I_{sc}	Short circuit current
I_p	Current due to parallel leakage
I_{on}	Reverse saturation current
I_m	Maximum current
IEP	Increase in energy production
$I-V$	Current - Voltage
k	Boltzmann constant
K_i	Temperature coefficient due to current
mc_p	Thermal mass
MPP	Maximum power point
$NSRDB$	National solar radiation database
$NOCT$	Nominal operating cell temperature

N_s	Number of cells in series
P	Power
P_{max}	Maximum power
PV	Photovoltaic
PV/T	Photovoltaic – thermal
$P - N$	Positive – negative junction
$P - V$	Power – Voltage
P_{mmp}	Maximum power on I-V curve
q	Electric charge
R_s	Shunt resistance
R_p	Resistance due to parallel resistor
$RMSE$	Root mean square error
t	Time
T_c	Cell temperature
T_m	Module temperature
T_a	Ambient temperature
T_n	Nominal temperature
$\tau\alpha$	Absorptance – transmittance
U	Overall heat transfer coefficient
V	Voltage
V_{oc}	Open circuit voltage
V_{tn}	Nominal thermal voltage
V_t	Thermal voltage
V_m	Maximum voltage
WS	Wind Speed

ABSTRACT

The purpose of this study is to develop a flexible computer tool to predict the power produced by a photovoltaic (PV) panel. The performance of the PV panel is dependent on the incident solar radiation and the cell temperature. The computer tool predicts voltage-current curves, power-voltage curves, and maximum power point values. Five different models are implemented to predict the temperature of the panel, and comparison between the different thermal models is good. A thermal capacitance approach that uses a simple relationship for the forced convection heat transfer coefficient is used to predict the cell temperature. Both the electrical and temperature models are verified through comparisons using PVWatts and validated by comparisons to measured values. The model is flexible in the sense that it can be applied to PV arrays of any size, at any location, and of different cell types. After being verified and validated, the model is used to investigate the effects of cooling on the photovoltaic panel to improve the panel efficiency and increase its power output. Typical results show that for every degree Celsius rise in temperature, the efficiency of the solar panel is reduced by 0.5%. The effect of cooling and the resulting increase in energy production in two different climatic zones are studied and discussed.

Keywords: photovoltaic panel, renewable energy, cooling, power, and temperature.

1. INTRODUCTION

The renewable energy industry across the world is increasing rapidly to offset the fossil fuel consumption. Renewables made up 26.2 percent of global electrical production in 2018, and that value is predicted to rise to 45 percent by 2040. Most of the increase will likely come from solar, wind, and hydropower as shown in Figure 1.1. According to the International Energy Agency [1] the development and the implementation of renewable energy technologies will depend on the government policies and economical support to make renewable energy cost effective.

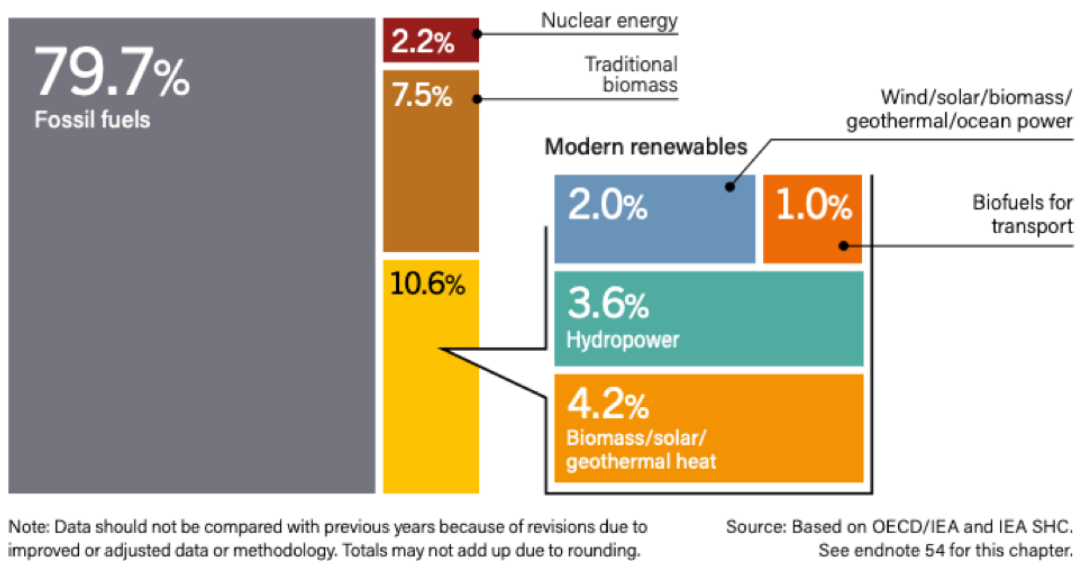


Figure 1.1: Estimated share of renewable energy compared to total energy consumption [1]

1.1 Photovoltaic Technology

In the last two decades, the contribution of solar energy to the total energy supply has grown. As shown in figure 1.2, solar energy in the last decade alone has experienced an average yearly growth rate of 42% [2]. Figure 1.3 shows the global photovoltaic power potential [3].

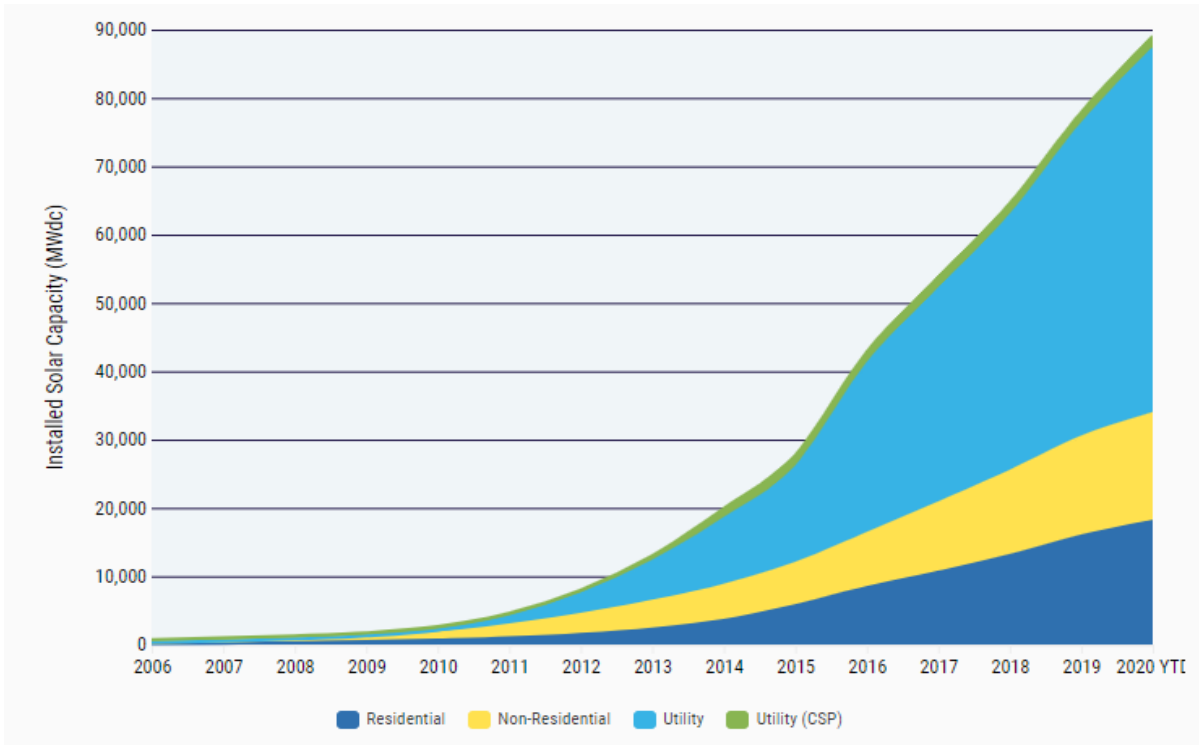


Figure 1.2: Cumulative U.S. solar installations [2]

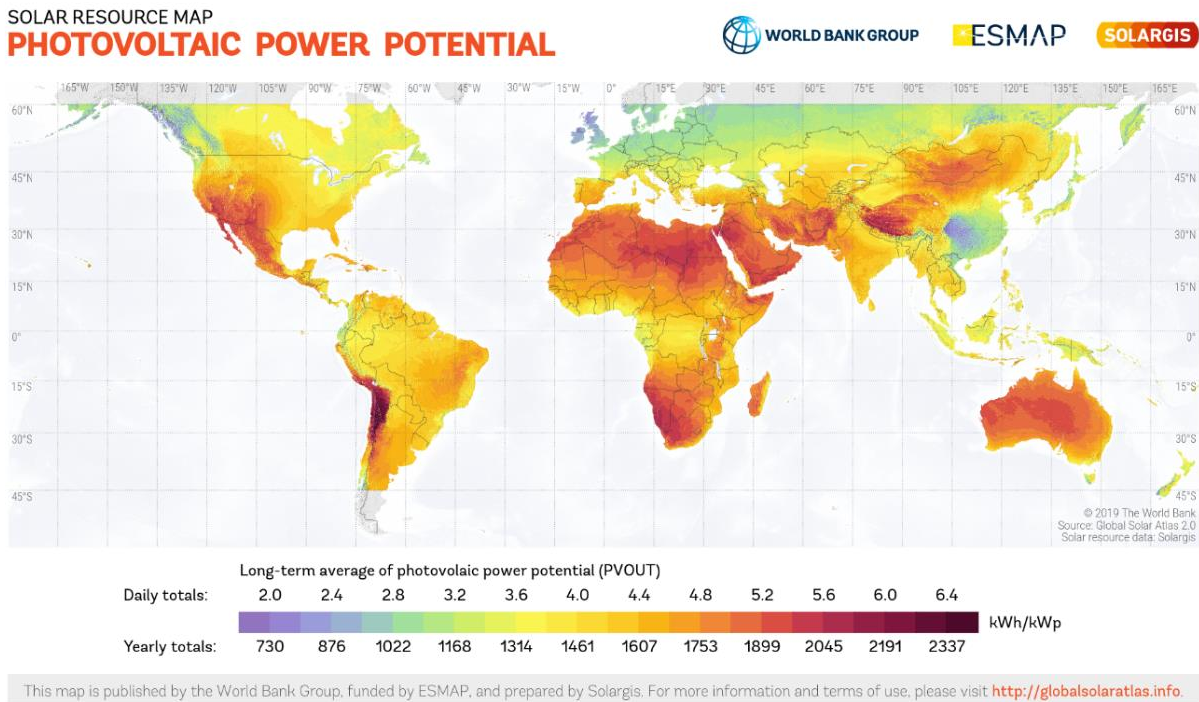


Figure 1.3: Photovoltaic power potential [3]

Energy from the sun is the most abundant and free energy available. However, in order to convert the electromagnetic radiation from the sun into a more useful form of energy such as electricity, devices are required. Solar cells made from silicon crystals are one such device. When the electromagnetic radiation from the sun strikes the cells, the electrons gain energy and are free to move. However, the movement of electrons is random, which does not result in any net current.

As outlined in [4]. To make the electrons move unidirectional, a driving force is needed. The driving force is provided with a P-N junction. Injection of boron with three valence electrons, into pure silicon, results in one hole for each atom. This is called P-type doping. Injection of phosphorus with five valence electrons, into pure silicon, results in one free electron for each atom. When these two materials are joined electrons from the N-side will migrate to the P-side and fill the holes available there.

A depletion region forms where there are no electrons and holes. Due to the electrons moving, the N-layer becomes slightly positively charged and the P-layer becomes negatively charged. An electric field forms between these negatively and positively charged layers —this electric field produces the driving force that is necessary to allow the electrons to flow in one direction [4]. A schematic showing a P-N junction and electron migration is shown in Figure 1.4.

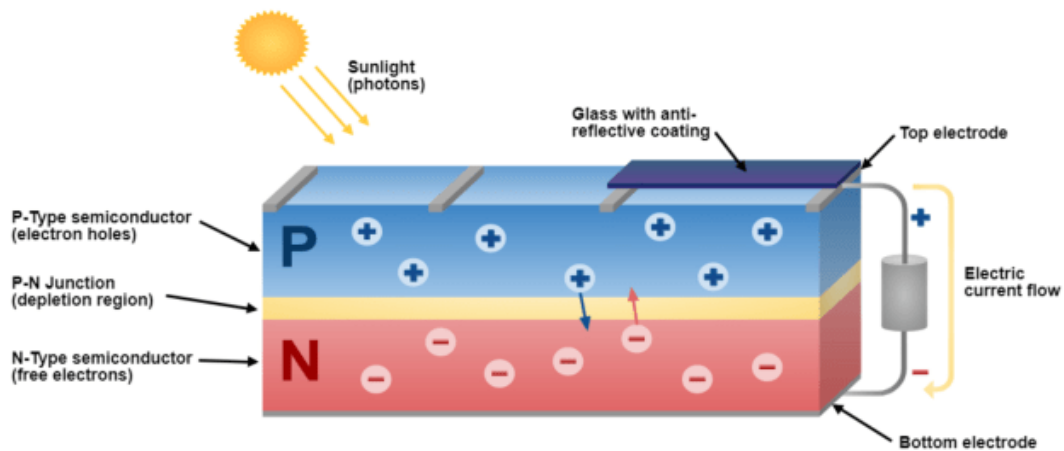


Figure 1.4: Schematic of a P-N junction [4]

Connection of a load between these two regions causes electrons to start flowing through the load; thus, the solar cell produces direct current.

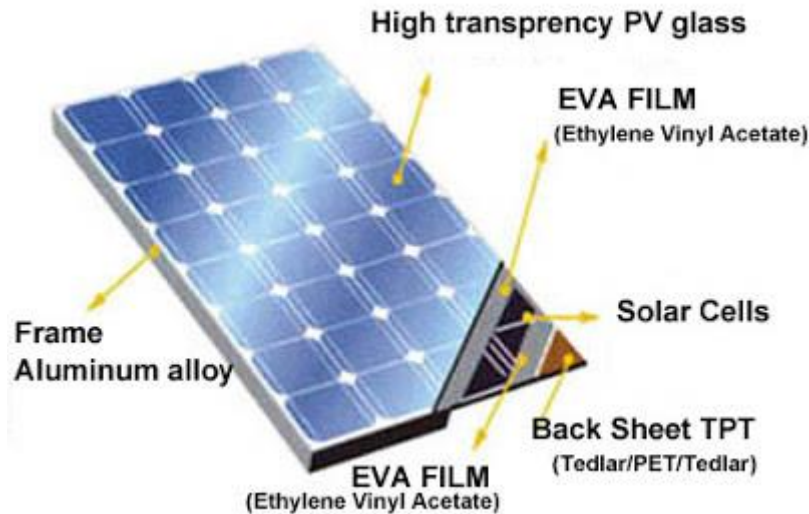


Figure 1.5: Solar panel layers [5]

Several solar cells are connected to create a solar panel. A solar panel, as shown in Figure 1.5, generally consists of three layers:

- 1- A layer of cells that are connected in series and parallel to each other.
- 2- A layer of EVA sheet on both sides of the solar cells to protect from shock, vibration, dust, and humidity.
- 3- High transparency glass.

Solar panels may be a part of system that uses charge controllers and stores electricity using batteries or they may use power invertors to convert DC to AC and are connected to the electrical grid.

Solar panels are exposed to temperature swings throughout the day and from day-to-day. Temperature variations are tough on solar panels because their electrical connections are metal. When the temperatures rise and fall, over time, different expansion and contraction rates in the metals can cause connections between the cells to break. Broken connections cannot conduct energy, so the panel loses power. Thus, researchers and engineers are motivated to improve solar panel longevity and efficiency by cooling the photovoltaics. Figure 1.6 shows solar cell efficiency

advancement throughout the last five decades. This data applies to wide variety of cells in a laboratory environment.

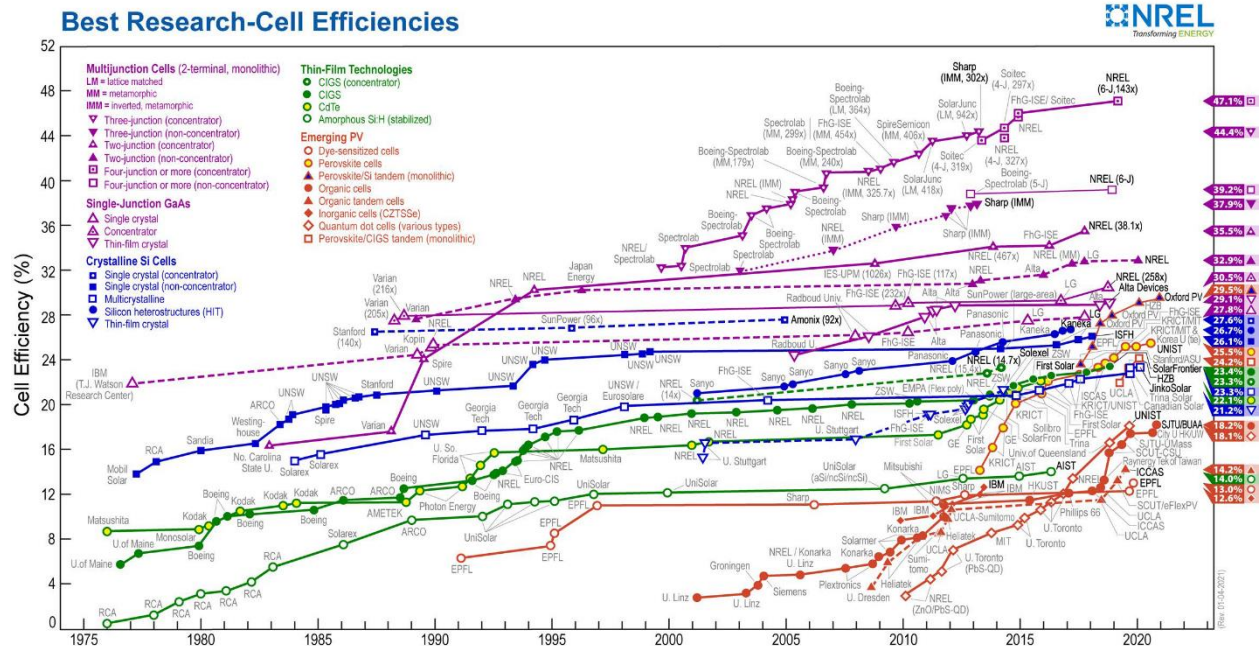


Figure 1.6: Research cell efficiencies [6]

1.2 Description of Solar Panel Cooling Methods

Only a small portion of the solar irradiance on the PV panel is converted to electricity—the rest is converted to heat causing the panel temperature to rise. In addition, high ambient temperatures can also cause the panel temperature to rise. Elevated panel temperatures are detrimental to panel performance, efficiency, and life span [7]. Non-uniform temperature distributions or hot spots reduce the efficiency and can permanently damage the panel [8]. Consequently, a wide variety of methods and devices have been proposed to cool PV panels [7-8].

Solar panel cooling methods can be classified into two types—active and passive. Active cooling involves the use of energy to cool the PV panel such as the use of a fan to blow air or a pump to circulate a coolant over the panel. A passive cooling system involves a design approach that naturally cools the PV such as the use of heat sinks or fins.

1.2.1 Heat Sinks

Heat sinks are one of the methods which uses a high thermal conductivity metal to transfer heat away from the photovoltaic module so that it can be removed by convection. A schematic for a heat sink attached at the back of the PV developed is shown in Figure 1.7. Popovici et al. [9] developed a numerical approach to show the decrease of temperature of the photovoltaic modules by using air-cooled heat sinks. The heat sink is a ribbed wall constructed of a high thermal conductive material.

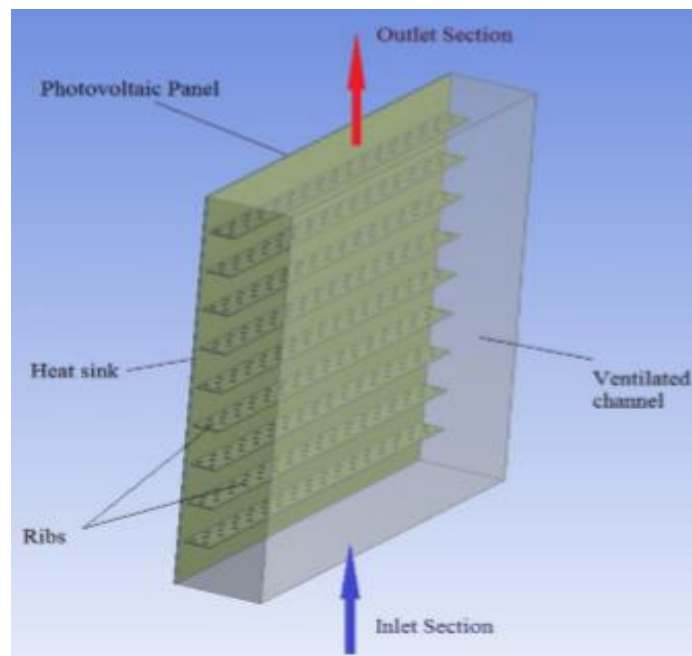


Figure 1.7: Schematic of modeling heat sinks to cool photovoltaics [9].

This heat sink system [9] increased the maximum power produced by the PV panel by 6.97% and 7.55% compared to the reference case for angles of the ribs from 90° and 45° , respectively. In addition, the temperature of the PV panel with no cooling was higher than the ambient temperature by 70%, while the temperature of the PV panel with cooling was higher than the ambient temperature by 30%. Reducing the cell temperature helped to maintain the efficiency and increase the power output.

A disadvantage of using heat sinks is that the set-up is relatively expensive for building the aluminum plate (fins and ribs) as shown in Figure 1.7. Also, the results are not generalizable to other environmental conditions, i.e., the data was taken on a clear sunny day; there is limited data for cloudy/cold days.

1.2.2 Fins

Simple fins attached to the panel can enhance heat loss and reduce the cell temperature. To estimate the heat loss from the PV panel, a standard fin model is employed with the following standard assumptions [10]:

- 1- Steady-state, one-dimensional heat conduction; therefore, the temperatures of the glass cover, solar cells, and plates change only in one direction.
- 2- The thermal capacity effects of the glass cover, solar cells, and back plate are neglected.

Alkhalidi et al. [10] reported that aluminum fins on the back of a PV panel resulted in:

- 1- an overall (average) increase the electrical efficiency by 1.75% and the output power by 2% and
- 2- a temperature reduction of over 20°C and over a 10% increase in power when incident the radiation at 1000 W/m².

However, the fins are relatively expensive, and measurements were not collected for extended periods of time—a feasibility study and cost analysis were not performed.

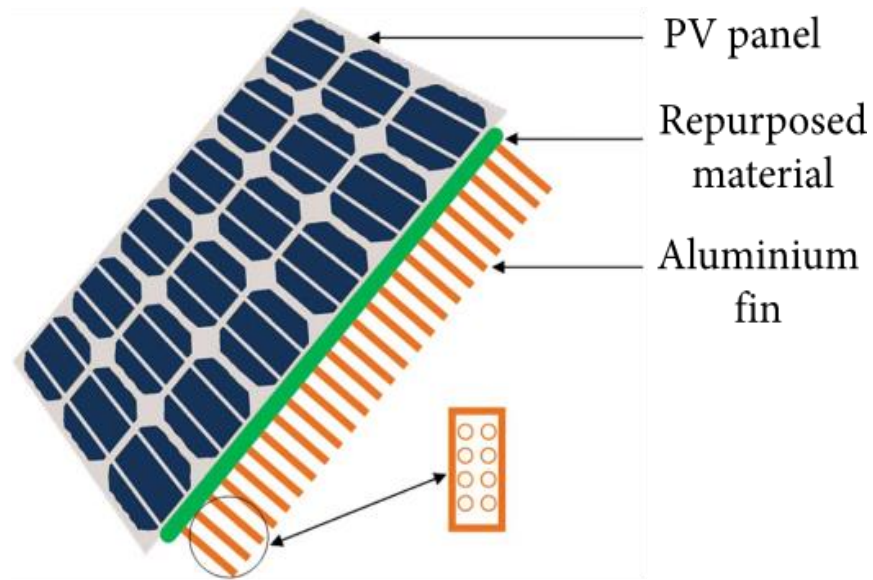


Figure 1.8: Schematic of fin array mounted to the back of a PV panel to enhance cooling [10].

1.2.3 Photovoltaic/Thermal (PVT) Systems

In this system, a fluid (water or air) flows through a channel as shown in Figure 1.9. The purpose of this device is to transfer the heat to the flowing fluid so that it can be carried away, instead of increasing the temperature of the PV panel.

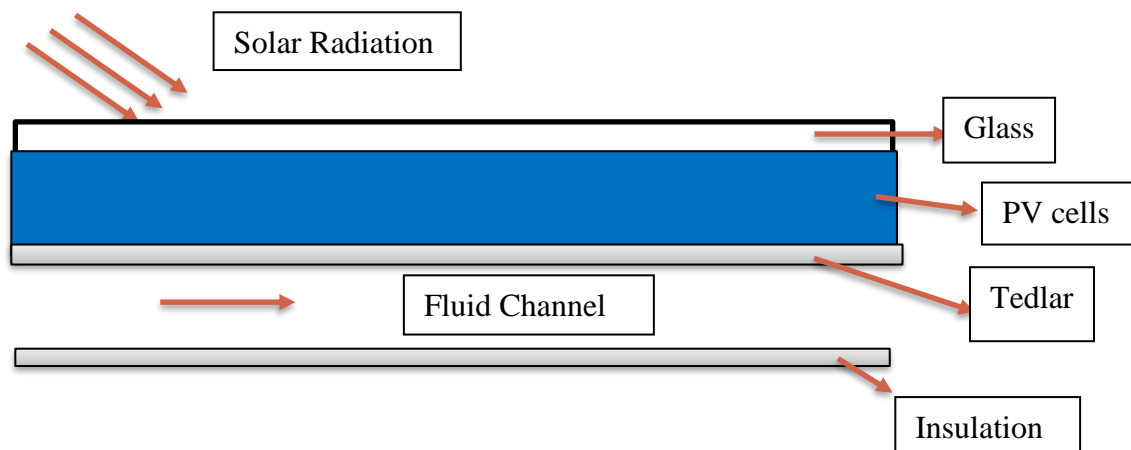


Figure 1.9: Schematic of passive cooling using PV/T.

Many different configurations have been proposed. In general, advantages of systems like those shown in Figure 1.9 include:

- 1- PV/T systems have the potential to capture the heat, producing high-temperature air or water, which can be used for space heating, boiler feedwater heating, industrial processing.
- 2- Under certain environmental conditions, the temperature reduction is significant resulting in a 10-15% increase electrical efficiency.
- 3- Careful design of the heat exchanger can greatly reduce temperature variation in the PV panel, thus promoting thermal homogeneity that will increase the longevity of the PV cell.

Several disadvantages of using PV/T systems include:

- 1- limited to very warm regions where excess water may not be available.
- 2- an increase in cost of labor, maintenance, and materials.
- 3- a need for additional power to operate a pump or fan.

1.2.4 Hybrid Thermoelectric Generation Systems (TEG)

Thermoelectric effect is the conversion of temperature differences to potential differences i.e. voltage [11]. In this device, the heat loss from the PV panel is transferred to a TEG system to generate additional power. A schematic of the system is shown in Figure 1.10.

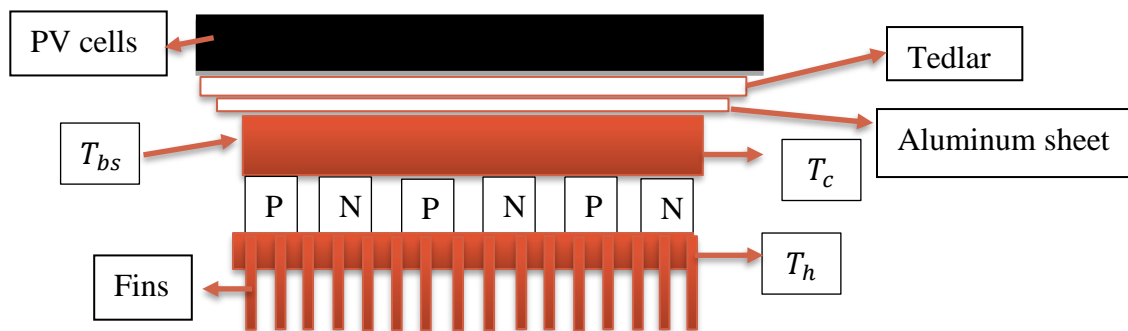


Figure 1.10: TEG with fins mounted to the back of a PV panel to enhance cooling [11].

Advantages of TEG devices include [11]:

- 1- They basically work like heat engines but are smaller and have no moving parts.
- 2- They can potentially increase the annual energy yield of 10-15% under certain climatic conditions.

Disadvantages of TEG devices [11]:

- 1- They are usually more expensive and less efficient than PV panels.
- 2- Cost of the TEG module along with maintenance is more than the average 12% annual energy increase.

1.2.5 Water Spraying

The idea of this device is spray water the panel to enhance cooling by convection and evaporation, thus reducing the cell temperature. A schematic of the proposed water spraying system is shown in Figure 1.11.

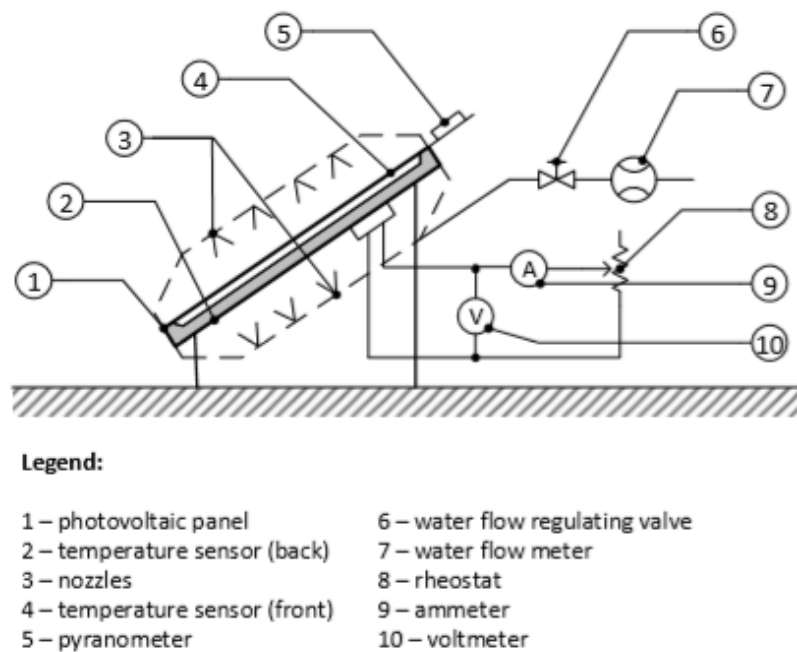


Figure 1.11: Schematic of water spraying to cool PV systems [12].

The results of the experiment are summarized in the Table 1.1.

Table 1.1: Water spraying cooling results [12].

Applied cooling options	Maximal power output (W)	Relative increase in power output (%)	Effective increase in power output (%)	Average panel temperature (°C)	Electrical efficiency (%)	Effective increase in el. efficiency (%)
Without cooling	35	-	-	56	13.92	-
Back surface cooling	39.9	14.0	5.4↑	33.7	15.59	3.6↑
Front surface cooling	40.1	14.6	6.0↑	29.6	15.42	2.5↑
Simultaneous cooling	40.7	16.3	7.7↑	24.1	15.92	5.9↑

Pros [12]:

- 1- Results show that an increase of 16.3% (effective 7.7%) in electric power output and a total increase of 14.1% (effective 5.9%) in PV electrical efficiency by using water spraying during peak hours.
- 2- A reduction in panel temperature from an average of 54°C to 24°C using simultaneous front and backside PV panel water spraying.
- 3- Feasible if applied to regions in Mediterranean climates with sufficient water availability.
- 4- Cleaning the PV provided increased longevity of the PV as well as increased its power production.

This preliminary study shows potential, but additional data, from a small prototype plant similar to the above needs to be collected to verify all aspects, e.g., operation, initial installation cost, and maintenance, etc. to see if PV water spray cooling is efficient in periods other than highest solar irradiation levels and for specific geographical locations, especially those that lack easy access to water.

1.3 Thesis Objectives and Scope of Work

The over-arching goal of this thesis is to develop a flexible computer tool to predict the power production of a solar panel. Then, to use the compute tool to investigate the potential to use panel cooling to increase efficiency. Specifically, the scope of the study is as follows:

- Discuss different cooling methods of photovoltaic arrays published in the literature.
- Implement a thermal model and computer simulation to predict the temperature of the PV cell based on ambient weather conditions.

- Implement an electric model and computer simulation to predict I-V and P-V characteristics of a panel and study the cooling effects on the overall maximum power point (MPP).
- Verify the computer tool by comparing to other models and by using other verification techniques.
- Validate the computer tool by cell temperature and panel power predictions to measurements.
- Investigate the effect of cooling on PV panel efficiency.
- Perform a feasibility study and basic cost analysis of the effect of cooling photovoltaic panels in two different geographic regions using weather conditions from Typical Meteorological Year Three or TMY3.

1.4 Thesis Organization

The following listed items outline the organization of the chapters presented. Additionally, a summary of each chapter is given.

Chapter 1: Introduction. This chapter establishes the premise of the work. Also, the chapter aims to create a basic understanding of the physics of the photovoltaic technology and their advancement. This chapter also aims at discussing cooling methods of photovoltaic based on a literature review. Previous works relevant to the topic of cooling of photovoltaics are summarized, and the characteristic of the different methods are discussed.

Chapter 2: Modeling and Simulation Overview. This chapter outlines the modeling and simulation process and describes the model parameters, input data, intermediate calculations, and output data. This chapter also describes the weather data used as an input to the model.

Chapter 3: Thermal Model. This chapter describes the temperature model used to predict the operating temperature of the photovoltaic, known as the cell temperature. It also compares the selected temperature model to other temperature models published in the literature.

Chapter 4: Electrical Model. Within this chapter, the focus is on simulating the power output and the effects of the solar irradiance, as well as the cell temperature on the performance of the Photovoltaic. I-V & P-V characteristics are simulated in this chapter.

Chapter 5: Model Verification. Both the thermal model detailed in Chapter 3 and the electrical model detailed in Chapter 4 are compared to other models and results in the literature-based process known as model verification. Both models are verified.

Chapter 6: Model Validation. Within this chapter, both electrical and thermal models are compared to data collected at Purdue University Fort Wayne campus. Both models are validated.

Chapter 7: Simulation Results. In this chapter, the cell temperature is modified to investigate the effects of cooling on the power output of the photovoltaic throughout the year. In order to enhance cooling of the panel, the wind speed is adjusted. Furthermore, the feasibility of cooling photovoltaics and the significance of cooling effects is discussed in two zones in the United States: Indiana and California. The purpose is to quantify a potential return on investment by cooling the panel.

Chapter 8: Conclusions. In this chapter conclusions of results are summarized. Furthermore, this chapter outlines possible next steps to be considered to improve this work.

2. MODELING AND SIMULATION OVERVIEW

In this chapter, an overview of modeling and simulation process is outlined. Model inputs, outputs, as well as model parameters are discussed.

Figure 2.1 [13] details the modeling and simulation process, including the critical steps of verification and validation.

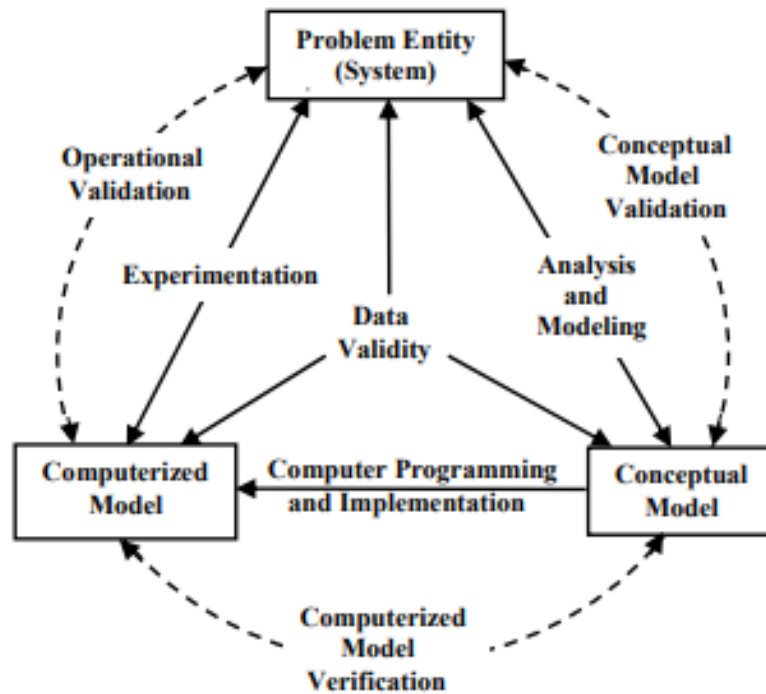


Figure 2.1: Simplified modeling and simulation process [13]

The model developed in this thesis predicts the power produced by photovoltaic model based on the Shockley Diode approach to solve for I-V and P-V characteristics [14-18]. Intermediate calculations include cell temperature, current, and voltage. Different models to predict the cell temperature are detailed in Chapter 3. A schematic of the modeling approach used in the thesis is shown in Figure 2.2.

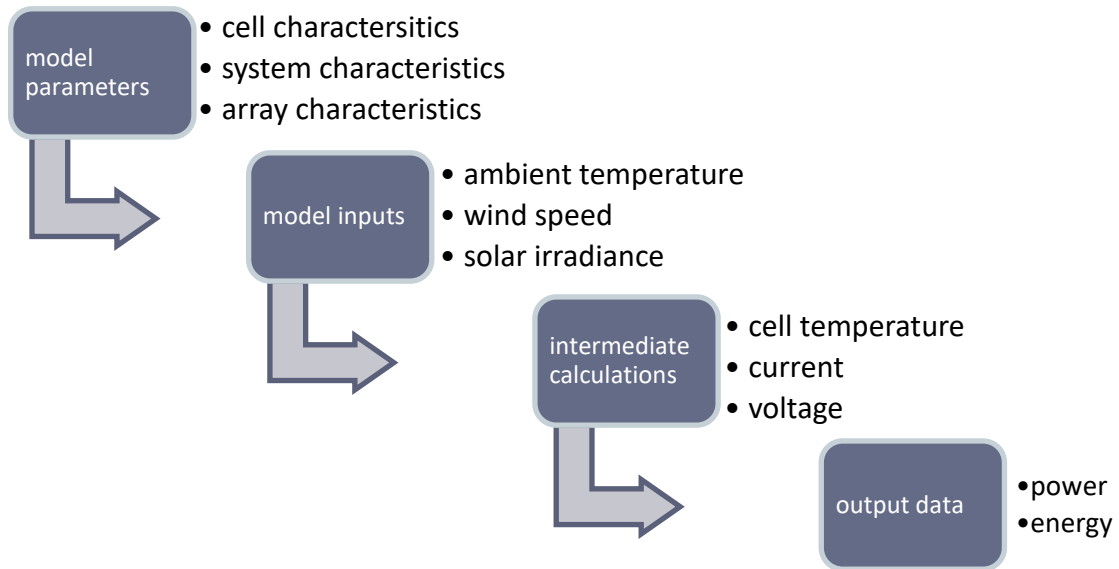


Figure 2.2: PV model flow chart

The mathematical models described in chapters 3 and 4 are converted to a MATLAB computer code. All computer simulations are performed using MATLAB 2019a.

2.1 Model Parameters

Model parameters are the data that are internal to the model and whose value are determined from specifications obtained from the manufacturer.

Cell characteristics are the electrical characteristics of a solar cell. Short circuit current, open circuit voltage and fill factor are some examples of cell characteristics. Effects of temperature and solar irradiance on short circuit current and open circuit voltage will be described in chapter 4.

System characteristics include the module type, tilt angle, and solar azimuth angle for the system set-up and configuration. The module type describes the photovoltaic module in the array. The module type used in this study is the silicon crystalline with a glass cover. The tilt angle is the

angle from the horizontal of the photovoltaic array, and the azimuth angle is the angle clockwise from the direction of the north, identifying the direction the modules face.

Array characteristics include the DC nominal system size (kW) at standard test conditions (STC), i.e. incident radiation of 1000 W/m², cell temperature of 25°C, and no wind speed. Other array characteristics include the type (fixed, adjustable, or tracking) and area (m²). Table 2.1 outlines the model parameters for the baseline system considered.

Table 2.1: Model parameters to the MATLAB simulation

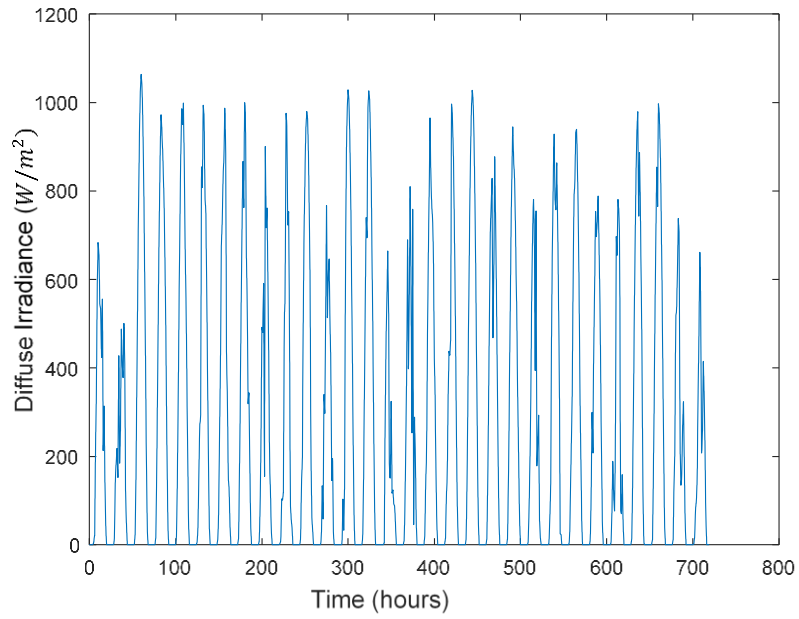
STC power rating	360 W
STC power per unit of area	185.5 W/m ²
Number of cells	72
Short circuit current, I _{sc}	9.71 A
Open circuit voltage, V _{oc}	48.1 V
Temperature coefficient of I _{sc}	0.04 %/K
Temperature coefficient of power	-0.39 %/K
Temperature coefficient of voltage	-0.149 V/K
Length	1956 mm
Width	992 mm
Band Gap of Silicon at STC	1.2
Diode ideality constant, a	2
PV cells absorptance-transmittance product, $\tau\alpha$	0.9
Thermal mass	11,000
Azimuth angle	180°
Tilt angle	7°
Array type	fixed

2.2 Model Inputs

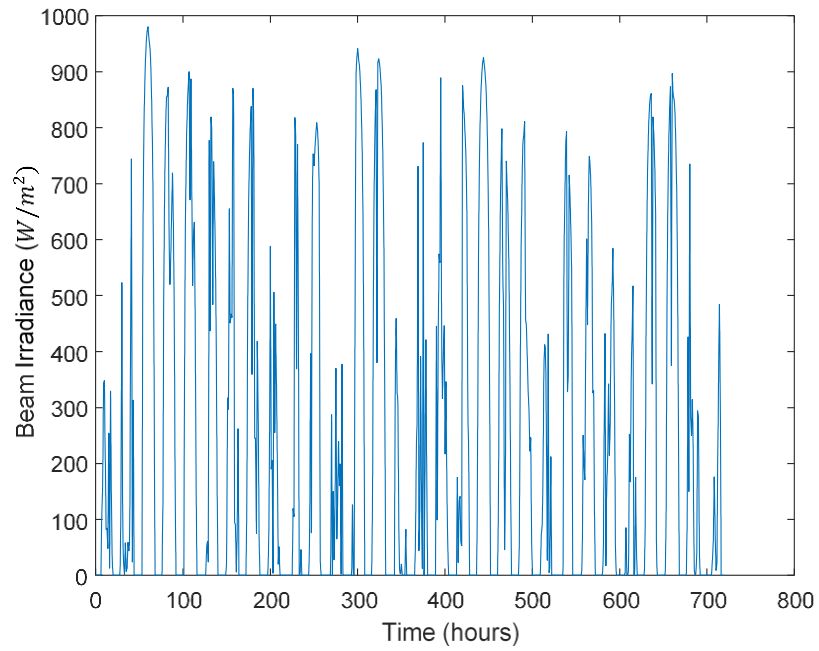
The inputs to the model are solar irradiance, wind speed and ambient temperature. These variable parameters are also referred to as weather data. Weather data refers to on-site measured weather parameters that are required for the evaluation of intermediate thermal and electrical calculations. Two different types of weather data are used in this study. Weather data from a national database is used for verification and to perform simulation studies. Actual weather data measurements are used for validation by comparing predicted PV array performance to an actual PV array.

The weather conditions are obtained from the National Solar Radiation Database (NSRDB) [19], which is complete median of hourly and a 30-minute values of meteorological dataset. Examples of NSRDB data used in this study are wind speed, plane of array irradiance and ambient temperature. The NSRDB covers the United States and various international locations. These data have been recorded at various locations and temporal as well as spatial scales to accurately represent regional solar irradiance climatic conditions. For a given location, the amount of solar energy can be predicted based on past climatic conditions [19].

The data collected from NSDRB is based on a Typical Meteorological Year (TMY). TMYs include one year of hourly dataset that best represents median weather conditions over a multiyear time frame as close as possible [19]. Although a TMY can be considered as a median, the techniques used to calculate it consider many factors other than a calculation of median values, including solar resource data and weather data (inputs) such as wind speed and ambient temperature. As outlined in [19], to predict a TMY, a multiyear data set is analyzed, and 12 months are chosen from that period that best represent the median conditions. For instance, a TMY developed from a dataset for the years 1998–2005 might use data from 2000 for February, 2004 for May, 1998 for November, and so on. The dataset used in this study is referred to as TMY3 [19]. An example of irradiance data from the Fort Wayne campus for the month of June TMY3 is shown in Figure 2.3.



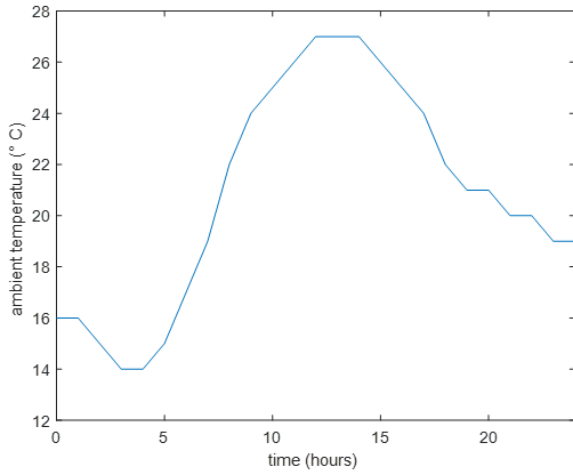
(a)



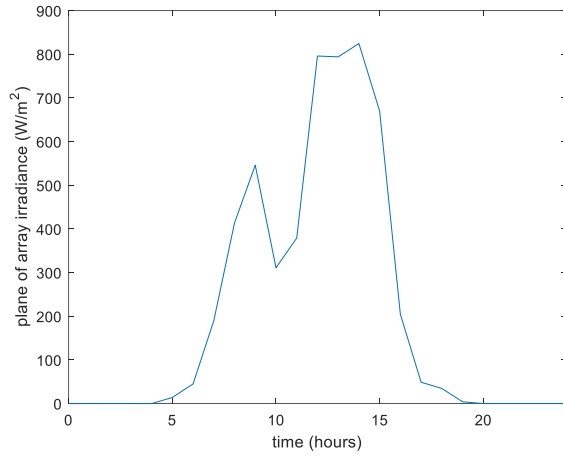
(b)

Figure 2.3: Solar irradiance data collected for the month of June (a) diffuse and (b) beam. Data from June TMY3.

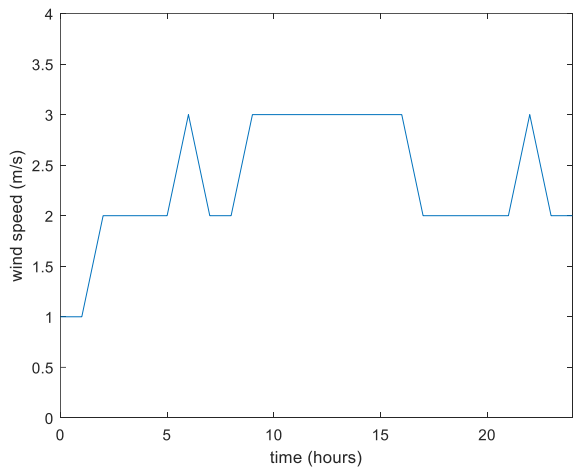
Additional sample input data, in hourly increments, is shown in Figure 2.4— (a) shows the ambient temperature, (b) shows the POA irradiance, and (c) shows the wind speed from 5 July of TMY.



(a)



(b)



(c)

Figure 2.4: Input data (a) ambient temperature, (b) solar irradiance, and (c) wind speed. Data from 5 June TMY3.

2.3 Intermediate Calculations

Intermediate calculations are calculations that are intermediate to the final simulation results. Chapters 3 and 4 detail the equations for the intermediate thermal and electrical calculations.

The weather data obtained from NSDRB [19] such as POA irradiance, wind speed, and ambient temperature is given on an hourly basis. Measured weather data can be obtained in a variety of time increments depending on the measurement devices. The time step in the model is flexible, i.e. cell temperature and panel power can be determined at any time increment. *For consistency and simplicity, a time step of one minute is used to obtain the results in this thesis.* Linear interpolation is used to generate additional input data.

Results for the cell temperature are obtained and shown in Figure 2.5. Input data, i.e. ambient temperature, solar irradiance, and wind speed, shown in Figure 2.4, are linearly interpolated at one-minute increments to calculate the cell temperature.

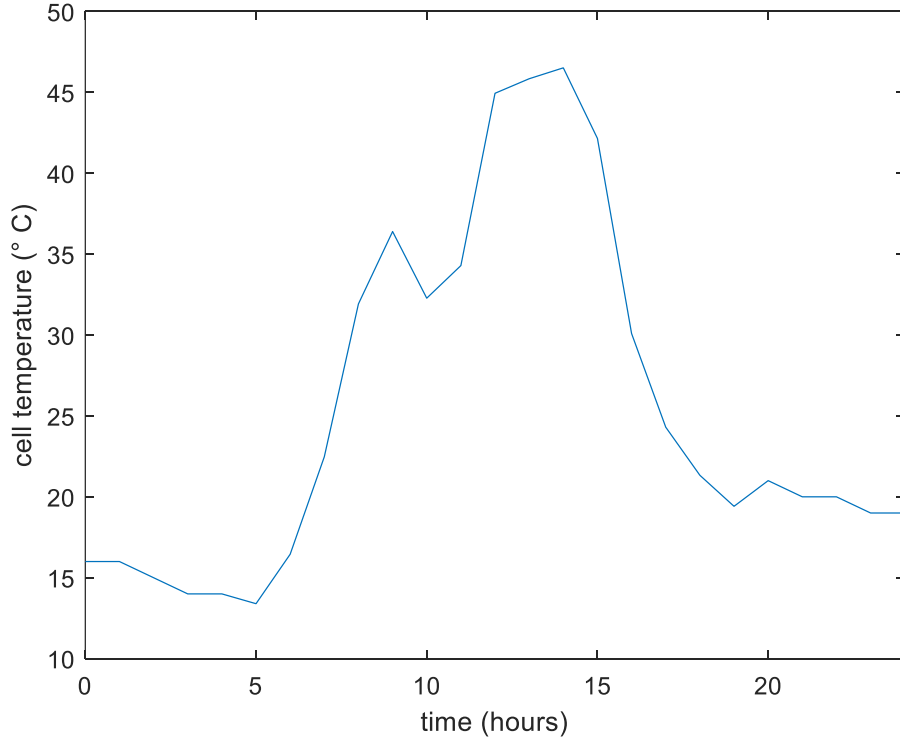


Figure 2.5: Intermediate calculation - cell temperature. Data from 5 June TMY3.

The cell temperature, calculated at increments of one minute, as well as the POA irradiance, interpolated at increments of one minute, are used to generate the I-V & P-V characteristics of the photovoltaic.

These P-V curves are obtained at a time step of one minute, and the maximum power point on the P-V curve are calculated. The maximum power point is thus computed at a time step of one minute.

Data is collected for the year at Kettler Building rooftop, Purdue University Fort Wayne, IN, with same inputs (refer to appendix B for detailed yearly inputs). There are 525,600 minutes in a leap year, the hourly weather conditions presented 8784 data points which were interpolated to 525,600 to get a time step of one minute.

2.4 Model Output

Output data and simulation results include the cell temperature and the power produced by the panel.

Verification is the process of checking that the model design (conceptual model) has been converted into a computer model with some accuracy [20]; in other words, “building the model right”. This is achieved by comparing the thermal and electrical model to other models based on literature review.

Validation, on the other hand, is the process of ensuring that the model is accurate for the purpose at hand; in other words, “building the right model”. Validation is ensuring that the data necessary for model building, model analysis and testing, and conducting the model experiments to solve the problem are accurate and correct [20-21]. Both the thermal model and the electrical model are validated experimentally by comparing the predicted data from the MATLAB simulation to the data measured experimentally.

The TMY3 data is used in chapter 5 for the verification process. However, exact weather conditions, such as irradiance and ambient temperature are used in chapter 6 to validate the computerized model. Chapters 5 and 6 detail verification and validation of the computer tool.

Comparison of different computational schemes and comparison to measured data indicate that the computer tool can accurately predict the cell temperature and panel power within the limitations described in this thesis.

In chapter 7, the value of the heat transfer coefficient and wind speed are changed to investigate the effects of cooling the photovoltaic panel. Simulations in different geographic locations are performed to evaluate the effect of cooling photovoltaics in different climatic conditions and carry out a simple feasibility study.

3. THERMAL MODEL

In this chapter, several thermal models are used to predict the temperature of the PV cell. The cell temperature is then used as an “input” to the electric model outlined in Chapter 4, to investigate the temperature effects on photovoltaic electrical power output.

3.1 Cell Temperature Calculation

In this section, five different thermal models are discussed, and results are obtained using MATLAB code. The models were developed by Ross et. al [22], Faiman et al [23], Sandia et al [24], Fuentes et al [25] and McAdams [26].

3.1.1 Ross Thermal Model

The most used model for finding the cell temperature is by using the normal operating condition temperature (NOCT) of the a PV cell with the relation developed by Ross [22]

$$T_c = T_a + \frac{T_{noct} - 20}{800} E_{POA} \quad 3.1$$

which is accurate only for PV free standing modules. The value of estimated NOCT is 45°C.

3.1.2 Faiman Thermal Mode

This model uses an energy balance between ambient temperature and cell with heat input due to the solar irradiance, i.e.

$$U(T_c - T_a) = a_m E_{POA} (1 - e). \quad 3.2$$

T_a is ambient air temperature, E_{POA} is the irradiance incident on the plane of the module or array, a_m is the absorptivity, and e is the efficiency of the PV module (default is 0.1). The thermal behavior is characterized by a thermal loss factor designed with a U -value. The U -value is based on a constant component and a factor proportional to the wind speed [23], i.e.

$$U = U_c + U_v WS, \quad 3.3$$

U_c is the constant heat transfer component, U_v is the heat transfer due to convection component, and WS is the wind speed. These U -factors depend on the mounting type of the modules (sheds, roofing, facade, ground, etc.). Thus, the cell temperature is given by [23]:

$$T_c = T_a + \frac{a_m E_{POA}(1 - e)}{U_c + U_v \times WS}. \quad 3.4$$

For free circulation, this U -coefficient refers to the front and back of the module, i.e., twice the area of the module. If the back of the modules is thermally insulated, the coefficient should be lowered, theoretically up to half the value (i.e., the back side does not participate in thermal convection and radiation transfer). In this study, the model is free standing, and the wind speed is 4 m/s on average, so that default U values are $U_c = 25 \text{ W/m}^2\text{K}$ and $U_v = 1.2 \text{ W/m}^2\text{K}$ [23].

3.1.3 Sandia Laboratory Temperature Model

Sandia [24] proposes the following model to estimate the module temperature:

$$T_m = E_{POA}(e^{a+b.WS}) + T_a. \quad 3.5$$

In Equation 3.5, T_m is the module temperature at the back of the module and not the cell temperature. The constants a and b are parameters that depends on module construction, materials, and the mounting configuration. For this study [24], a glass cell module with an open rack mount is used. Thus, the values of a and b are -3.47 and -0.0594 respectively. The cell temperature can be related to the module temperature in the following expression:

$$T_c = \frac{E_{POA}}{E_o} \times (T_c - T_m) + T_m. \quad 3.6$$

where E_o is a reference solar ration value at standard test conditions.

3.1.4 Fuentes PV-Watts Model

The Fuentes model accounts for the effects of the thermal capacitance of the photovoltaic and runs a numerical integration between time steps to include the thermal transient behavior. The thermal model utilizes the total incident plane of array irradiance data, wind speed data, and ambient temperature data to calculate the cell temperature. PVWatts version 5 [25] assumes a height of 5 m above the ground when correcting the wind speed in the NSRDB dataset and that the installed nominal operating cell temperature (INOCT) of the module is 45°C.

3.1.5 Thermal Capacitance Model with McAdams's Relation

The thermal analysis below is performed for a single PV cell based on an energy balance. The temperature of all PV cells is assumed to be the same, thus this analysis can be applied to the whole PV module. The photovoltaic cell temperature is computed from the heat balance:

$$mC_{p-module} \frac{dT_c}{dt} = Q_{in} - Q_{conv} . \quad 3.7$$

The heat incident and absorbed by the PV solar cell can be calculated by the following:

$$Q_{in} = \alpha GA \quad 3.8$$

where G is the incident solar radiation and a is the absorptivity. The heat transfer by convection is determined from:

$$Q_{conv} = h_{conv}A (T_c - T_{\infty}). \quad 3.9$$

Substitution into Equation 3.7 and use of a first-order representation for the derivative yields an expression for the cell temperature, viz.:

$$T_{i+1} = T_i + \frac{A[a_m E_{POA} - h_{conv}(T_i - T_a)]\Delta t}{mC_{p-module}} . \quad 3.10$$

The value of the heat transfer coefficient is approximated using McAdam’s relation (1954) [26]:

$$h_{conv} = 5.7 + 3.8 \times WS \quad 3.11$$

3.2 Comparison of Thermal Models

The five thermal models described in this chapter are compared in Figure 3.1. The input data for all of the models is from 16 June TMY3. Agreement between the models is good with the largest difference occurring during peak irradiance hours of 12:00 PM – 3:00 PM.

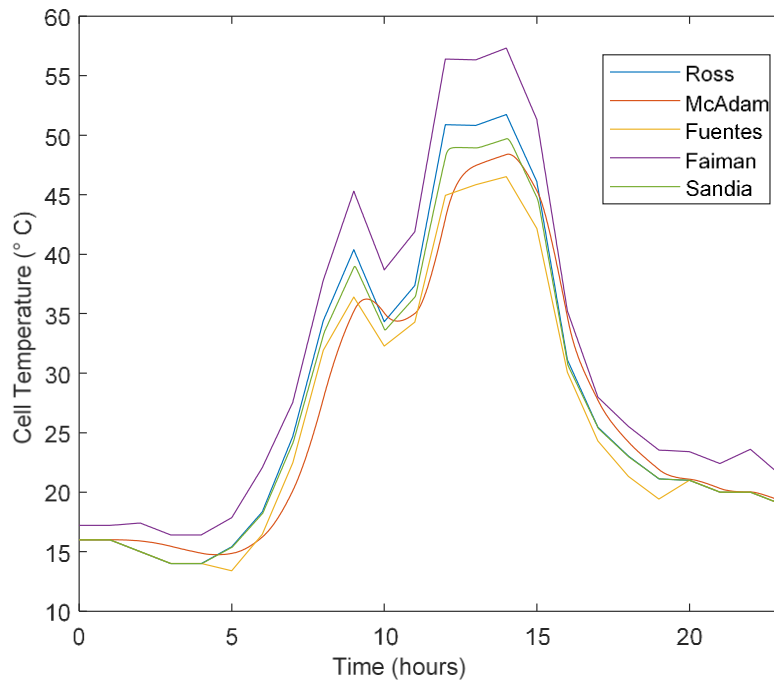


Figure 3.1: Comparison of thermal models for cell temperature calculation. Input data from 16 June TMY3.

Although all models show similar temperature predictions, the thermal capacitance model with McAdam’s relationship for the heat transfer coefficient is used for the rest of this study. The thermal capacitance model is robust, flexible, and accounts for the thermal capacity of the PV panel and the effect of the wind speed over the panel.

4. ELECTRIC MODEL

To evaluate the performance of the solar panel, an electrical model that predicts the I-V and P-V characteristics of the photovoltaic is developed. A PV cell equivalent circuit is shown in Figure 4.1. A solar cell is composed of an electrical diode, a resistance, and a shunt resistance [14-17].

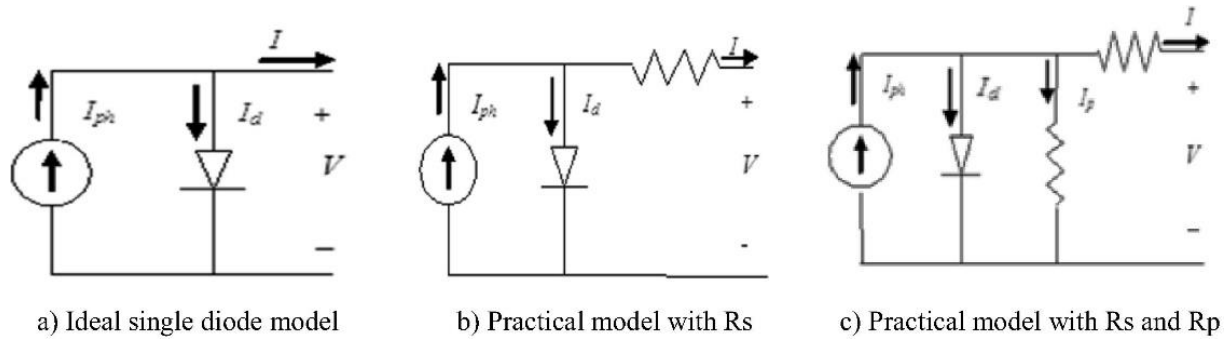


Figure 4.1: The equivalent circuit of a solar cell and a PV device [22]

The mathematical model of the PV cell is developed by analysis of the circuit shown in Figure 4.1c.

4.1 Mathematical Model

The first step is to find the thermal voltage. The thermal voltage is dependent on the cell temperature. The nominal voltage in Equation 4.1 is dependent on the nominal temperature and the thermal voltage in Equation 4.2 is dependent on the cell temperature [14-15], i.e.

$$V_{tn} = N_s \left[\frac{(k \times T_n)}{q} \right] \tag{4.1}$$

$$V_t = N_s \left[\frac{(k \times T_c)}{q} \right] \tag{4.2}$$

The nominal temperature sometimes is referred to as the reference temperature of the cell at standard test conditions (STC). The cell temperature at STC is $25^\circ\text{C} + 273 = 298 \text{ K}$.

The next step is to calculate the reverse saturation current and the saturation current using equations:

$$I_{rs} = \frac{I_{sc}}{\exp\left(\frac{V_{oc}}{a \times V_{tn}}\right) - 1} \quad 4.3$$

$$I_0 = I_{rs} \times \left(\frac{T_n}{T_c}\right)^3 \times \exp\left[\frac{(q \cdot E_g)}{(a \cdot k)}\right] \times \left(\frac{1}{T_n} - \frac{1}{T_c}\right). \quad 4.4$$

According to Figure 4.1.a, the output current at the standard test conditions (STC) is:

$$I = I_{ph} - I_{0n} \left[\exp\left(\frac{V}{a}\right) - 1 \right]. \quad 4.5$$

Since the nominal photovoltaic current cannot be easily obtained, Equation 4.5 is written as

$$I_{sc} = I_{pvn} - I_{0n} \left[\exp\left(\frac{0}{a}\right) - 1 \right] = I_{pvn} \quad 4.6$$

when the PV cell is short circuited. But this equation is only valid for an ideal case, so the equality is not strictly correct. Therefore, this equation can be written as:

$$I_{sc} \approx I_{pvn}. \quad 4.7$$

The photocurrent is dependent on the solar irradiance and the temperature, where K_i is the coefficient temperature of short circuit current provided by the manufacturer, and G_n is the nominal solar irradiance at STC, i.e., 1000 W/m² so that

$$I_{ph} = \left(\frac{G}{G_n}\right) \times [I_{sc} + K_i \times (T_c - T_n)]. \quad 4.8$$

The diode current is proportional to the saturation current and is given by

$$I_d = I_0 * \left\{ \exp \left[\frac{V + I * R_s}{(a * V_t)} \right] - 1 \right\}, \quad 4.9$$

which follows from Figure 4.1.b. Using Figure 4.1.c, the leak current in the parallel resistor is calculated by:

$$I_p = \frac{V + I * R_s}{R_p} \quad 4.10$$

Finally, application of Kirchhoff's law, yields the current produced by the PV panel viz.,

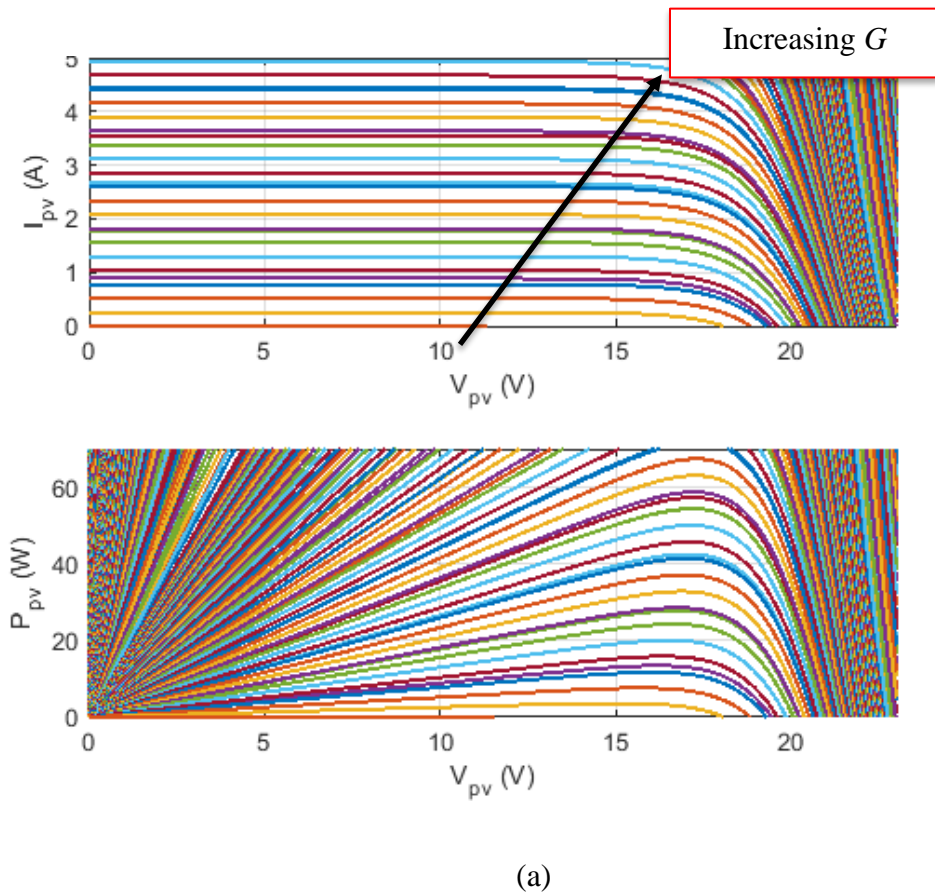
$$I = I_{ph} - I_d - I_p. \quad 4.11$$

4.2 I-V & P-V Characteristics with Constant Temperature

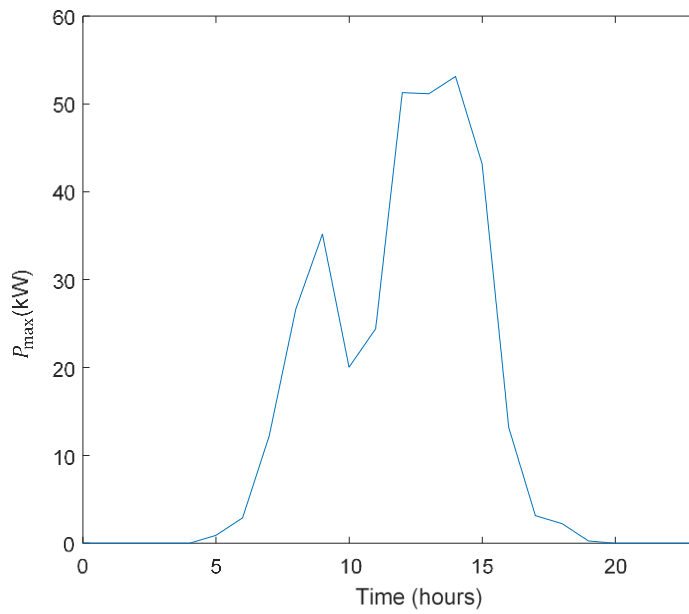
With the use of the cell temperature as an intermediate value and solving for current I , yields the I - V as well as the P - V characteristics. Figure 4.2.a shows clusters of data with increasing incident radiation, while the cell temperature is kept constant at 25°C. In reality, increasing the incident radiation increases the maximum power which is desirable, but it also increases the cell temperature which negatively affects the cell performance. Figure 4.2.b shows the maximum power point, which is the maximum point on a power (P - V) curve that has the highest value of the product of its corresponding voltage and current, or the highest power output, and that can be found using Equation 4.12:

$$P_{mpp} = V_m \times I_m \quad 4.12$$

Figure 4.2.a shows the I - V and P - V curves at a time step of every minute for 1440 minutes for 16 June TMY3, but with the temperature fixed 25°C. Figure 4.2.b shows the maximum power point.



(a)



(b)

Figure 4.2: Variation of plane of array irradiance with constant temperature, (a) I - V & P - V curves and (b) predicted maximum power point.

4.3 I-V & P-V Characteristics with Constant Radiation

Figure 4.3 shows the PV panel characteristic when incident radiation is fixed at 800 W/m^2 and cell temperature changes every minute based on environmental conditions of 16 June TMY3.

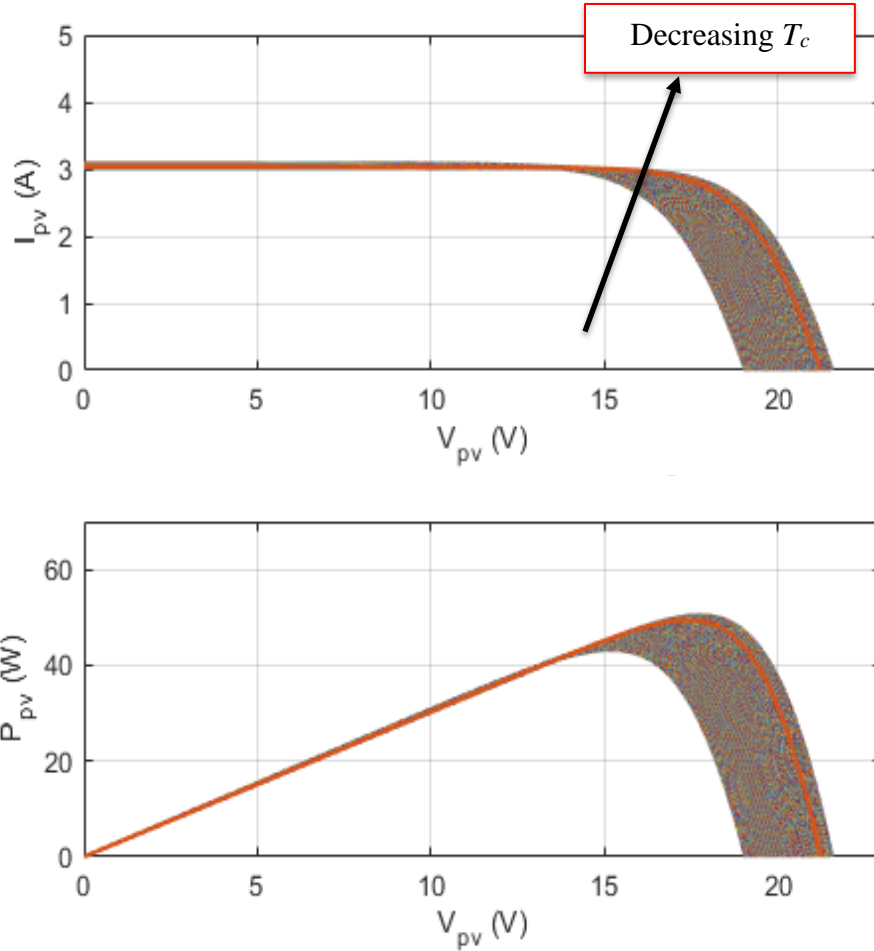
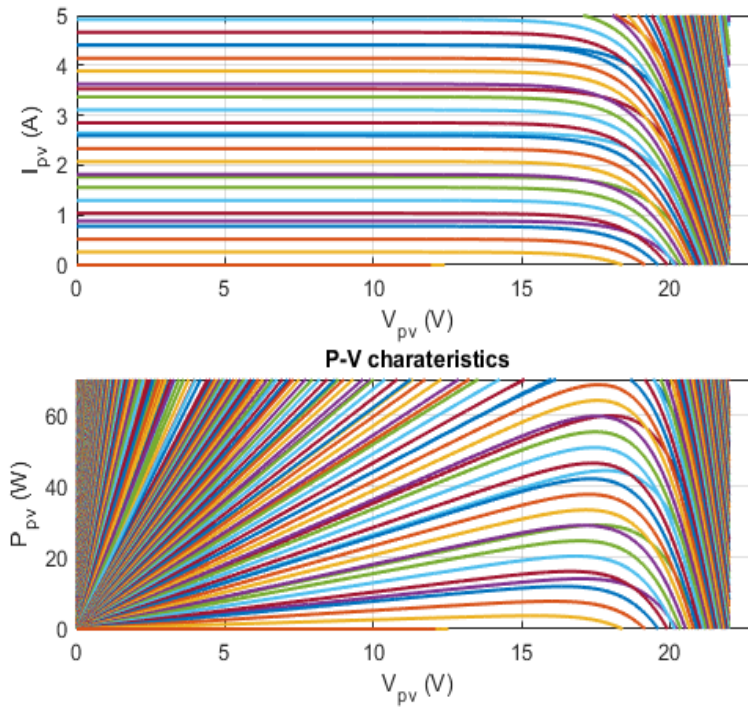


Figure 4.3: I-V & P-V curves for variation of cell temperature with constant POA irradiance.

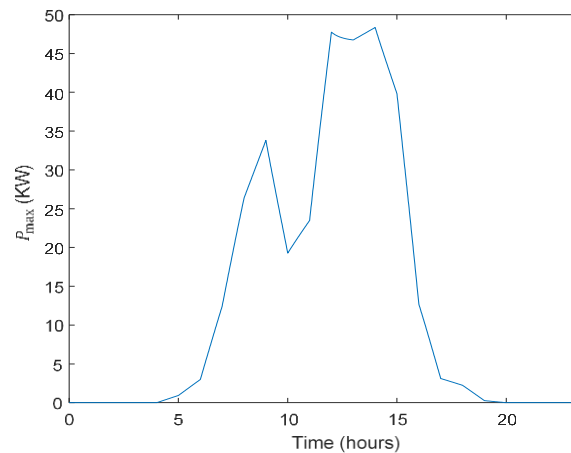
Figure 4.3 shows the I-V and P-V curves obtained at a time step of every minute for 1440 minutes for 16 June TMY3, but with the solar irradiance kept constant. As shown in Figure 4.3, the short circuit current (when $V_{pv} = 0$) is nearly unaffected with changing temperature, compared to Figure 4.2 which showed significant effects on the both the short circuit current and the open circuit voltage as well as the maximum power point and the fill factor. When keeping the solar radiation constant and decreasing the temperature, the open circuit voltage increases as does the maximum power point, the efficiency, and the fill factor.

4.4 I-V & P-V Characteristics with Weather Data

Figure 4.4.a shows the I-V and P-V characteristics using the ambient weather conditions of 16 June TMY3 as input. The maximum power point is obtained every minute and is presented in Figure 4.4.b for 1440 points throughout the day.



(a)



(b)

Figure 4.4: Variation of plane of array irradiance and constant temperature, (a) I-V & P-V curves and (b) predicted maximum power point for 16 June TMY3.

An increase in the solar radiation increases the maximum power output, while a increase in the cell temperature decreases the maximum power output (but to a lesser extent). Various factors that might increase the solar irradiance such as adjusting the inclination angle, changing the mounting location, or modifying the setup by adding mirrors etc. which may increase the power output compared to decreasing cell temperature; but these factors are not considered in this study. The focus of this study is reduction of the cell temperature to increase the conversion efficiency of the PV panel.

5. MODEL VERIFICATION

In this chapter, both the thermal and electrical models are verified. Verification is the process whereby the model and simulation are shown to be constructed correctly and behave as expected.

5.1 Verification of Thermal Model

The thermal model to predict the cell temperature has been verified by:

- 1- Comparing the thermal model to other thermal models published in the literature.
- 2- Comparing the output (cell temperature) to the input (ambient temperature).
- 3- Varying one of the input parameters (solar irradiance) and observing the effects on the output (cell temperature).

5.1.1 Comparison of Thermal Models

Five different thermal models are compared in section 3.2. Figure 3.1 shows the predicted cell temperature for the five different models. All models follow the same trend, and the predicted temperatures are similar. A thermal capacitance model with a simple relationship [17] for the forced convection heat transfer coefficient that depends on the wind speed is used for the rest of this study.

5.1.2 Behavior of the Thermal Model

This technique involves checking if the model's output and/or behavior is reasonable. Figure 5.1 shows the ambient and cell temperatures on a typical summer day, i.e., 16 June TMY3. As expected, the cell temperature is higher than the ambient temperature during periods of high solar irradiance. During periods of no solar irradiance, i.e. evening hours, the cell temperature and the ambient temperature are the same.

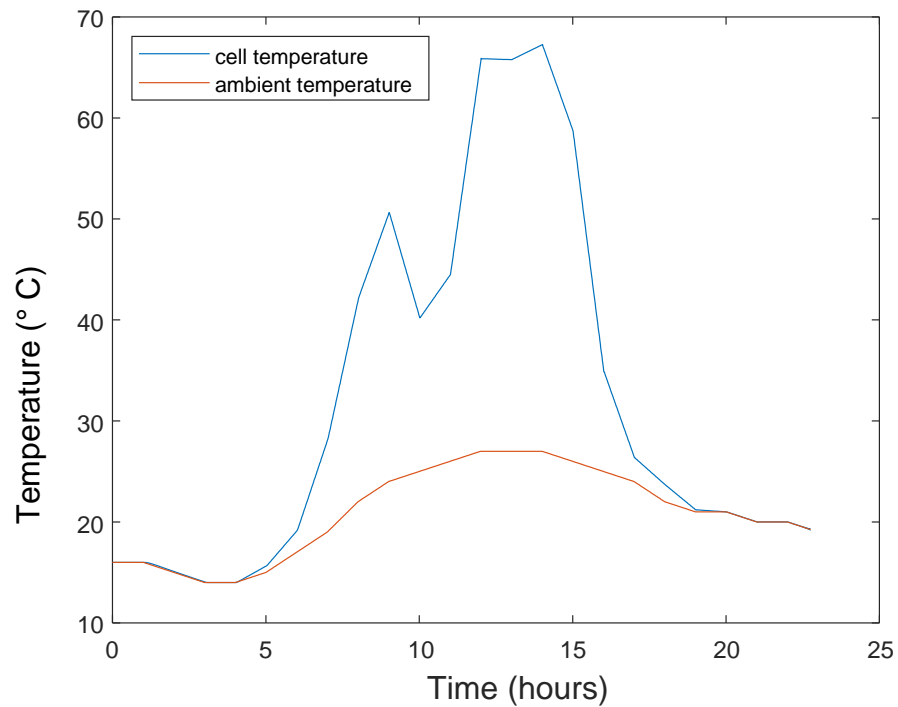
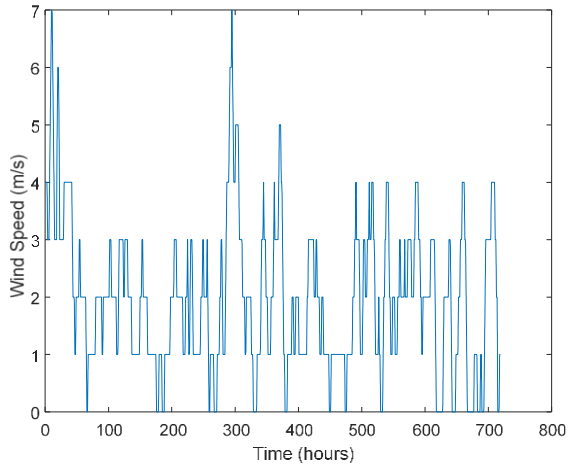
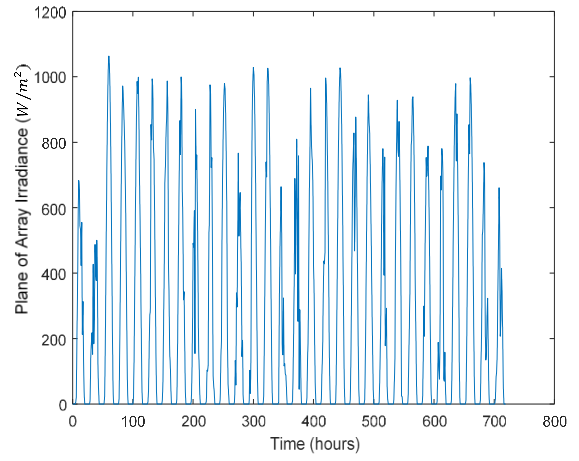


Figure 5.1: Cell and ambient temperatures compared. Input data from 16 June TMY3.

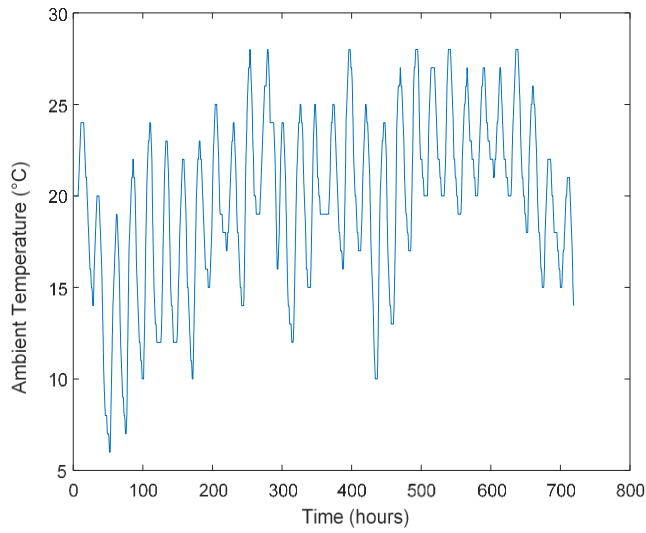
A similar check is performed for an entire month, i.e. June TMY3. The input data for June TMY3 is shown in Figure 5.2. Figure 5.3 shows the ambient temperature and the cell temperature. As expected, the cell temperature is considerably higher than the ambient temperature during periods of high incident solar radiation. During evening, periods of low solar irradiance, the ambient temperature and the cell temperature coincide.



(a)



(b)



(c)

Figure 5.2: Input data (a) wind speed, (b) plane of array irradiance, and (c) ambient temperature. Data from June TMY3.

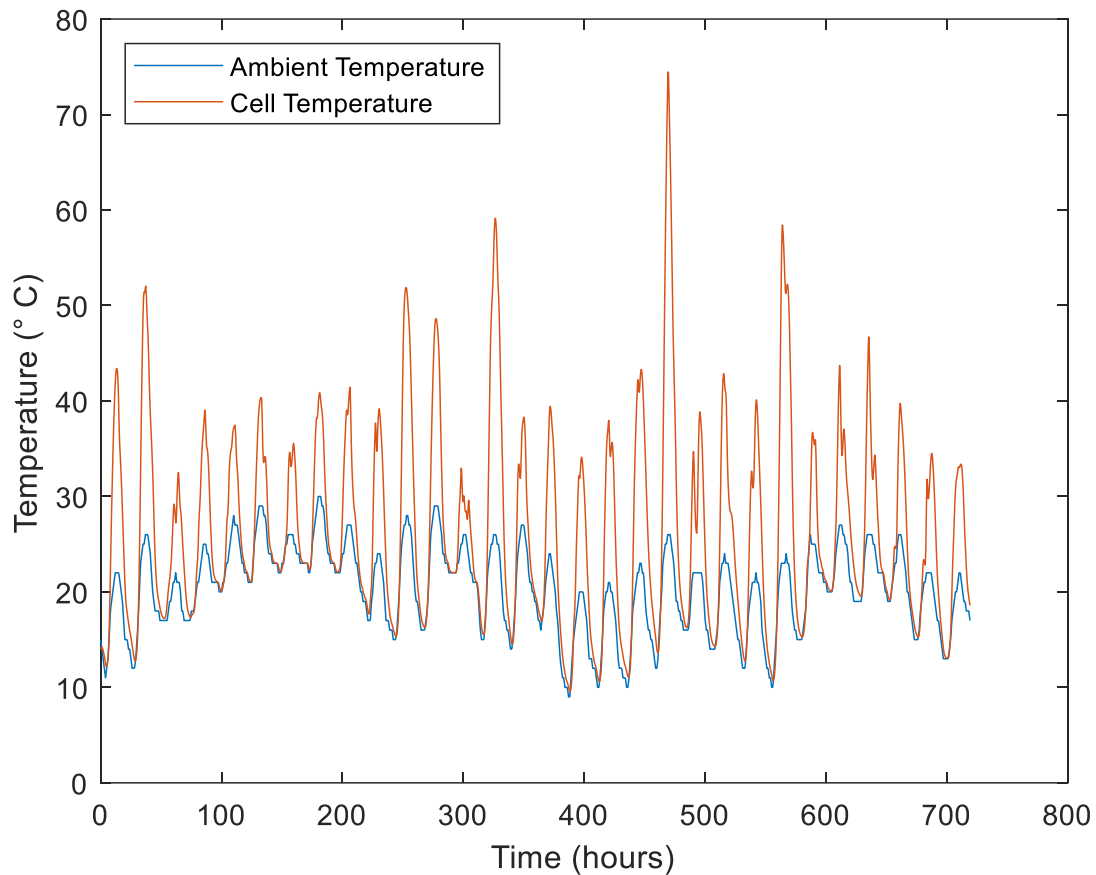


Figure 5.3: Cell temperature (output) compared to ambient temperature (input) for June TMY3.

5.1.3 Thermal Model Parameter Sensitivity

This technique consists of changing the input values to demonstrate predictable model behavior, i.e. the model and simulation output should behave as expected. A test is performed by altering the input data set. The time increment is one minute and the input to the model is ambient temperature and POA irradiance, G . The ambient temperature is kept uniform throughout an hour. However, the value of G is halved after 20 minutes. The predicted outcome is that the cell temperature will be lower as is shown in Figure 5.4.

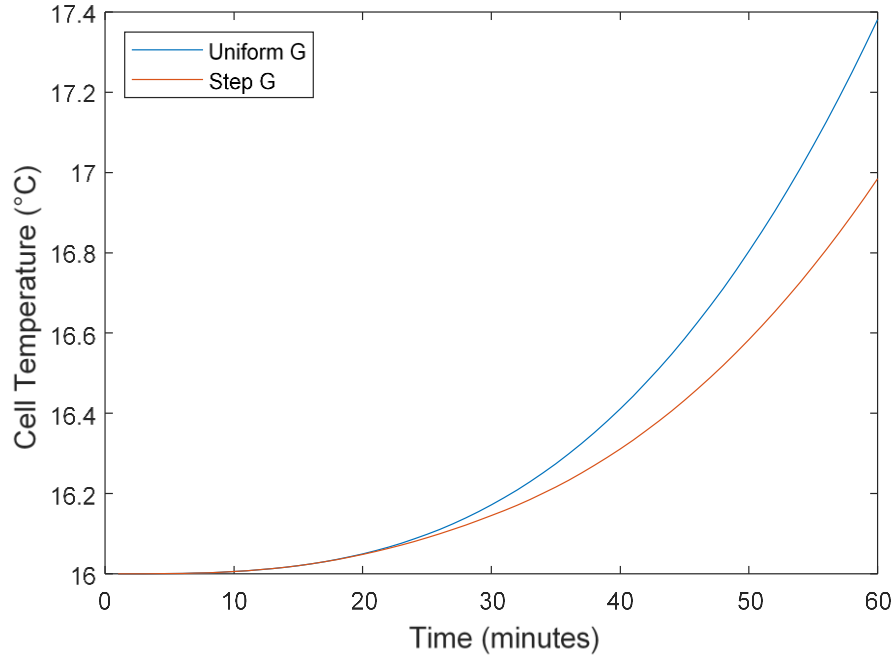


Figure 5.4: Parameter variability sensitivity analysis.

5.2 Verification of Electrical Model

Verification of the electrical model is done by comparing the results to those predicted by PV-Watts. The PVWatts calculator, developed by NREL lab, predicts the electrical power based on *averaged* solar cell characteristics, however, the model described in chapter 4 utilizes Shockley’s diode model [14-17] with manufacturer’s cell parameters to calculate the power output more accurately. For comparison, the PVWatts calculator hourly results were linearly interpolated to obtain panel power at a time step of one minute.

Figure 5.5 shows the predicted power simulation results obtained from the model compared to the results from the PVWatts calculator. Input data is from 20 June TMY3. As shown in Figure 5.5, the variances in predicted power, i.e. simulation, to the results produced via PVWatts are minimal, with approximately a 4% difference during four hours around noon. Results for the predicted power for the 8640-hourly data in TMY3 are shown in Figure C.4 in appendix C.

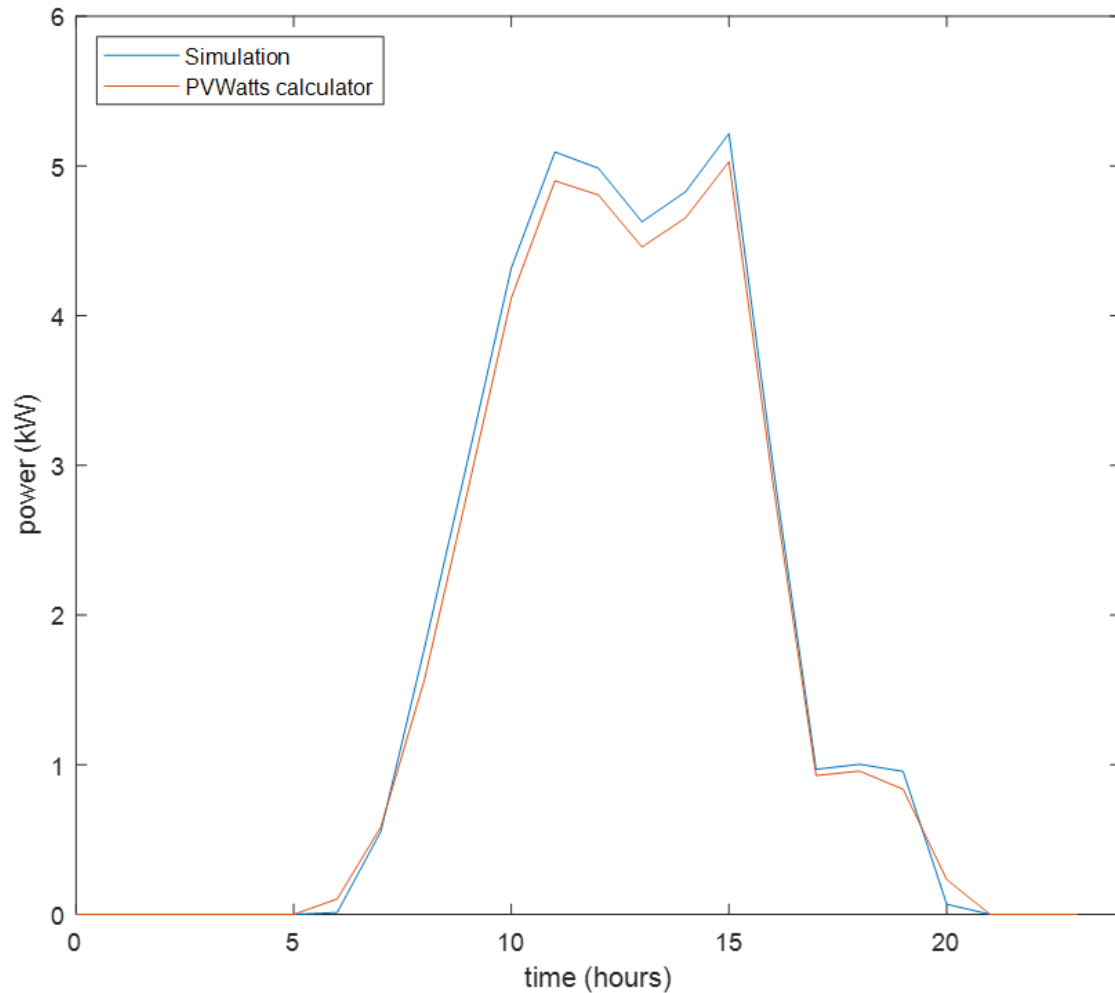


Figure 5.5: Predicted power simulation results and PVWatts power results compared. Input data from 20 June TMY3.

The PVWatts calculator also generates a monthly total energy data. The power produced throughout the day using the computer simulation is utilized to generate the predicted energy in kW-h. The energy in kW-h is the area under the power – time graph, i.e.

$$E = \frac{1}{60} \int P dt \quad 5.1$$

The results presented in Figure 5.6 below shows the DC energy output predicted, using the electrical model presented in chapter 4, i.e. simulation, compared to the DC annual energy output predicted using the PVWatts calculator.

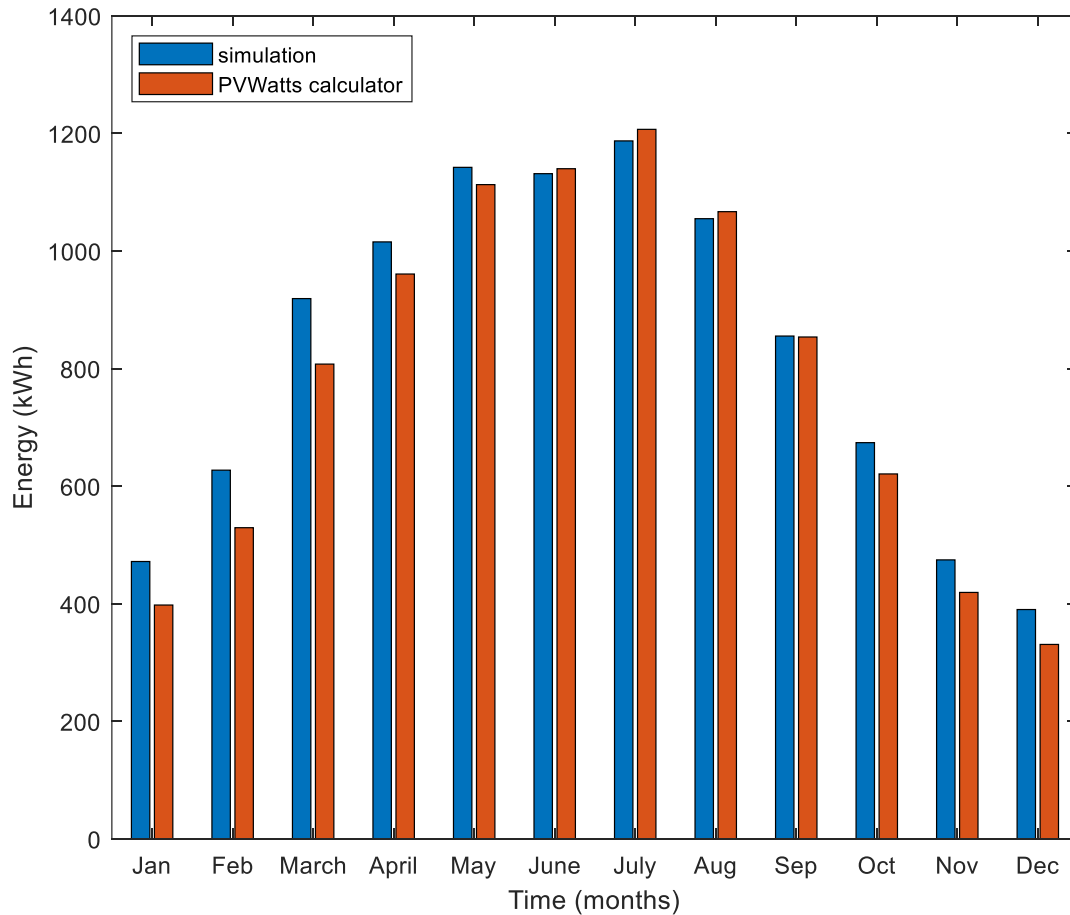


Figure 5.6: PVWatts annual energy results and annual energy simulation results compared. Input data TMY3

The same input data (TMY3) and model parameters are used for the simulation and PVWatts. The input data were solar irradiance and the cell temperature. PV parameters included the system size, i.e. a 7.6 kW DC array, the same geographical location, azimuth angle etc. The difference between the simulation described in this study and the results from the PVWatts calculator is that PVWatts calculator assumes a typical, i.e. generic, module type without taking into consideration all of the cell characteristics that are shown Table 2.1. For example, the module type in PVWatts is the

standard module type with the cover type of glass with a temperature coefficient of $-0.47 \text{ \%}/^{\circ}\text{C}$. The simulation described in this study uses all of the cell characteristics that are shown in Table 2.1 that are based on information presented in the module data sheet specifications.

To compare the results, the percent difference between the simulation and the PVWatts calculator is shown in Table 5.1. The differences were the highest during the winter months, when power produced is low and lowest during summer months. The monthly percent differences ranged from 15.7% to 0.19% with an overall annual percent difference of 5%.

Table 5.1: Comparison of monthly PVWatts energy results and simulation results. Input data TMY3.

Month	Simulation (kWh)	PVWatts (kWh)	% Difference
January	471.8	397.8	15.7
February	627.2	529.3	15.6
March	919	807.6	12.1
April	1015.4	960.7	5.39
May	1142.2	1112.8	2.57
June	1131.5	1139.9	-0.74
July	1187.2	1206.8	-1.65
August	1054.9	1066.8	-1.13
September	855.3	853.7	0.19
October	673.9	620.7	7.89
November	474.5	419.2	11.7
December	390.1	330.8	15.2
Total	9943	9446.1	5.00

6. MODEL VALIDATION

To validate the computer tool, the 7.6 kW roof ballast array mounted on Kettler Hall (Purdue University Fort Wayne), shown in Figure 6.1, is used. The array consists of 21 Heliene modules (360 W). Each module has a P370 MPPT optimizer that tracks the I - V curve and records the maximum power point. Data were recorded over a period of two weeks among which four clear sky days were chosen for the data analysis. The performance of the photovoltaic array was characterized by recording the temperature of the photovoltaic cell and the power output at different times throughout the day. The maximum power point from the array was obtained by tracing the I - V curve every 15 minutes.

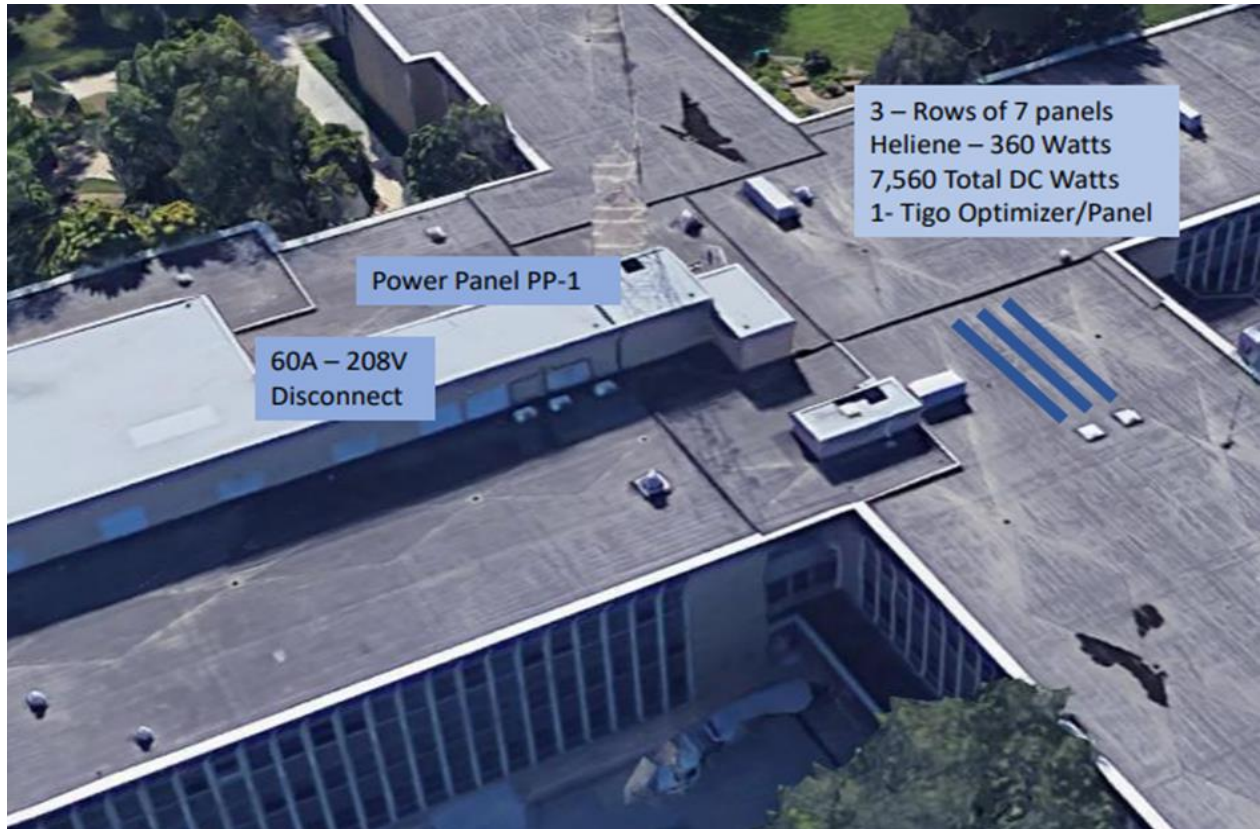


Figure 6.1: Roof-mounted PV array at Kettler Hall in Purdue University Fort Wayne campus.

6.1 Temperature and Solar Irradiance Measurements

Cell and ambient temperatures, as well as solar irradiance measurements were obtained with the Solar Survey 100. The device, as shown in Figure 6.2, also includes a data logging capability with USB interface for downloading and transferring the data to a PC. This allows for plane of array irradiance and temperature values to be recorded at 15-minute intervals. The Solar Survey 100 also has a built-in inclinometer to measure array angle and verify the tilt angle parameter.

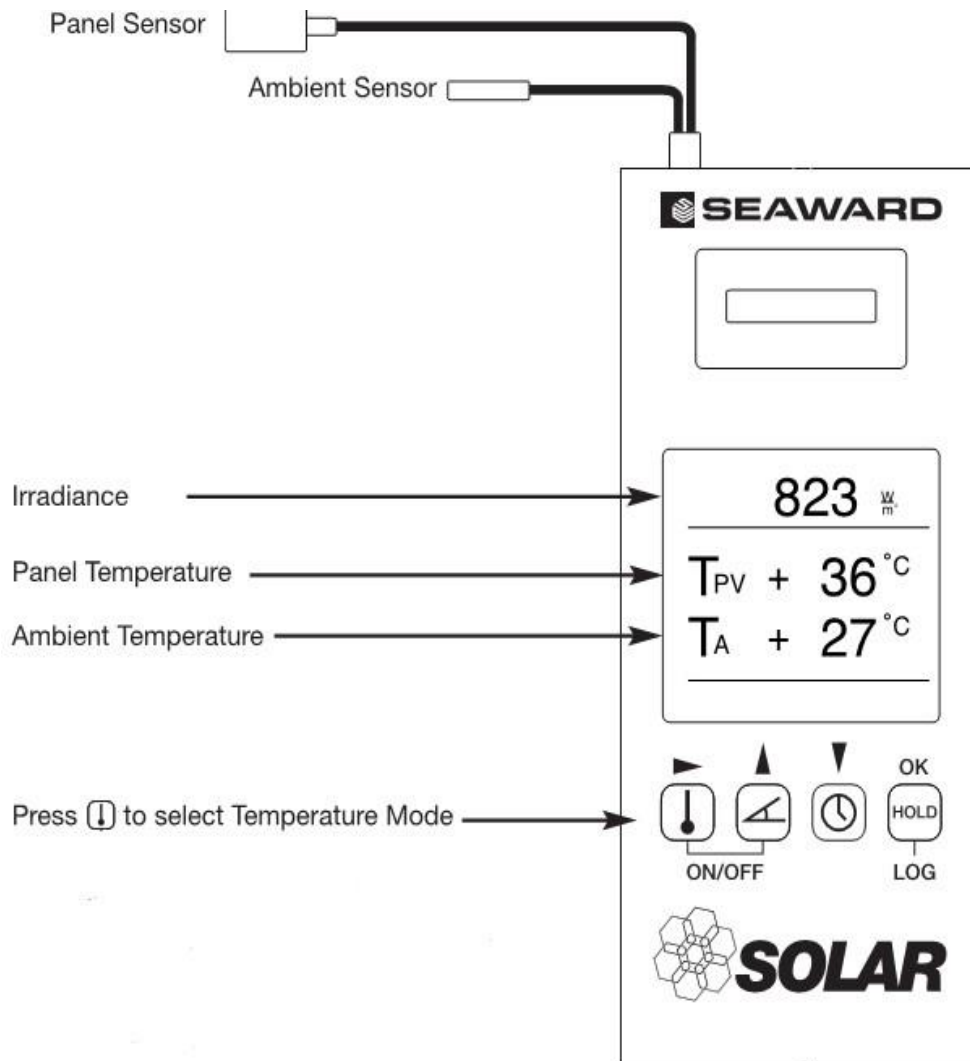


Figure 6.2: Solar Survey 100 temperature and solar irradiance data logger.

6.2 Array Maximum Power Point Measurements

The P370-5NC4ARS power optimizer developed by SolarEdge [27] is a DC/DC converter designed to support 60 and 72-cell modules up to 370 W, 60 V and 11 A (Isc). The SolarEdge Tigo Optimizer is a P370-5NC4ARS which is connected to each panel, replacing the electrical solar junction box. Each power optimizer maximizes the power output from each panel through constant tracking of the maximum power point individually. In addition, the power optimizers monitor the performance of each panel and communicate performance data to the SolarEdge interface for cost effective enhanced maintenance [27].

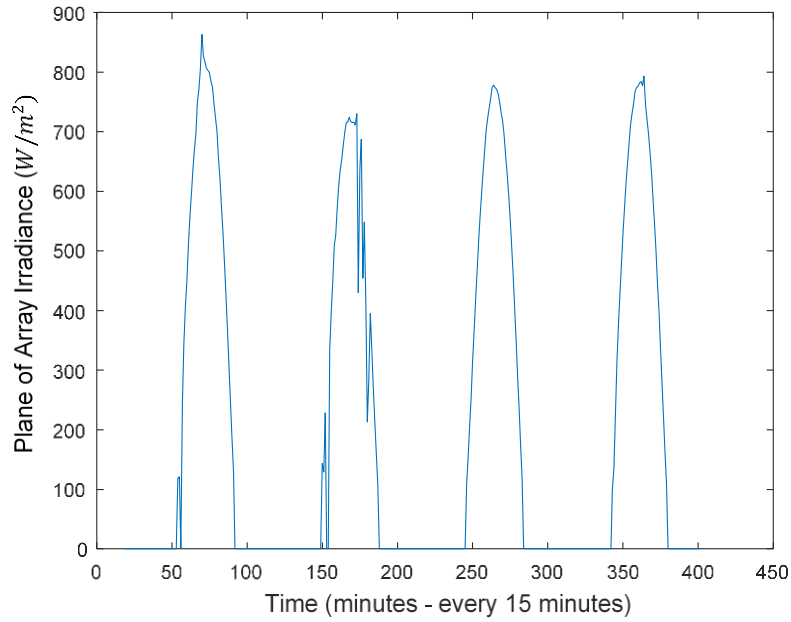


Figure 6.3: 7.6 kWp PV array mounted on the Kettler Hall rooftop at Purdue University Fort Wayne campus.

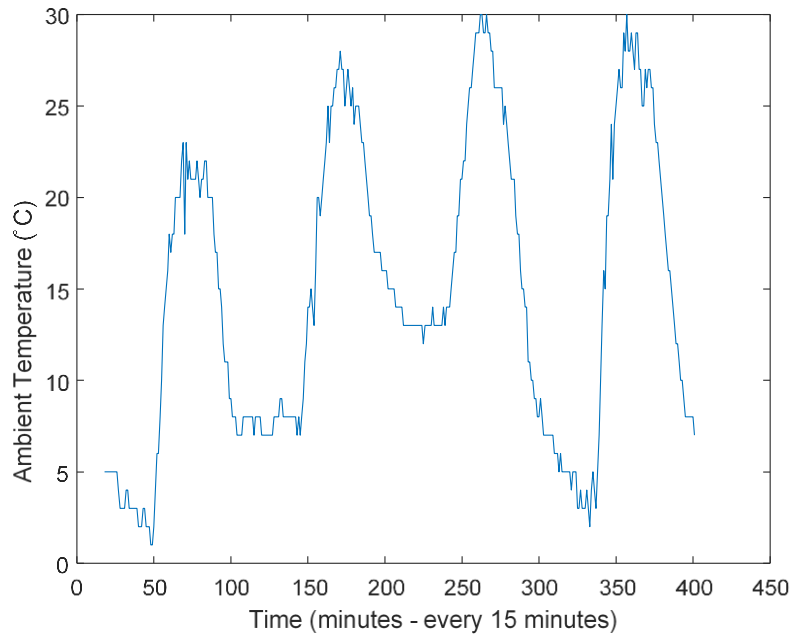
The data was recorded over period of four days, i.e., from 5 October 2020 through 8 October 2020 from sunrise to sunset. Table 2.1 shows model and cell parameters as well as PV array characteristics. The PV panel array is shown in Figure 6.3. The tilt angle is approximately 7 degrees, and the azimuth angle is approximately 200 degrees.

6.3 Description of Input Data Collected

Figure 6.4, below, shows the measured input data for the four clear sky days in October.



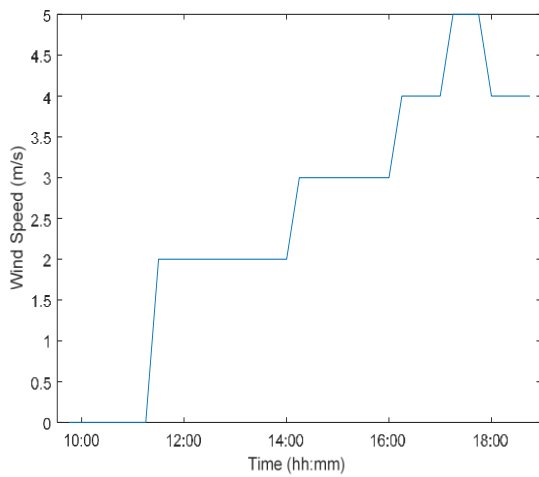
(a)



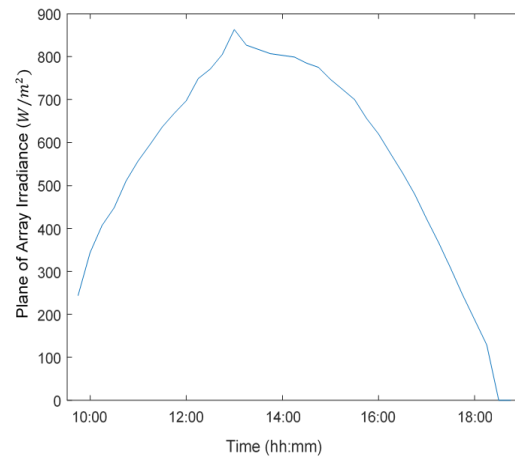
(b)

Figure 6.4: Input data. (a) irradiance and (b) ambient temperature. Data recorded 5 October – 8 October 2020.

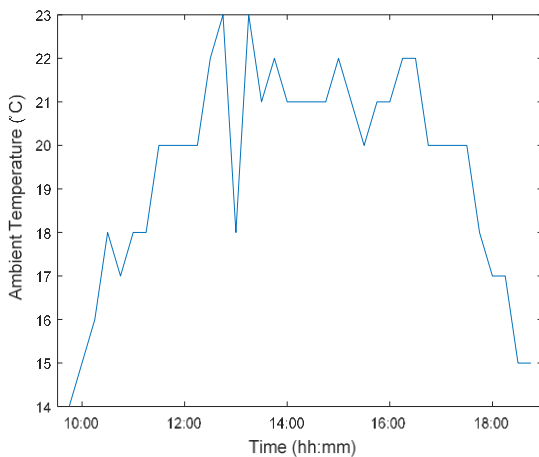
The Solar Survey 100 meter described in section 6.1 was used to record the plane of array irradiance and the ambient temperature at the Purdue Fort Wayne Campus. A wind speed aerometer was not available to measure the wind speed; thus, the value of measured wind speed was approximated using the nearest weather station data, located at the Fort Wayne airport. The data collected from the weather station is hourly data. For consistency, the wind speed data was also interpolated to a time step of one minute. Figure 6.5 shows the three input data parameters used in the simulation i.e., wind speed, solar irradiance, and the ambient temperature obtained on 5 October 2020.



(a)



(b)



(c)

Figure 6.5: Input data (a) wind speed, (b) plane of array irradiance, and (c) ambient temperature. Data for 5 October 2020.

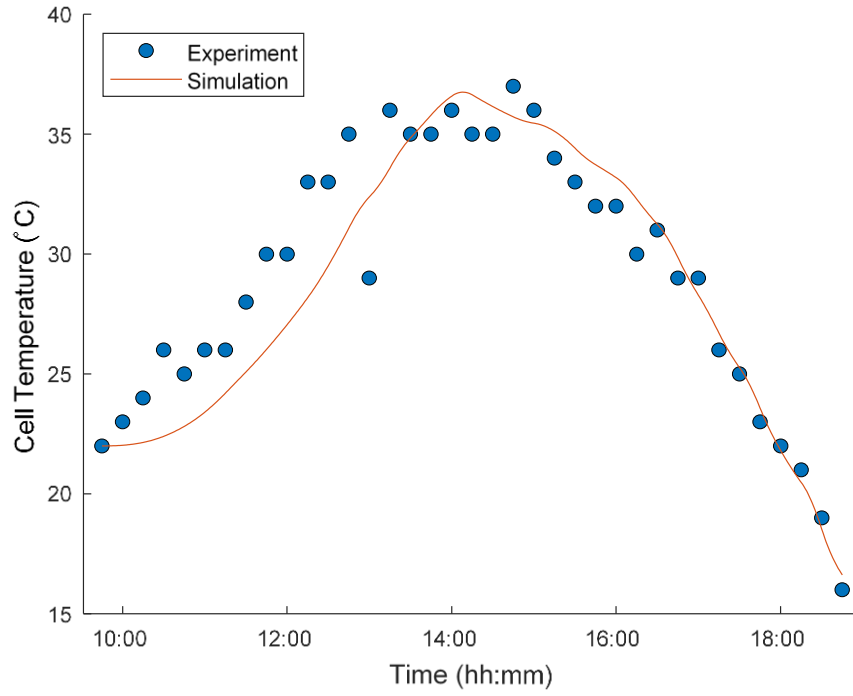
6.4 Simulation Results

The four clear sky days selected are used as an input data to the computer tool. A comparison between the measured cell temperatures and electrical power and those predicted by the thermal model and electrical models is shown in Figures 6.6-6.8.

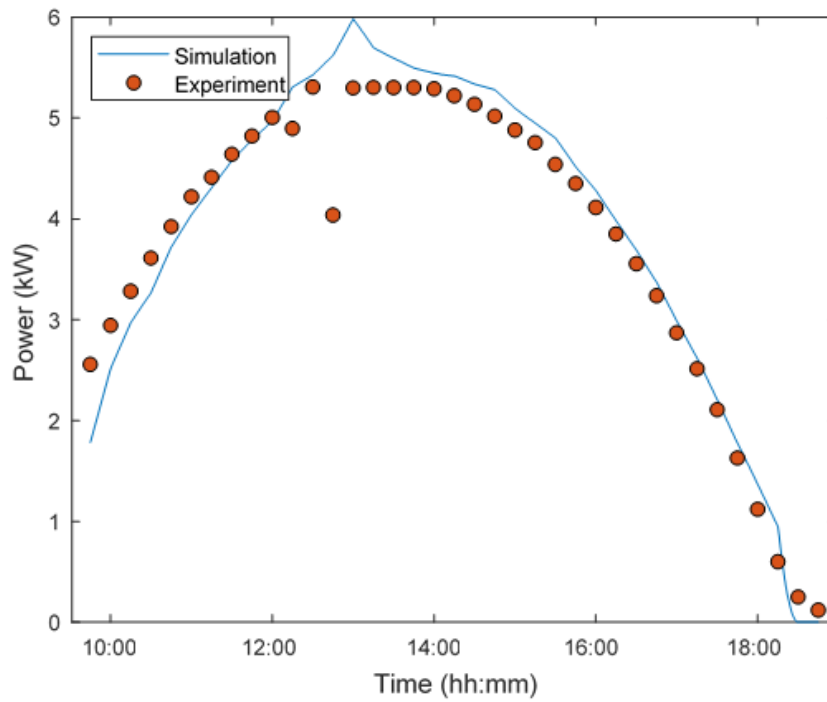
The data measured i.e., solar irradiance and ambient temperature and the data collected i.e., wind speed was used to calculate an intermediate calculation, the cell temperature. The intermediate calculation, cell temperature and the plane of array irradiance was then used to obtain current and voltage readings by varying the load as described chapter 4. The intermediate calculations are used to obtain the maximum power point on an I-V curve. The cell temperature is measured experimentally by the means of a probe and is then compared to the calculated predicted cell temperature from the simulation. Comparisons are shown in Figures 6.6.a and 6.7.a.

The experimental recorded data for the DC electrical power is obtained using the PV optimizer, and the data was recorded on the SolarEdge database. The experimental recorded data was hourly. The maximum predicted power point calculated using the MATLAB code i.e., simulation was then compared to the experimental recorded data. Figures 6.6 through 6.8 show the comparison results from October 5th through October 8th.

The data was collected over a period of 9 hours from 9:45 AM till 18:45 PM as the radiation could not be measured before 9:45 AM. Note that the plane of array irradiance readings less than 100 W/m² are not detected by the Solar Survey meter.

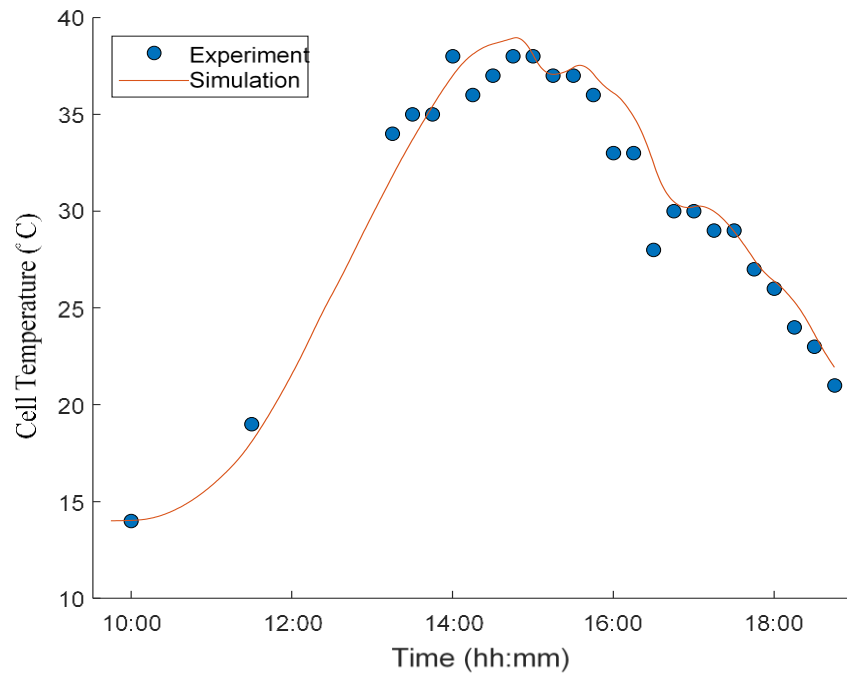


(a)

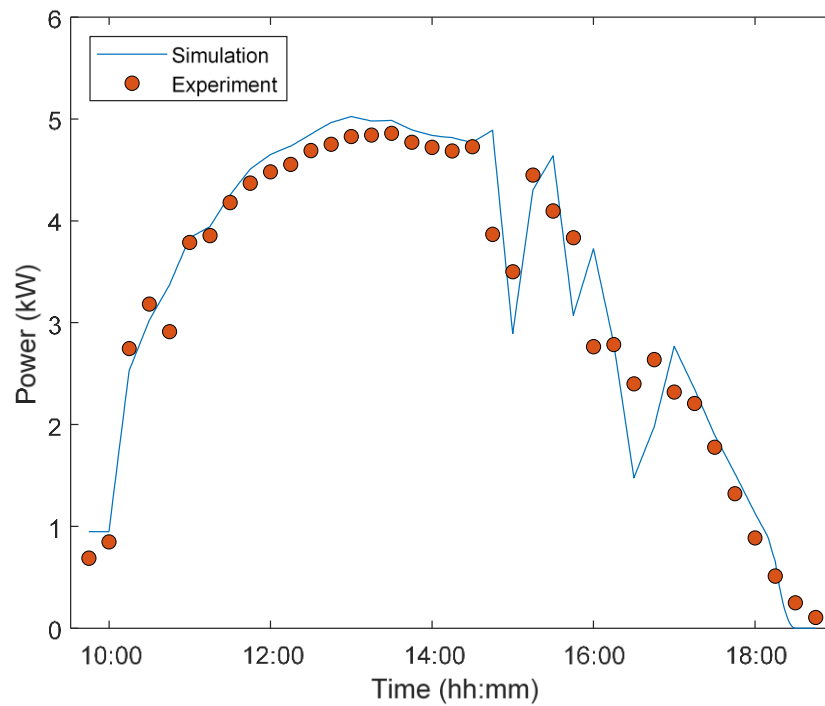


(b)

Figure 6.6: Comparison between measurement and simulation prediction (a) cell temperature and (b) power. Input data from 5 October 2020

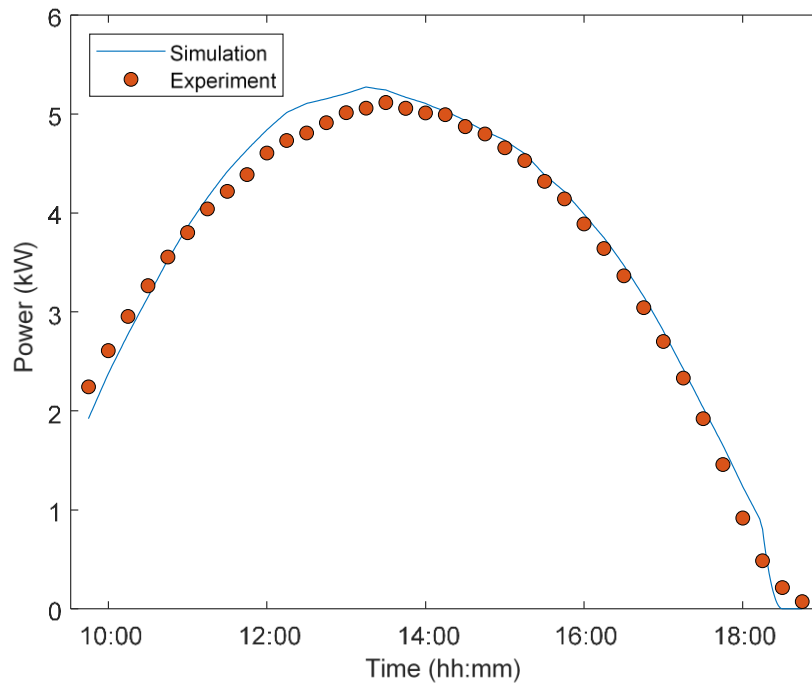


(a)

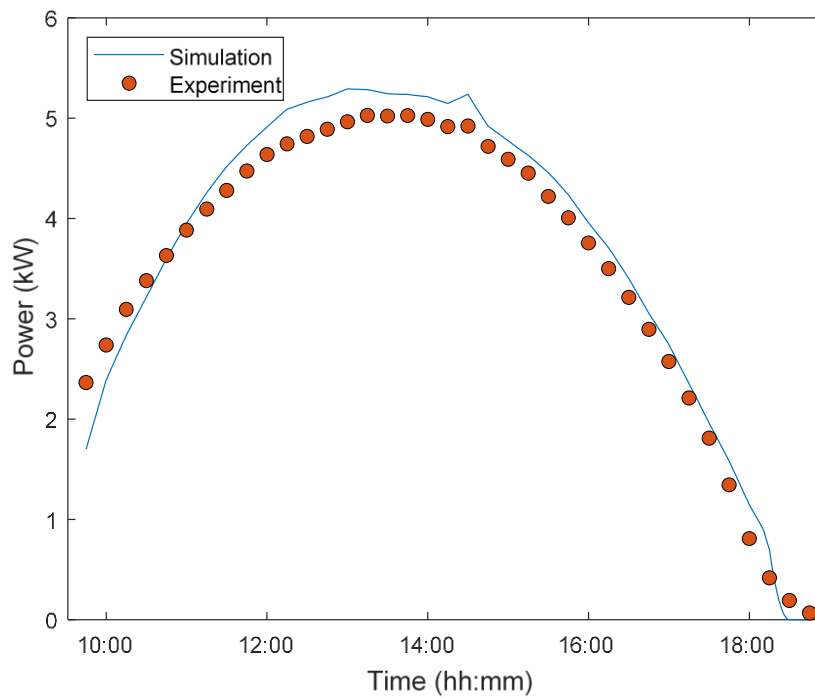


(b)

Figure 6.7: Comparison between measurement and simulation prediction (a) cell temperature and (b) power. Input data from 6 October 2020



(a)



(b)

Figure 6.8: Comparison between the power measurement and simulation prediction. Input data from (a) 7 October 2020 and (b) 8 October 2020.

6.5 Discussion of Simulation Results

In Figures 6.6.a and 6.7.a, the cell temperature curves of the simulation prediction and the experiment follow the same general trend. Although the model predicts a lower cell temperature, the difference between the curves is relatively constant. The root-mean-square error (RMSE) between the predicted temperature and the measured temperature is calculated by:

$$\text{RMSE} = \left[\frac{1}{N} \sum_{x=1}^N (T_{pred,x} - T_{exp,x})^2 \right]^{\frac{1}{2}} \quad 6.1$$

where N is the number of observations, i.e. 36 points between 9:45 AM and 18:45 PM measured at a time step of 15 minutes. The RMSE is shown in Table 6.1.

Table 6.1: RMSE cell temperature measurement compared to simulation on Oct. 5th and Oct. 6th.

Date	Cell Temperature RMSE (°C)
Oct-05	2.1
Oct-06	1.5

The thermal model predicts a lower cell temperature during early morning hours. The computer simulations are performed with the parameters and inputs indicated in Table 2.1 with using the wind speed dataset recorded at a station located approximately 14 miles from the setup, the Fort Wayne airport weather station. That local wind speed provides a better estimate to the observed wind speed. More accurate measurement of wind speed may improve the agreement between the measured and predicted values.

The thermal model in computer tool uses McAdam's relation for the heat transfer coefficient [26]. This relationship was obtained in a controlled environment, i.e., performed experiments on a heated copper plate mounted vertically in wind tunnel. The reported correlation, based on experimental data of Jurges [18], between the forced convective heat transfer coefficient and wind speed as:

$$h_{conv} = 5.7 + 3.8 \times WS \quad 6.2$$

To better account for the realistic wind conditions encountered by the panels on the building rooftop, such as unsteady flow, turbulence, shifting flow direction, the heat transfer coefficient is adjusted to

$$h_{exp} = 11.4 + 7.6 \times WS \quad 6.3$$

which is twice the relationship reported in [26].

Experiment conditions and different sizes and orientation of the panels, necessitate the use of a modified coefficient. Natural wind flow over the surface of an inclined photovoltaic panel cannot be exactly simulated in wind tunnel as natural wind is not steady. The amount of stream turbulence in natural environment can be higher. Therefore, a higher value of wind heat transfer coefficient is expected in natural environment than in controlled environment such as a wind tunnel [18].

Figures 6.6.b, 6.7.b and 6.8 show the simulated and measured DC power. The computer tool uses input parameters from tables 2.1 and 2.2. The measured and simulated results show good agreement with slight differences, mainly during peak hours. October 7 and 8 were clear sky days and the results are very closely aligned. It is possible that dust, partial shading (meaning some shading on some solar panels not exactly where the solar irradiance meter was mounted) or simply due to dust accumulation and flying objects providing shading (on some modules) contributed to some of the differences. The predicted power overall, however, is a close representative of the measured power.

6.6 Relationship between Efficiency and Cell Temperature

To investigate how the efficiency varies with cell temperature, a relationship of power output and temperature is obtained. The power output varies with cell temperature and plane of array irradiance.

$$\text{Efficiency} = \frac{(\text{DC Power Output})}{E_{POA} \times \text{Area}} \times 100\% \quad 6.4$$

$$\Delta T = T_{cell} - T_{ambient} \quad 6.5$$

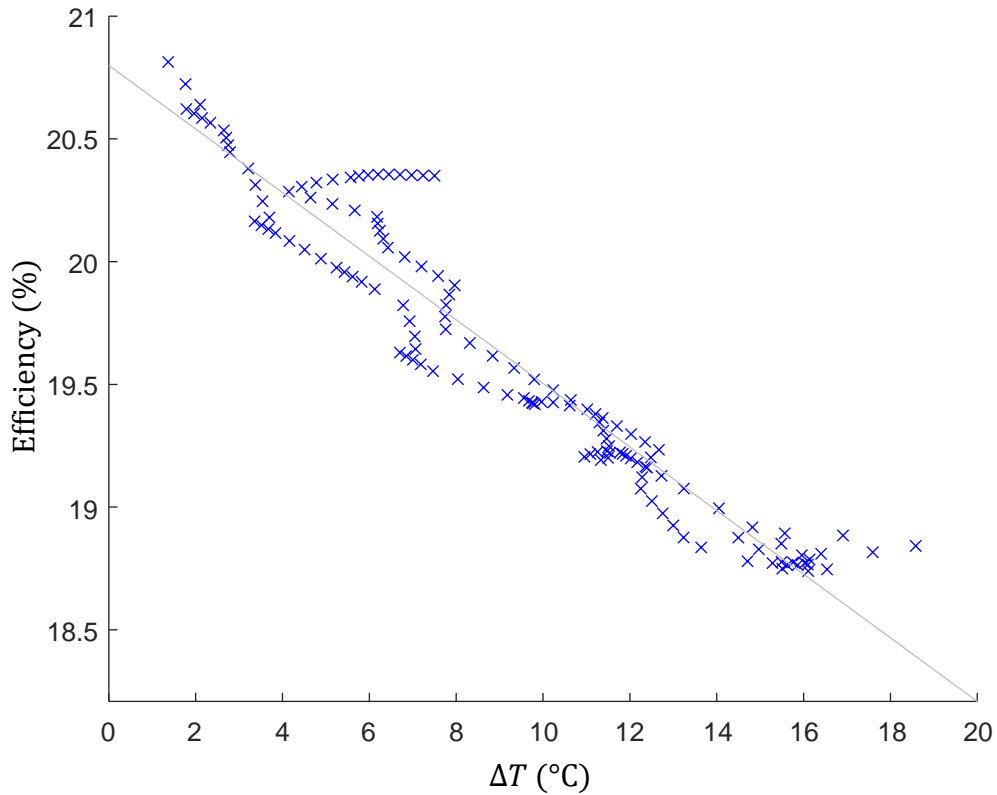


Figure 6.9: Relationship between efficiency and rise in cell temperature. Input data from 5 Oct. 2020.

As shown in Figure 6.9, the rise in cell temperature above the ambient decreases the efficiency of the PV panel. It can be approximated that for every degree Celsius rise in temperature, the efficiency of the solar panel is reduced by 0.5%. This agrees very closely with the value of 0.45% reported in [7]. It can also be noted that at 16°C difference in temperature and above the effects on the efficiency appears to level off.

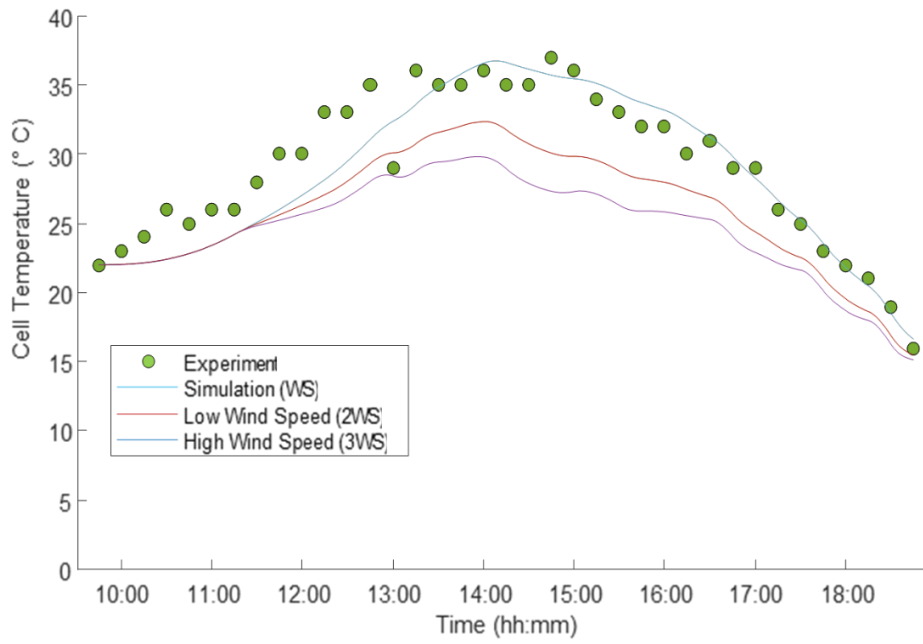
7. EFFECT OF COOLING ON PHOTOVOLTAIC PERFORMANCE

To investigate the effect of cooling, the values of wind speed are modified to effectively cool the photovoltaic panel. In this study, the values of wind speed are doubled and tripled. These values could be achieved experimentally by placing a fan behind the solar modules and modulate the fan speed as required to achieve the desired wind speed. The effects of cooling vary with other ambient conditions and are not only limited to wind speed. For example, wind direction, whether it is a sunny day or a cloud day, and humidity for example impact the cell temperature. The impact of those parameters requires a complex model, and there are no means for accurately capturing all of that data. The aim of this study is to simply vary the wind speed and examine the impact on the cell temperature and the power output.

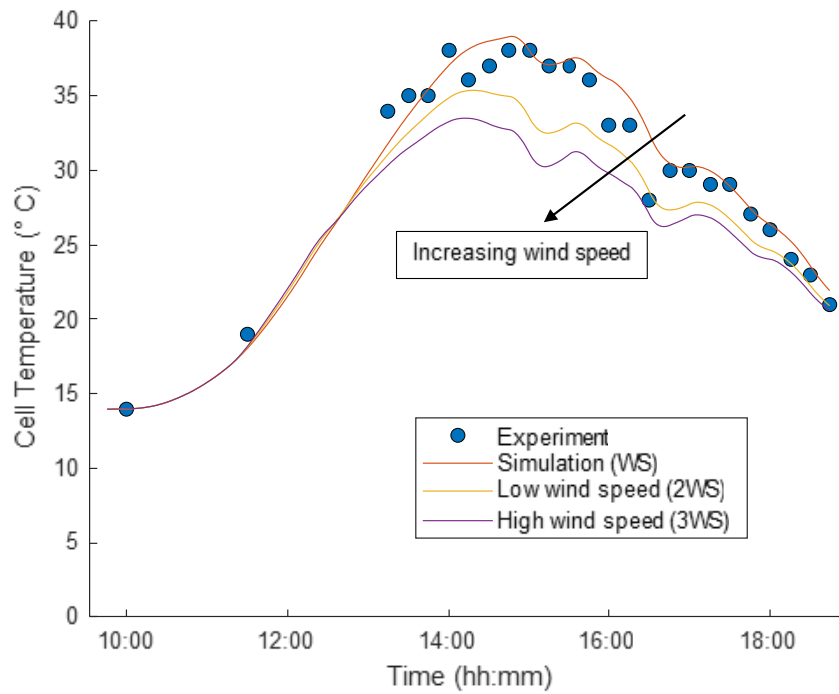
7.1 Use of Measured Data to Simulate Cooling Effects

Figures 7.1 and 7.2 show the results of the effect of cooling by varying wind speeds. The inputs for the simulation are the measured ambient temperature and plane of array irradiance collected on 5 October and 6 October 2020 as shown in Figure 6.4.

The results from Figure 7.1, as well as the solar irradiance recorded on 5th and 6th October 2020 are used to investigate the DC power time-monitoring output and the effects of cooling the PV array on its performance, these results are presented in Figure 7.2. As seen in Figure 7.2, adjusting the wind speed has minimal effects on the power output before 13:00 PM. This is due to the module temperature only changing from 30°C to 27°C as shown in Figure 7.1. The highest temperature difference between low wind speed and high wind speed was obtained at 14:30 PM. This is reflected on the power output results as shown in Figure 7.2.a.

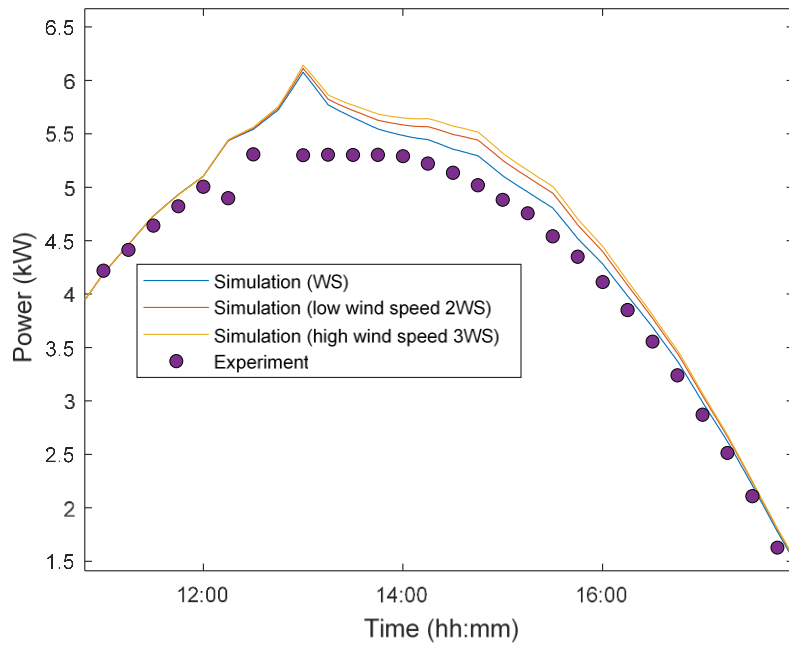


(a)

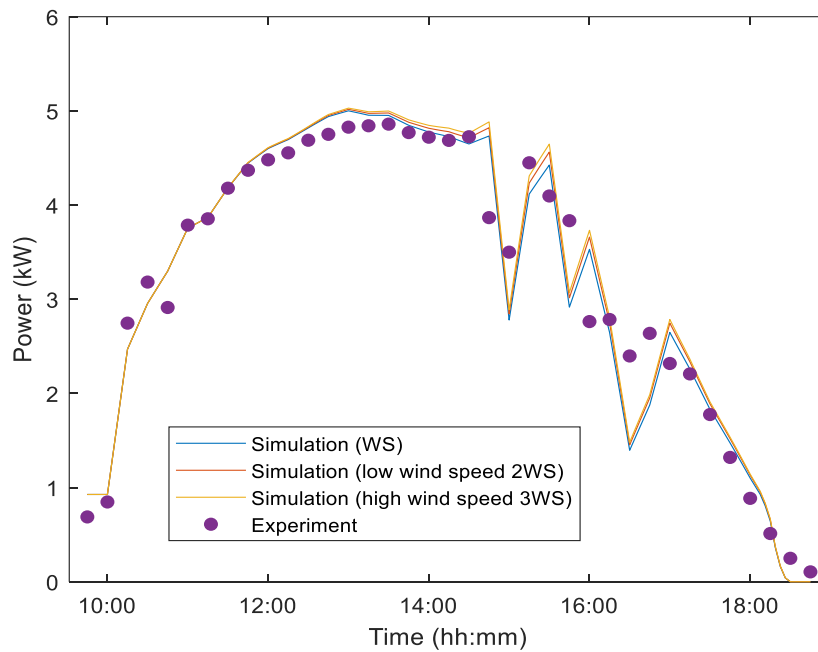


(b)

Figure 7.1: Effect of varying wind speed on cell temperature. Input data from (a) 5 Oct. 2020 and (b) 6 Oct. 2020.



(a)



(b)

Figure 7.2: Effects of varying wind speed on the power output. Input data from (a) 5 Oct. 2020 and (b) 6 Oct. 2020.

Figure 7.2.b shows the effects of cooling on the DC power output of the array for 6 October 2020. The effect of cooling was even less significant on Oct. 6 as it was cloudier than 5 October 2020.

7.2 Using TMY3 Data to Simulate Cooling Effects

In this section the simulation will run on a hot day, June 17th using data input from NSDRB, TMY3. Cooling effects will thus be investigated. Figure 7.3 shows real time monitored experimental data for the power output of the array.

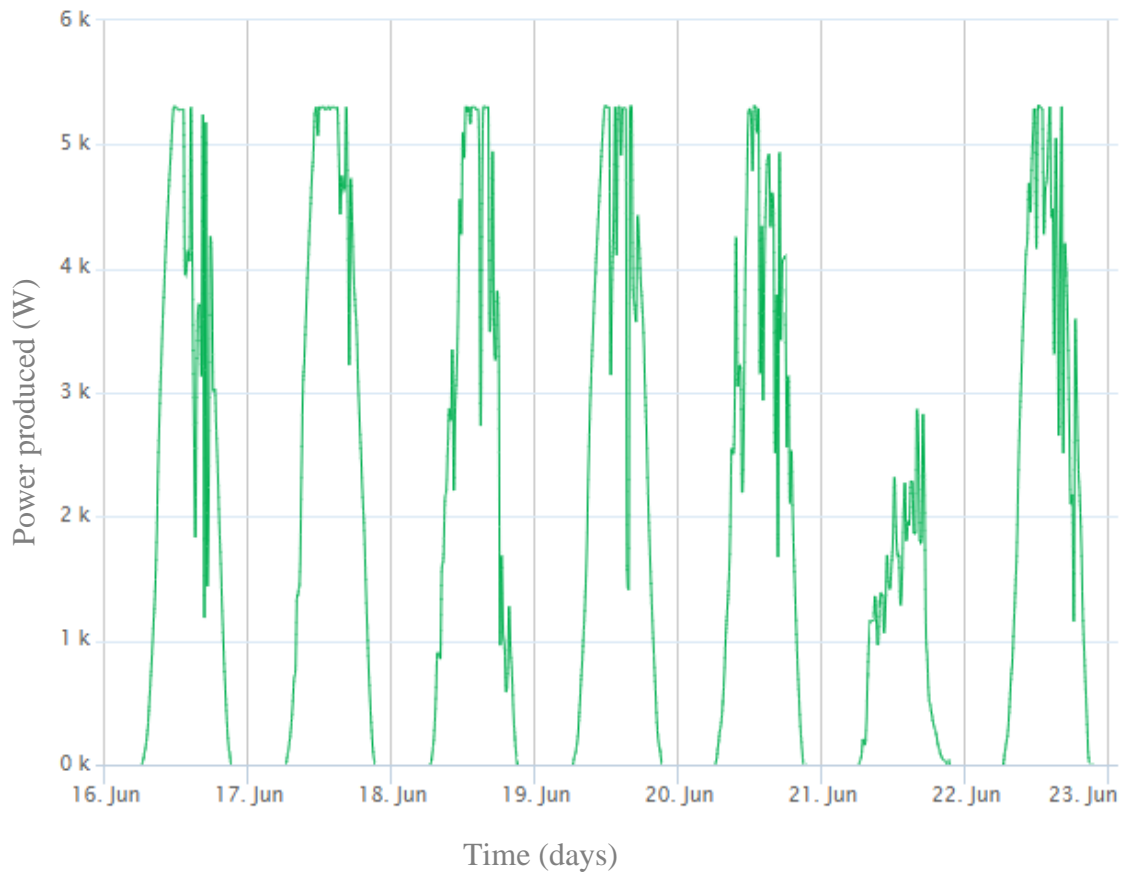


Figure 7.3: Experimental data measured for the array from 16 Jun. 2020- 23 Jun. 2020.

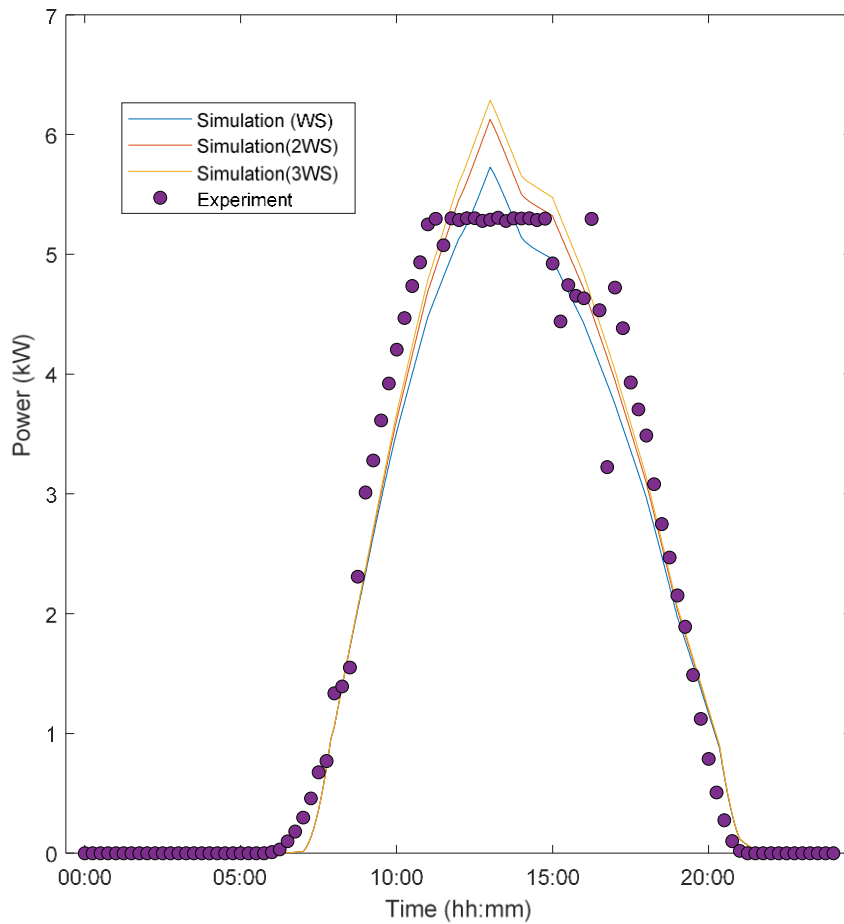


Figure 7.4: Cooling effects on DC power output. Input and recorded data from 17 June TMY3.

Figure 7.4 shows the simulated power using TMY3 conditions for a hot day, June 17th, and the effects of varying the wind speed on the predicted power, compared to the actual measured power from the array of June 17th. The results show that, as expected, the effects of cooling are most significant during periods of high irradiance and thus higher cell temperatures.

7.3 Effect of Increasing Wind Speed during Peak Hours

The previous section investigates the effect of doubling and tripling the wind speed on the cell temperature and the power output of the PV array. As shown in Figures 7.1 through 7.4, the most useful time of the day to implement is during peak irradiance hours, mainly from 11:00 AM till 15:00 PM. It is not economically feasible to cool the panels 24 hours/day 7days/week. Depending

on the geographical location and peak hours, it is vital to consider cooling effects in summer months and peak irradiance hours only.

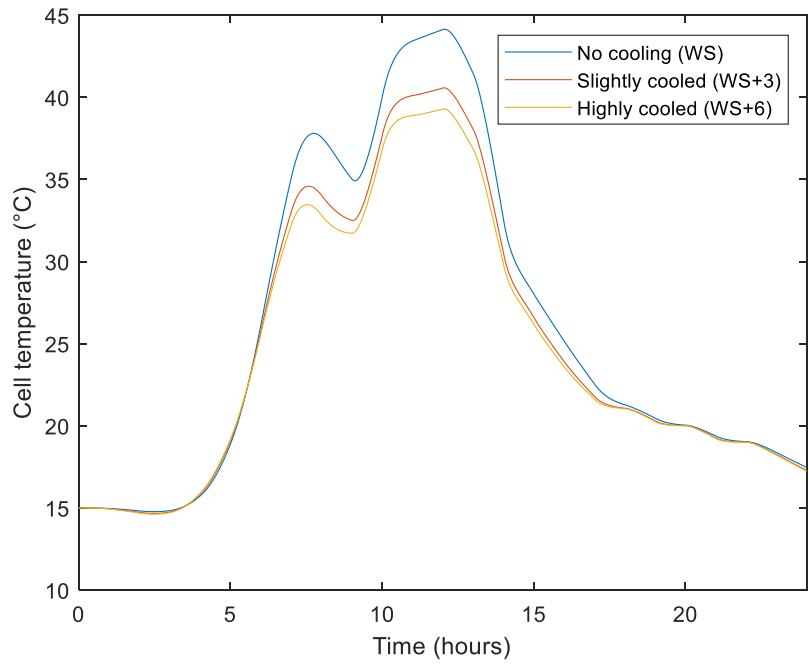
An operation strategy can be developed by studying the typical peak hours in a geographical location and developing a control sequence of operation such that the fan operates during peak ambient temperatures. The speed of the fan can be modulate based on the outside air temperature and be adjusted to provide cooling as required to maintain the temperature of the cell at 25°C. In this study, it is observed that in Fort Wayne, IN – the summer peak hours were 6 hours.

To simulate the effects of cooling, the wind speed is adjusted according as follows:

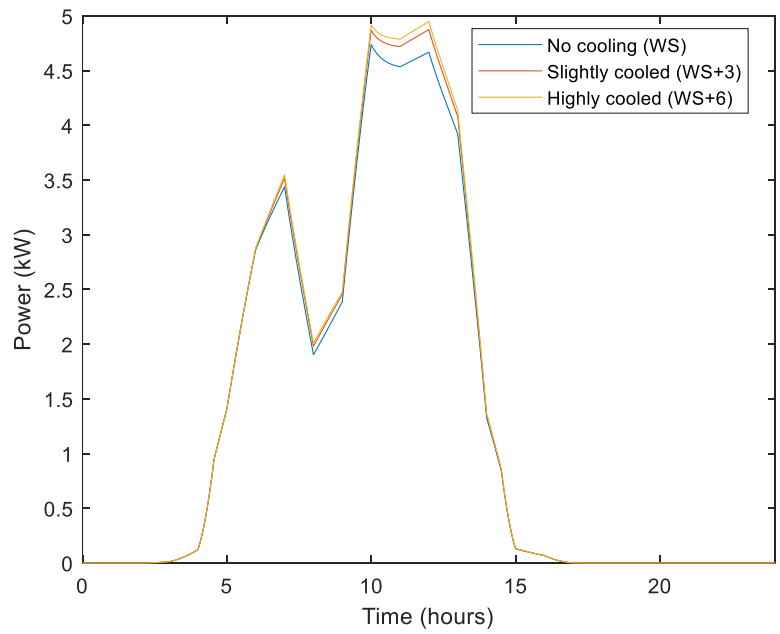
$$\begin{aligned} \text{No cooling} &= WS & 7.1 \\ \text{Slightly cooled} &= WS + 3 & 7.2 \\ \text{Highly cooled} &= WS + 6 & 7.3 \end{aligned}$$

Assuming that the speed of the fan is 3 mph at a low rpm, and 6 mph at a high rpm and adding those constant speeds to the value of the predicted wind speed from the ambient conditions. Wind speed is not the only ambient condition that effects the cell temperature of the photovoltaic. Humidity, shading effects, wind direction and ambient temperatures etc. have effects on the heat transfer coefficient. Accounting for all these variable and unknown factors, however, is too complex and the purpose of this study is to simulate effects of cooling on the overall power output while assuming a clear sunny day.

Figure 7.5 shows the effect of cooling on the cell temperature and the power output. As shown in Figure 7.5.a, slightly cooling the PV reduced the cell temperature from around 45°C to around 37°C at 13:00 PM. While highly cooling the PV reduced the cell temperature to approximately 35°C at the same time. Similarly, as shown in Figure 7.5.b, slightly cooling the PV increased the power output to from around 4.5 kW to around 5 kW at 13:00 PM. While highly cooling the PV increased the power output to approximately 5.2 kW at the same time. Slightly cooling the PV panel shows a higher relative increase in power compared to highly cooling the PV panel.



(a)



(b)

Figure 7.5: Effects of varying wind speed during peak hours on (a) cell temperature and (b) power output. Input data from 5 June TMY3.

7.4 Effect of Geographical Location

NSDRB data are utilized and input data such as the plane of array irradiance, wind speed, and ambient temperature of two different locations are modified to analyze the significance of cooling in a warm region and a cold region as shown in Figure 7.6. In this study, two geographical locations are studied. The first is simulating energy productions in Fort Wayne, IN, and comparing the annual energy to a warmer region in San Diego, California.

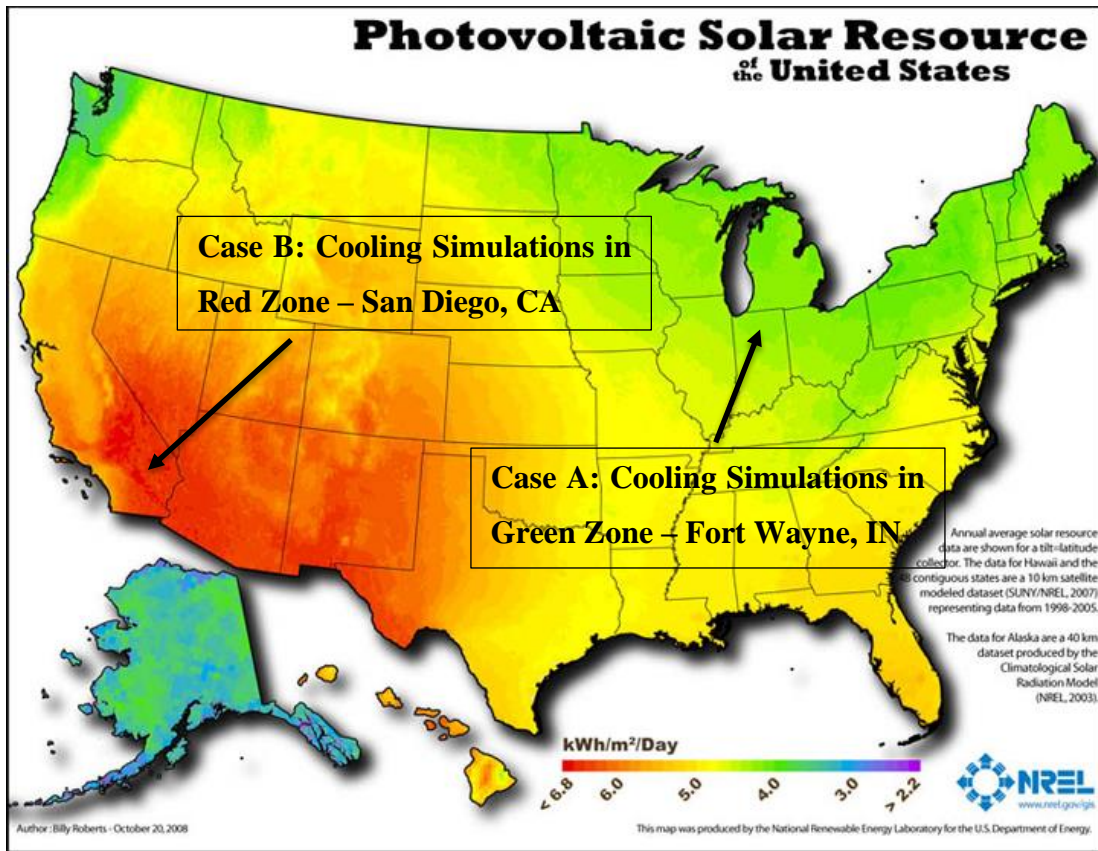


Figure 7.6: Photovoltaic solar resource of the United States [28]

7.4.1 Effect of Wind Speed on Annual Energy Production and Costs – Fort Wayne, IN

The proposed model in Chapter 3 and 4 is simulated for the year at Kettler Hall Purdue Fort Wayne campus, IN, with same inputs as outlined previously (refer to appendix B for detailed yearly inputs). There are 525,600 minutes in a leap year, the hourly weather conditions presented 8784 data points which were interpolated to 525,600 to get a time step of one minute.

Figure 7.7 shows the effect of cooling on the power output energy production by increasing the wind speed. To further analyze the energy costs and harvesting of energy by cooling, Figure 7.8 shows the IEP, “increase in energy production” throughout the year. The increase in energy production is defined in Equation 7.4 and 7.5.

$$IEP_{\text{Increase to Low WS}} = \frac{1}{60} \left(\int P_{2WS} dt - \int P_{WS} dt \right) \quad 7.4$$

$$IEP_{\text{Increase to High WS}} = \frac{1}{60} \left(\int P_{3WS} dt - \int P_{WS} dt \right) \quad 7.5$$

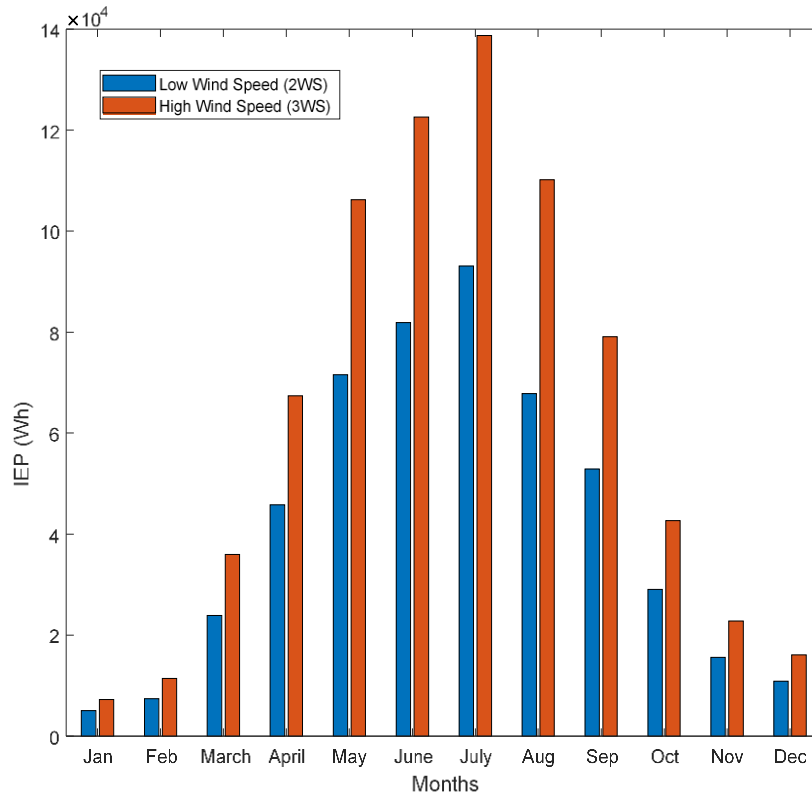


Figure 7.7: Simulation of increase in energy production due to increasing wind speed for a 7.6 kWp roof mounted PV array in Fort Wayne, IN. Input data TMY3.

The average industrial electricity rate in Fort Wayne, IN where the data was collected is 5.43¢/kWh. This average (industrial) electricity rate in Fort Wayne is 14.35% less than the Indiana average

rate of 6.34¢/kWh. The average (industrial) electricity rate in Fort Wayne is 18.59% less than the national average rate of 6.67¢/kWh [29]. Figure 7.8 shows the cost of savings for the increase in energy production due to panel cooling compared to the of the existing system.

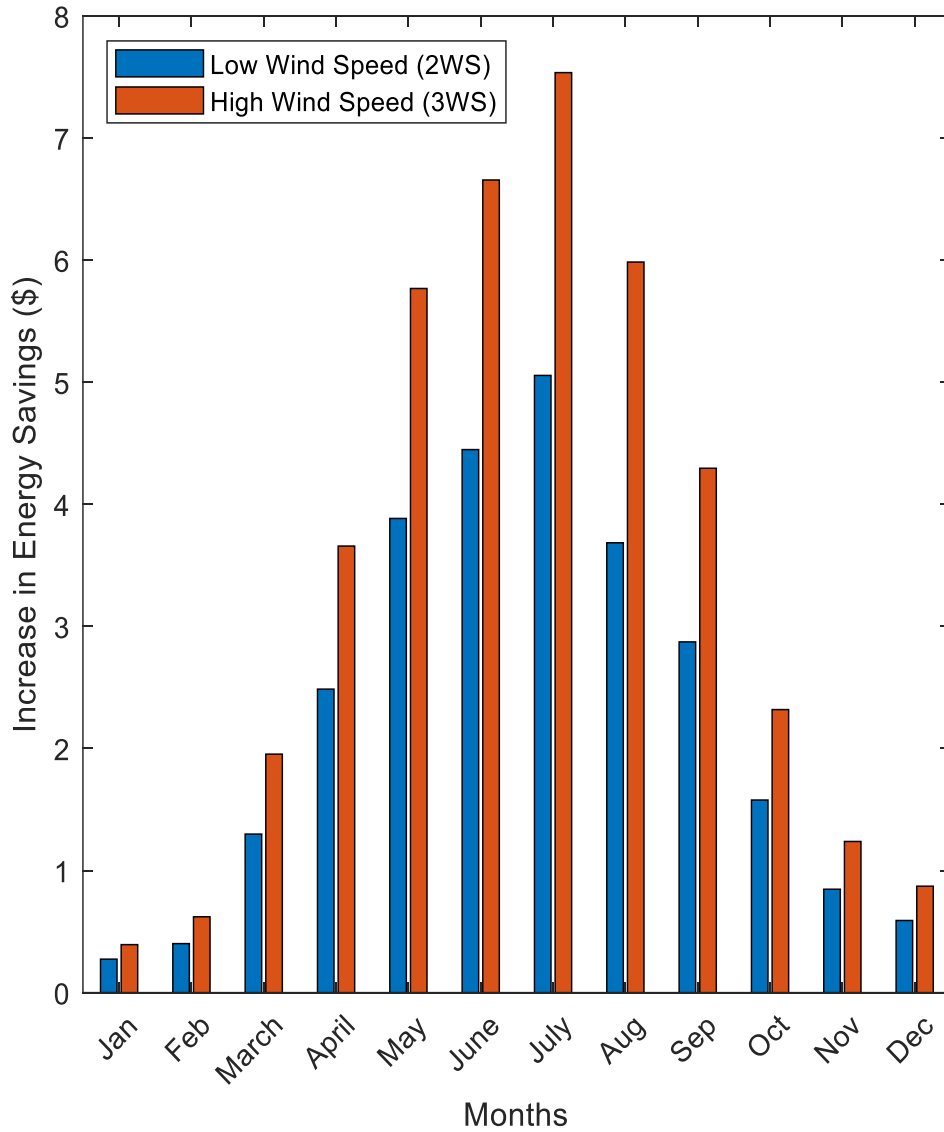


Figure 7.8: Savings from cooling the photovoltaic array for a 7.6 kWp roof mounted PV array in Fort Wayne, IN. Input data TMY3.

7.4.2 Effect of Wind Speed on Annual Energy Production and Costs – San Diego, CA

The 7.6 kW peak solar array is now modeled in San Diego, California. Figure 7.9 shows the predicted energy production from the PV panel array along with the predicted energy production with two levels of panel cooling. The effects of cooling are greatest during the summer months, as expected. In general, lower-level cooling, indicated by a lower adjusted wind speed provides relatively more of a benefit.

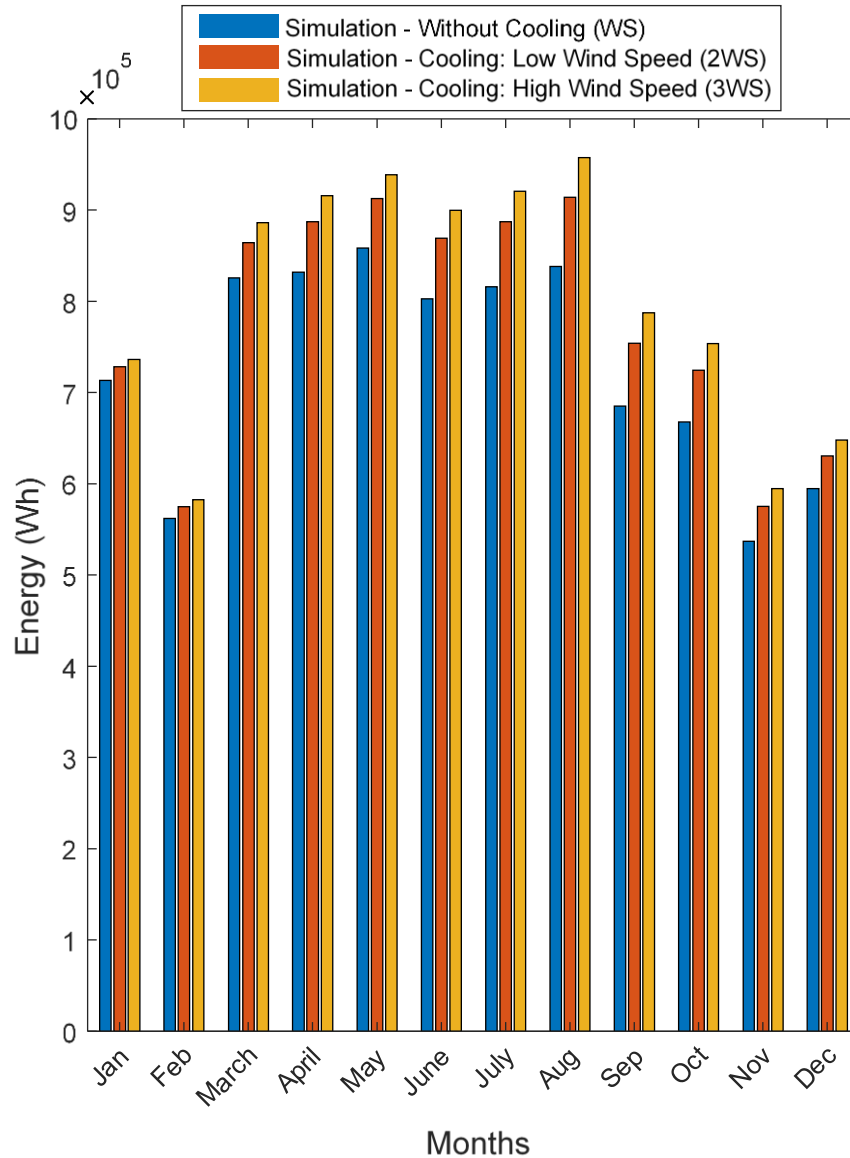


Figure 7.9: Annual energy simulation results by varying wind speed in San Diego, California. Input hourly data from TMY3.

Increase in energy calculations are calculated using Equations 7.4 and 7.5 and the results are shown in Figure 7.10.

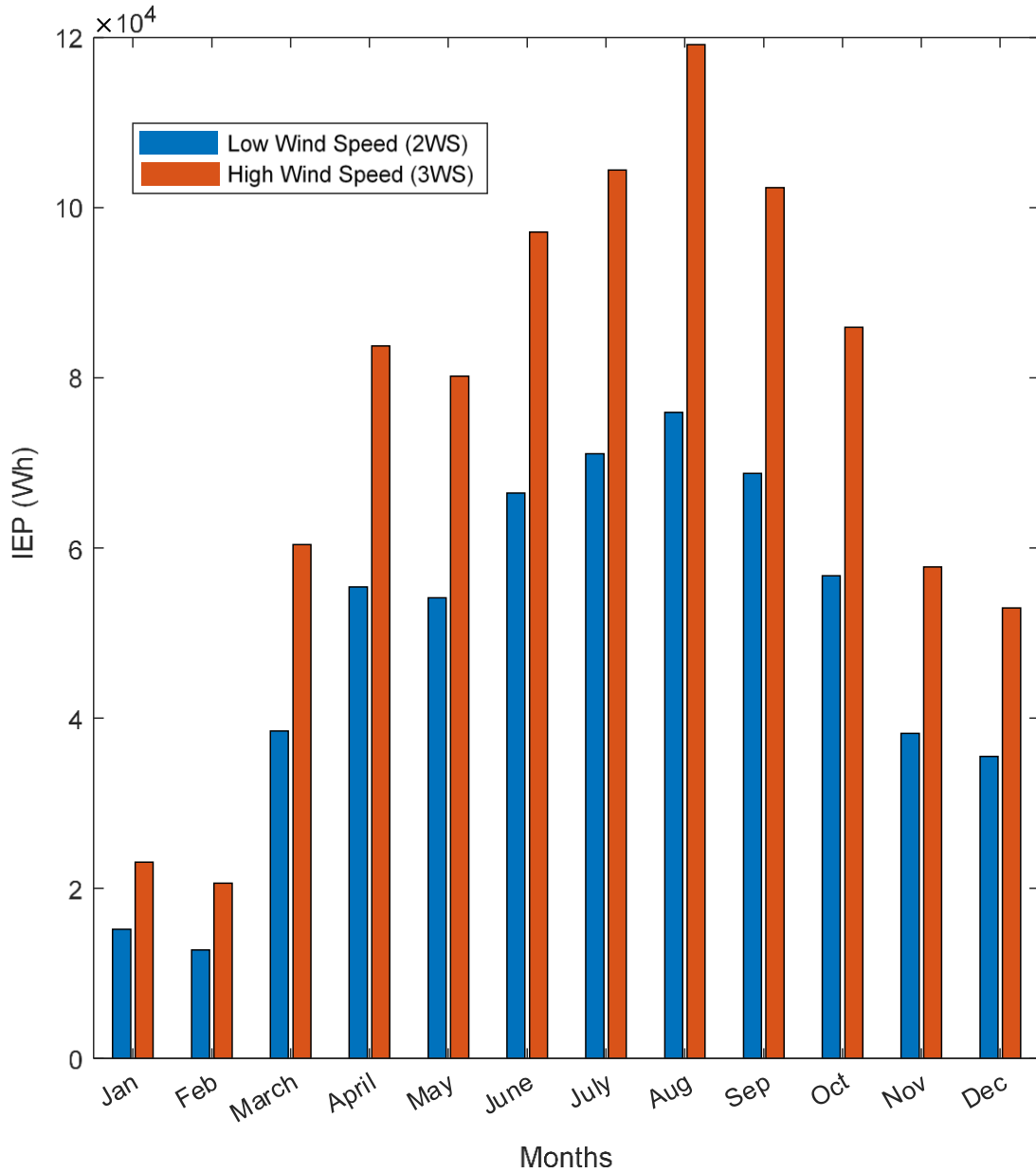


Figure 7.10: Simulation of increase in energy production due to increasing wind speed, based on a 7.6 kWp roof mounted PV array in San Diego, CA. Input data TMY3.

The average residential electricity rate in San Diego is 16.35¢/kWh. This average (residential) electricity rate in San Diego is 6.58% greater than the California average rate of 15.34¢/kWh [30]. Figure 7.11 shows the savings for the increase in energy production of the existing set-up, if located in San Diego, California.

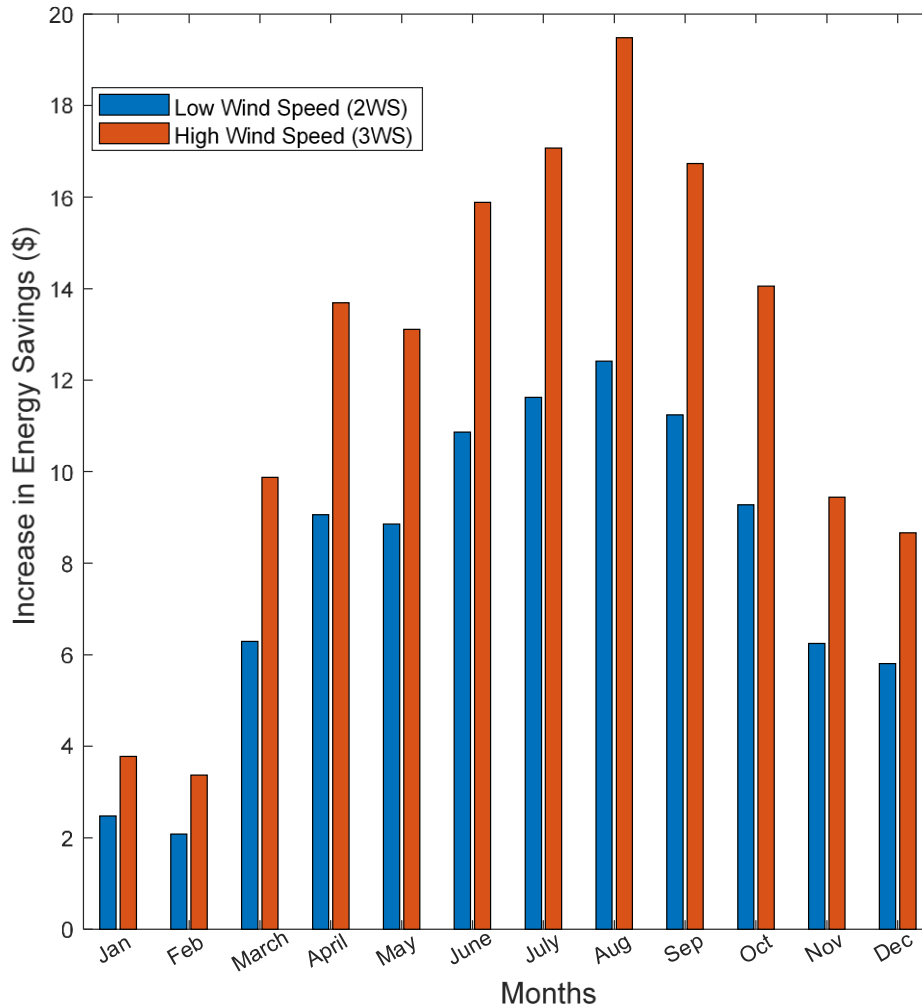


Figure 7.11: Savings from cooling the photovoltaic array, based on a 7.6 kWp roof mounted PV array in San Diego, CA. Input data TMY3.

7.5 Return on Investment for Cooling Solar Arrays

To justify the investment of cooling a PV array, the following must be considered:

- 1- kWh cost of electricity in the geographic location.
- 2- The area of the solar array.
- 3- The ambient conditions of the geographic location (relative humidity, ambient temperature, and wind speed).
- 4- Accessibility of cooling methods such as water and heat sinks.
- 5- Political and economic support in that location.
- 6- Initial cost of cooling and annual recurring costs of cooling.

The IEP of San Diego was larger than that of Fort Wayne. Both locations showed a larger relative increase in energy of 2xWS to WS compared to 3xWS to WS. This indicates that any efforts to further enhance cooling methods will not justify the costs of further cooling.

Table 7.1 summarizes the IEP for the two geographic locations as well as the cost savings. Note that the costs of electricity are approximately three times higher in San Diego, CA compared to Fort Wayne, IN.

Table 7.1: Summary of annual energy savings due to cooling.

Location	Annual IEP due to 2WS	Annual IEP due to 3WS	Annual Savings due to 2WS	Annual Savings due to 3WS
Fort Wayne, IN	381.5 kW-h	575.5 kW-h	\$20.72	\$31.20
San Diego, CA	588.6 kW-h	887.8 kW-h	\$96.24	\$145.16

As shown in Table 7.1, the increase in energy production and cost savings is higher in San Diego, CA compared to Fort Wayne, IN. The increase in energy produced in San Diego is approximately twice of that of Fort Wayne. Cooling photovoltaics in green zones as shown in Figure 7.6 such as in Fort Wayne, IN is not as profitable. At an annual savings of \$20 and a life expectancy of 20 years. The only feasible cooling mechanism should cost around \$400 to breakeven. It is unlikely

that the initial investment of cooling would be justified in green zones as shown in United States map. If we consider the case of San Diego, CA – there is more irradiation, which means higher power, but also higher temperatures resulting in lower efficiency. The effects of cooling are much more significant. At a savings annual rate of around \$100 annually per 7.6 kWp array, and at a life expectancy of 20 years, the savings of cooling could reach around \$2000 per 7.6 kW.

It is profitable and energy efficient to cool photovoltaics in red zones shown in Figure 7.6. Tripling the wind speed at 20 years would save around \$3000 per 7.6 kWp. If the design of further cooling is costlier than the cost of annual savings, cooling PV is not be feasible. Overall, cooling PV arrays in red zones may be justified on a residential as well as industrial scale.

The results presented in Figure 7.6 shows the effects of cooling and varying wind speed on the power output to be significant during peak noon hours. This is due to the higher temperature levels of the cells of the array during noon hours. Thus, it is vital to cool the Photovoltaic during peak hours only – to minimize the cooling costs. Depending on the cooling technique, whether it is an active cooling method, or passive, optimizing the power output may be done to ensure the cooling is efficient and cost effective. An example would be modulating the flow rate of the refrigerant passing at the back of the module or modulating the speed of the fan to increase wind speed and enhance the module's energy production.

8. CONCLUSIONS

A computer tool is developed to predict the cell temperature and power produced by a photovoltaic panel. The model is flexible and robust—it can handle a variety of PV array configurations and input data (solar irradiance, ambient temperature, and wind speed) from national databases or measurements.

Five different thermal models to predict the cell temperature are compared. A thermal capacitance model is used in this study. I-V & P-V characteristics are generated by varying the load (parallel and shunt resistances). Both the thermal model and electrical model are verified and validated. Verification is performed by relating changes in input data to changes in the output data and by comparing to other methods. Validation is performed by comparing the simulation results to measured data obtained from a photovoltaic array on Kettler Hall at the Purdue University Fort Wayne campus.

Results from the simulation show that under typical conditions, the PV panel efficiency decreases 0.5% for every 1°C above the nominal temperature 25°C. Thus, reduction of the cell temperature will increase the efficiency of the panel.

A cooling strategy based on adjusting the wind speed is investigated in chapter 7. Simulations are performed using both measured input data and data from national databases. Numerous cooling techniques are discussed in chapter 1 that can reduce photovoltaic module temperature and thus improve efficiency. However, the manufacturing cost of some PV cooling techniques may be higher as compared with their potential power increase, and thus a detailed cost analysis is needed to justify producing certain PV cooling techniques.

To simulate the effects of cooling, the wind speed is adjusted to increase the value of the heat transfer coefficient. Results show a decrease in cell temperature and an increase in output power with increase in wind speed. The simulations conducted in a hot region where the ambient temperatures are higher show a greater increase in power compared to a cooler region. The savings

from cooling photovoltaics may be justified in warmer locations (red and yellow zones) compared to colder regions (green zones).

8.1 Recommendations

- The correlations used to estimate the heat transfer coefficient do not take into effect complex, natural variation in wind speed and direction. Alternative expressions for the heat transfer coefficient should be investigated.
- To obtain irradiance measurements, the Solar Survey 100 was mounted on one module, the passage of partial clouds across some modules resulted in the variances of the power. It is recommended to install several irradiance meters across the array and take an average of the plane of array irradiance readings.
- The wind speed is an approximation; it is recommended to install a calibrated anemometer to measure the wind speed.
- It is recommended to validate the effects of cooling in a hot region with measurements.
- Further evaluations of cost analysis of cooling methods are suggested to investigate the return on investments.
- Where cooling is feasible, harvesting the heat and utilizing it to heat water such as in PV/T (Photovoltaic-Thermal) systems is worth evaluating in different zones across the country.

APPENDIX A. MANUFACTURER'S DATA SHEETS

72M

DIMENSIONS FOR HELIENE 72M SERIES MODULES

I-V CURVE FOR HELIENE 72M SERIES

CERTIFICATIONS

ELECTRICAL DATA (STC)

Parameter	Unit	385	380	375	370	365
Peak Rated Power	P_{mppt} (W)	385	380	375	370	365
Maximum Power Voltage	V_{mppt} (V)	41.76	41.20	40.67	40.23	39.90
Maximum Power Current	I_{mppt} (A)	9.24	9.23	9.22	9.21	9.20
Open Circuit Voltage	V_{oc} (V)	49.70	49.55	48.96	48.66	48.50
Short Circuit Current	I_{sc} (A)	10.06	9.98	9.90	9.77	9.75
Module Efficiency *	Eff (%)	20.01	19.65	19.34	19.09	18.82
Maximum Series Fuse Rating	MF (A)	20	20	20	20	20
Power Output Tolerance		[- 0, + 4.99] Wp				

STC - Standard Test Conditions: Irradiation 1000 W/m² - Air mass AM 1.5 - Cell temperature 25 °C
* Calculated using maximum power based on full positive output tolerance [-0, +4.99] Wp

MECHANICAL DATA

Dimensions (L x W x D)	1956 x 992 x 40 mm (77 x 39 x 1.6 inch)
Weight	22 kg (48.5 lbs)
Output Cables	1.2 m (47.2 inch) symmetrical cables with MC4 type connectors
Junction Box	IP-67 rated with 3 bypass diodes
Frame	Double webbed 15 micron anodized aluminum alloy
Front Glass	Low-iron content, high-transmission PV solar glass
Solar Cells	72 Monocrystalline cells (156.75 x 156.75 mm)

CERTIFICATIONS

UL Certification	ULC/ORD-C1703-1, UL1703 UL61215 & UL61730
IEC Certification	Optional

Helene modules are certified under the California Energy Commission (CEC) Listing Report.

TEMPERATURE RATINGS

Nominal Operating Cell Temperature (NOCT)	+45°C (±2°C)
Temperature Coefficient of P_{max}	-0.39%/°C
Temperature Coefficient of V_{oc}	-0.31%/°C
Temperature Coefficient of I_{sc}	0.06%/°C

PACKAGING CONFIGURATION

Modules per box:	26 pieces
Modules per 53' trailer:	780 pieces

MAXIMUM RATINGS

Operational Temperature	-40°C - +85°C
Max System Voltage	1000V (*1500V) *Optional

WARRANTY

10 Year Manufacturer's Workmanship Warranty
25 Year Linear Power Guarantee

(Refer to product warranty page for details)



CAUTION: READ SAFETY AND INSTALLATION INSTRUCTIONS BEFORE USING THE PRODUCT.

Figure A.1: Manufacturer's data specification sheet for a single monocrystalline photovoltaic module used at Kettler Hall at Purdue University Fort Wayne campus.

/ Power Optimizer

Frame-Mounted

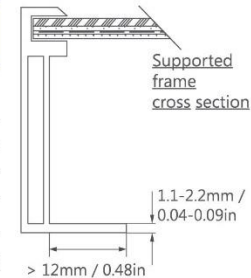
P370 / P401 / P404 / P500

OPTIMIZER MODEL (TYPICAL MODULE COMPATIBILITY)	P370 (FOR HIGH-POWER 60-CELL AND FOR 72-CELL MODULES)	P401 (FOR HIGH POWER 60/72-CELL MODULES)	P404 (FOR 60-CELL AND 72-CELL, SHORT STRINGS)	P500 (FOR 96-CELL MODULES)	
INPUT					
Rated Input DC Power ⁽¹⁾	370	100	405	500	W
Absolute Maximum Input Voltage (Voc at lowest temperature)	60		80		Vdc
MPPT Operating Range	8 - 60		12.5 - 80	8 - 80	Vdc
Maximum Short Circuit Current (Isc)	11	11.75	11	10.1	Adc
Maximum Efficiency	99.5				%
Weighted Efficiency	98.8				%
Oversoltage Category	II				
OUTPUT DURING OPERATION (POWER OPTIMIZER CONNECTED TO OPERATING SOLAREEDGE INVERTER)					
Maximum Output Current	15				Adc
Maximum Output Voltage	60		85	60	Vdc
OUTPUT DURING STANDBY (POWER OPTIMIZER DISCONNECTED FROM SOLAREEDGE INVERTER OR SOLAREEDGE INVERTER OFF)					
Safety Output Voltage per Power Optimizer	1 ± 0.1				Vdc
STANDARD COMPLIANCE					
EMC	FCC Part15 Class B, IEC61000-6-2, IEC61000-6-3				
Safety	IEC62109-1 (class II safety), UL1741				
RoHS	Yes				
Fire Safety	VDE-AR-E 2100-712:2013-05				
INSTALLATION SPECIFICATIONS					
Maximum Allowed System Voltage	1000				Vdc
Dimensions (W x L x H)	139 x 165 x 40 / 5.5 x 6.5 x 1.6	129 x 153 x 29.5 / 5.08 x 6.02 x 1.16	139 x 165 x 48 / 5.5 x 6.5 x 1.9		mm / in
Weight (including cables)	775 / 1.7	655 / 1.5	895 / 2.0	870 / 1.9	gr / lb
Input Connector	MC4 ⁽²⁾				
Input Wire Length	0.16 / 0.52				m / ft
Output Connector	MC4				
Output Wire Length	1.2 / 3.9				m / ft
Operating Temperature Range ⁽³⁾	-40 to +85 / -40 to +185				°C / °F
Protection Rating	IP68 / NEMA6P				
Relative Humidity	0 - 100				%

- (1) Rated power of the module at STC will not exceed the optimizer "Rated Input DC Power". Modules with up to +5% Power tolerance are allowed
(2) For other connector types please contact SolarEdge
(3) For ambient temperature above +85°C / +185°F power de-rating is applied. Refer to Power Optimizers Temperature De-Rating Technical Note for more details

PV SYSTEM DESIGN USING A SOLAREEDGE INVERTER ⁽⁴⁾		SINGLE PHASE HD-WAVE	SINGLE PHASE	THREE PHASE	THREE PHASE FOR 277/480V GRID	
Minimum String Length (Power Optimizers)	P370/ P401/ P500 ⁽⁵⁾	8		16	18	
	P404	6		14 (13 with SE3K) ⁽⁶⁾	14	
Maximum String Length (Power Optimizers)		25		50	50	
Maximum Nominal Power per String		5700 ⁽⁷⁾	5250 ⁽⁷⁾	11250 ⁽⁸⁾	12750	W
Parallel Strings of Different Lengths or Orientations		Yes				

- (4) It is not allowed to mix P404 with P370/P401/P500 in one string
(5) The P370/P401/P500 cannot be used with the SE3K three phase inverter (available in some countries; refer to Three Phase Inverter SE3K-SE10K datasheet)
(6) Exactly 10 when using SE3K-RW0108NN4
(7) If the inverters rated AC power ≤ maximum nominal power per string, then the maximum power per string will be able to reach up to the inverters maximum input DC power Refer to: <https://www.solareedge.com/sites/default/files/se-power-optimizer-single-string-design-application-note.pdf>
(8) For SE27.6K, SE55K, SE82.8K: It is allowed to install up to 13,500W per string when 3 strings are connected to the inverter and when the maximum power difference between the strings is up to 2,000W; inverter max DC power: 37,250W

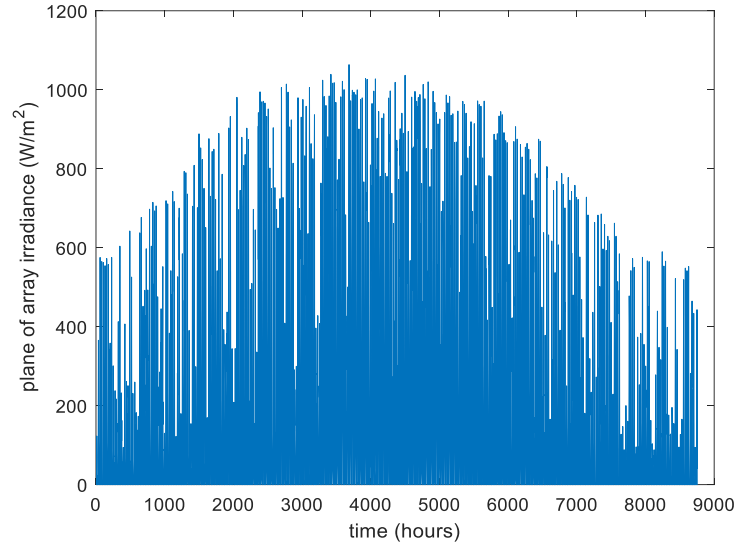


© SolarEdge Technologies, Inc. All rights reserved. SOLAREEDGE, the SolarEdge logo, OPTIMIZED BY SOLAREEDGE are trademarks or registered trademarks of SolarEdge Technologies, Inc. All other trademarks mentioned herein are trademarks of their respective owners. Date: 12/2020/V01/ENG ROW. Subject to change without notice.

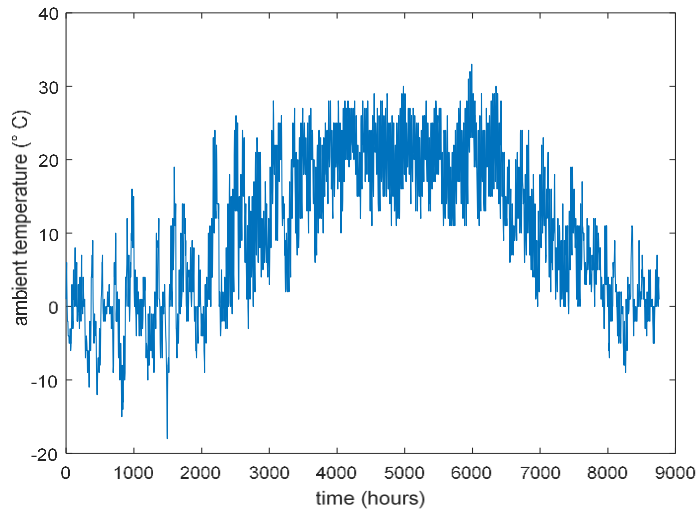
CE

Figure A.2: P370 power optimizer mounted at the back of each PV module, used to track, and record maximum power point.

APPENDIX B. ANNUAL HOURLY DATA

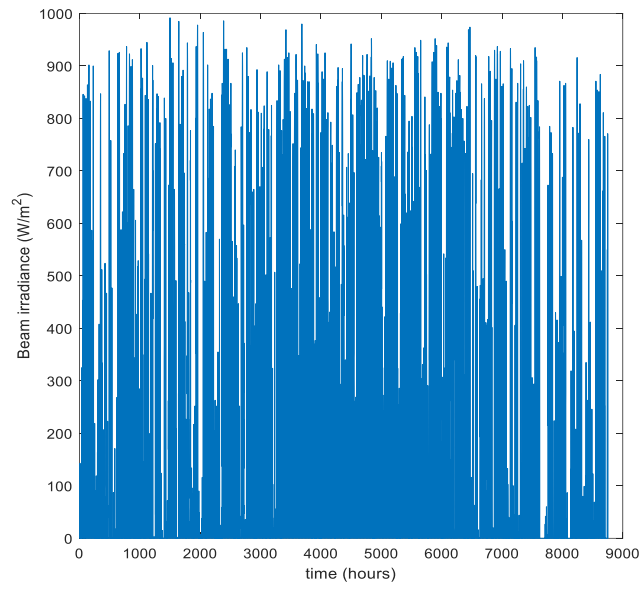


(a)

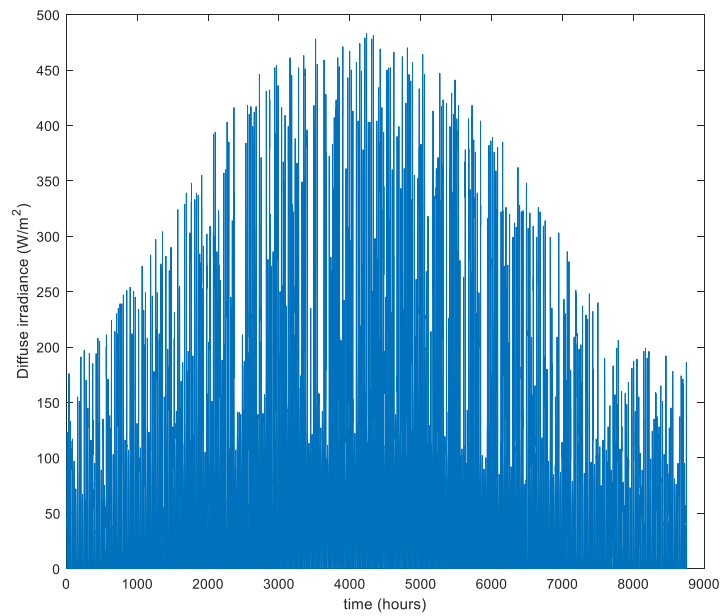


(b)

Figure B.1: Annual hourly model input data. Weather data set based on TMY3, NREL (prospector), Purdue University Fort Wayne campus. (a) irradiance (b) ambient temperature



(a)



(b)

Figure B.2: Annual hourly irradiance data. Weather data set based on TMY3, NREL (prospector), Purdue University Fort Wayne campus. (a) beam (b) diffuse

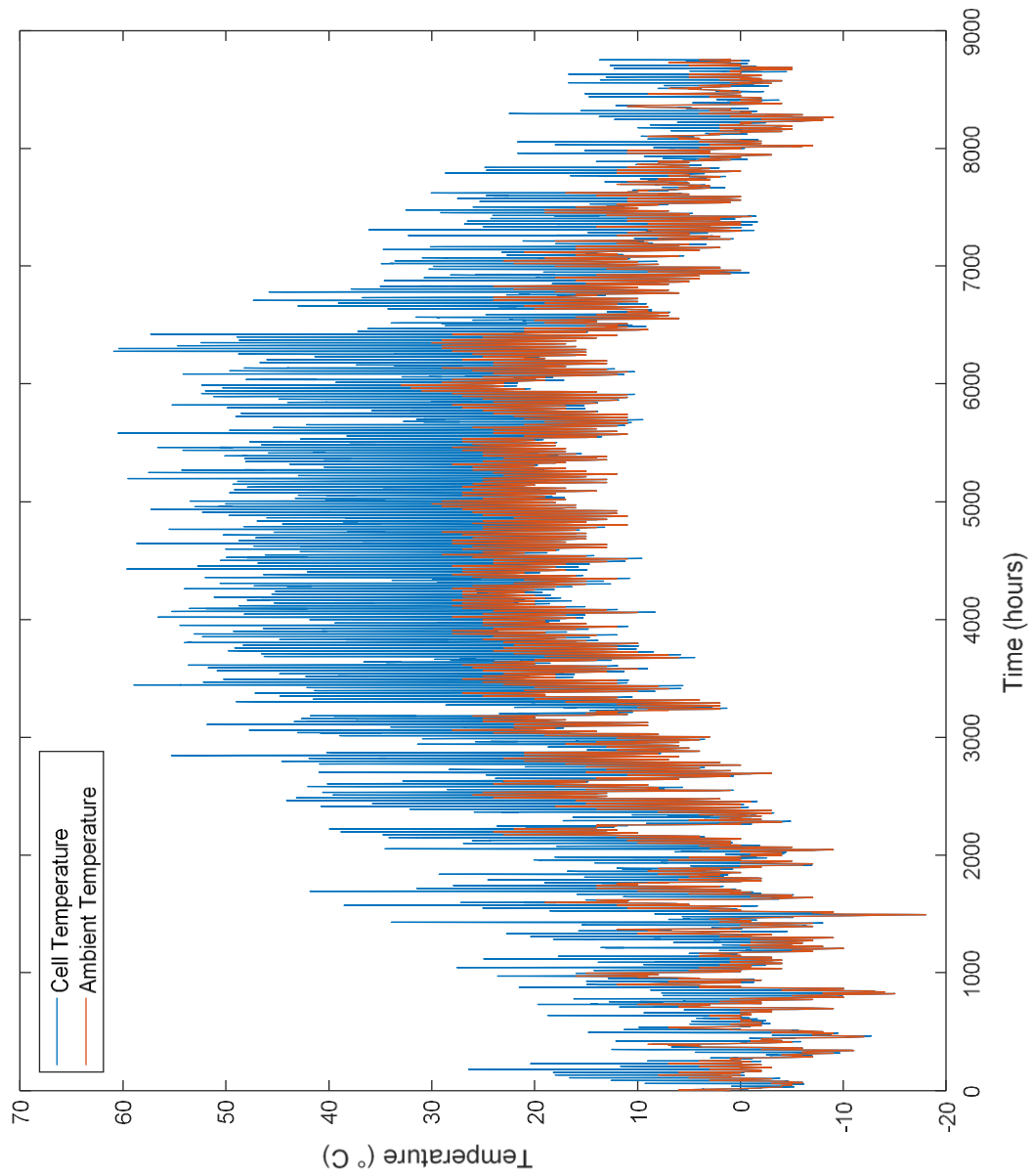


Figure B.3: Annual hourly model output (cell temperature) compared to input (ambient temperature). Input weather data set based on TMY3, NREL (prospector), Purdue University Fort Wayne campus.

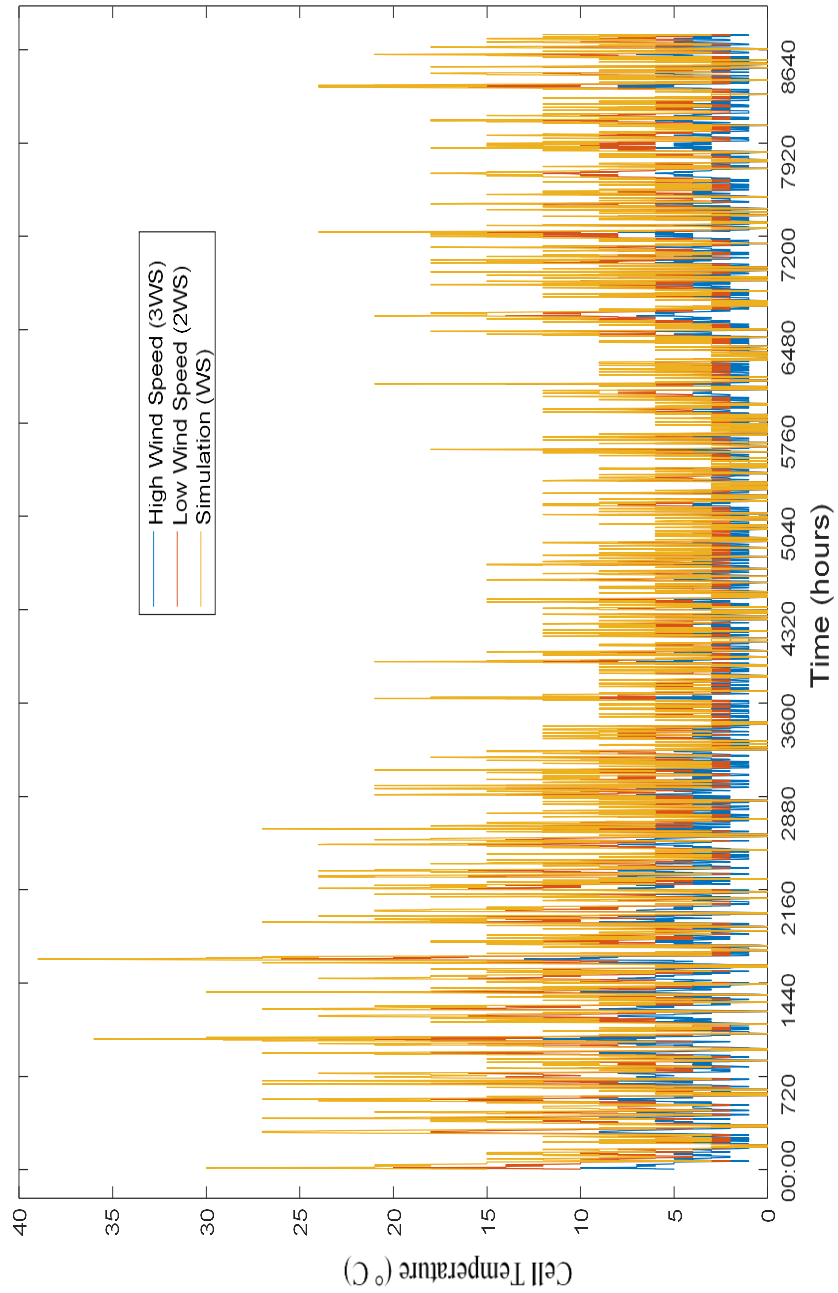


Figure B.4: Effect of varying wind speed on cell temperature. Input weather data set based on TMY3, NREL (prospector), Purdue University Fort Wayne campus.

APPENDIX C. PVWATTS CALCULATOR

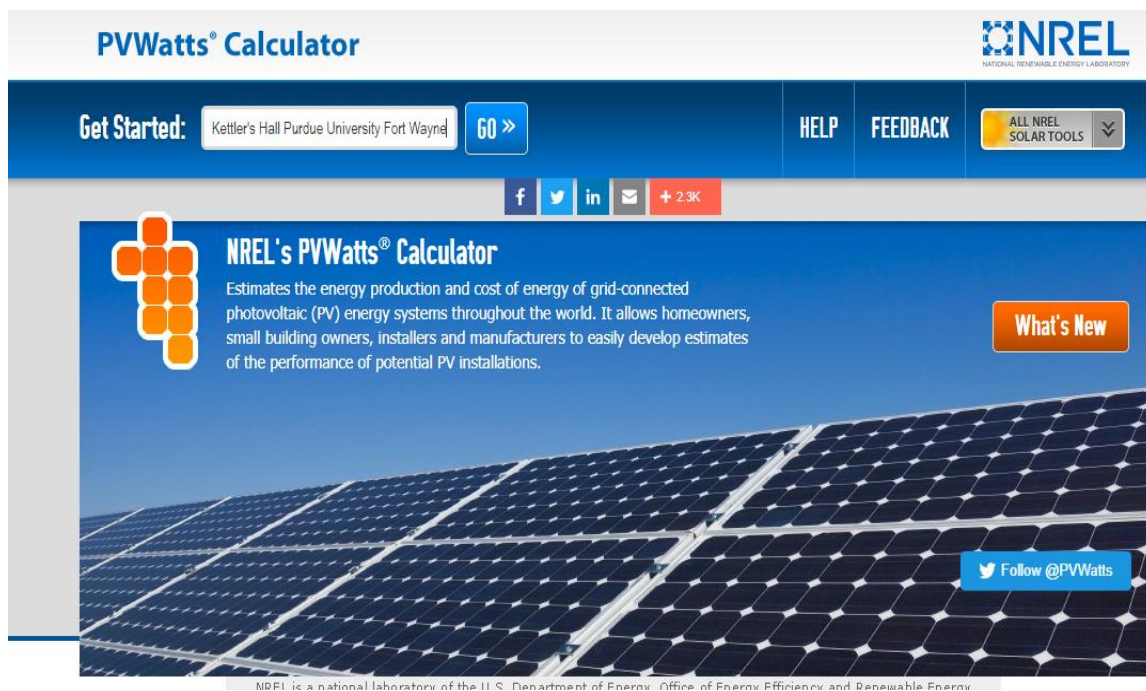


Figure C.1: PVWatts calculator, location input window.

My Location **Kettler's Hall Purdue University Fort Wayne** [» Change Location](#) **HELP** **FEEDBACK** **ALL NREL SOLAR TOOLS**

RESOURCE DATA SYSTEM INFO RESULTS

SOLAR RESOURCE DATA

The latitude and longitude of the solar resource data site is shown below, along with the distance between your location and the center of the site grid cell. Use this data unless you have a reason to change it.

Solar resource data site

Lat, Lon: 41.09, -85.14

1.2 mi

Go to system info

Resource Data Map

The blue rectangle on the map indicates the NREL NSRDB grid cell for your location. If your location is outside the NSRDB area, the map shows a pin for the nearest available NREL international data site instead of a rectangle. If you want to use data for a different NSRDB grid cell, double-click the map to move the rectangle. *Dragging the rectangle will not move it.* Use the Legacy Data Options check boxes to show pins for legacy data sites. Click a legacy data pin to use legacy data instead of the recommended NSRDB data. See [Help](#) for details.

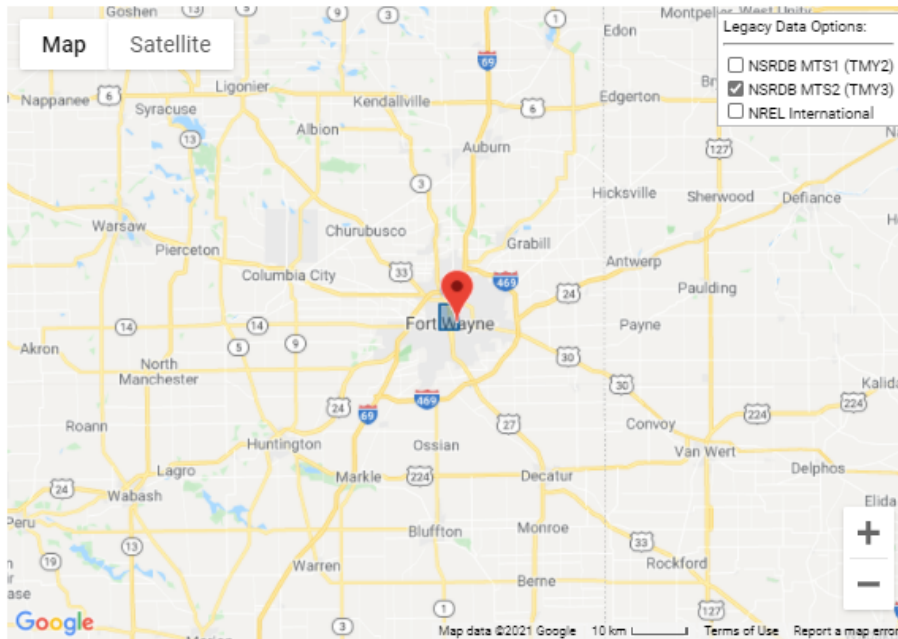


Figure C.2: PVWatts calculator, TMY3 legacy data selection, input window.

PVWatts[®] Calculator **NREL**
NATIONAL RENEWABLE ENERGY LABORATORY

My Location *Kellter's Hall Purdue University Fort Wayne* HELP FEEDBACK ALL NREL SOLAR TOOLS

RESOURCE DATA **SYSTEM INFO** RESULTS

Go to
resource
data

SYSTEM INFO

Modify the inputs below to run the simulation.

DC System Size (kW):

Module Type:

Array Type:

System Losses (%):

Tilt (deg):

Azimuth (deg):

+ Advanced Parameters

Draw Your System

Click below to customize your system on a map. (optional)



Go to
PVWatts[®]
results

RETAIL ELECTRICITY RATE

To automatically download an average annual retail electricity rate for your location, choose a rate type (residential or commercial). You can change the rate to use a different value by typing a different number.

Rate Type:

Rate (\$/kWh):

Figure C.2: PVWatts calculator, system parameters, input window.

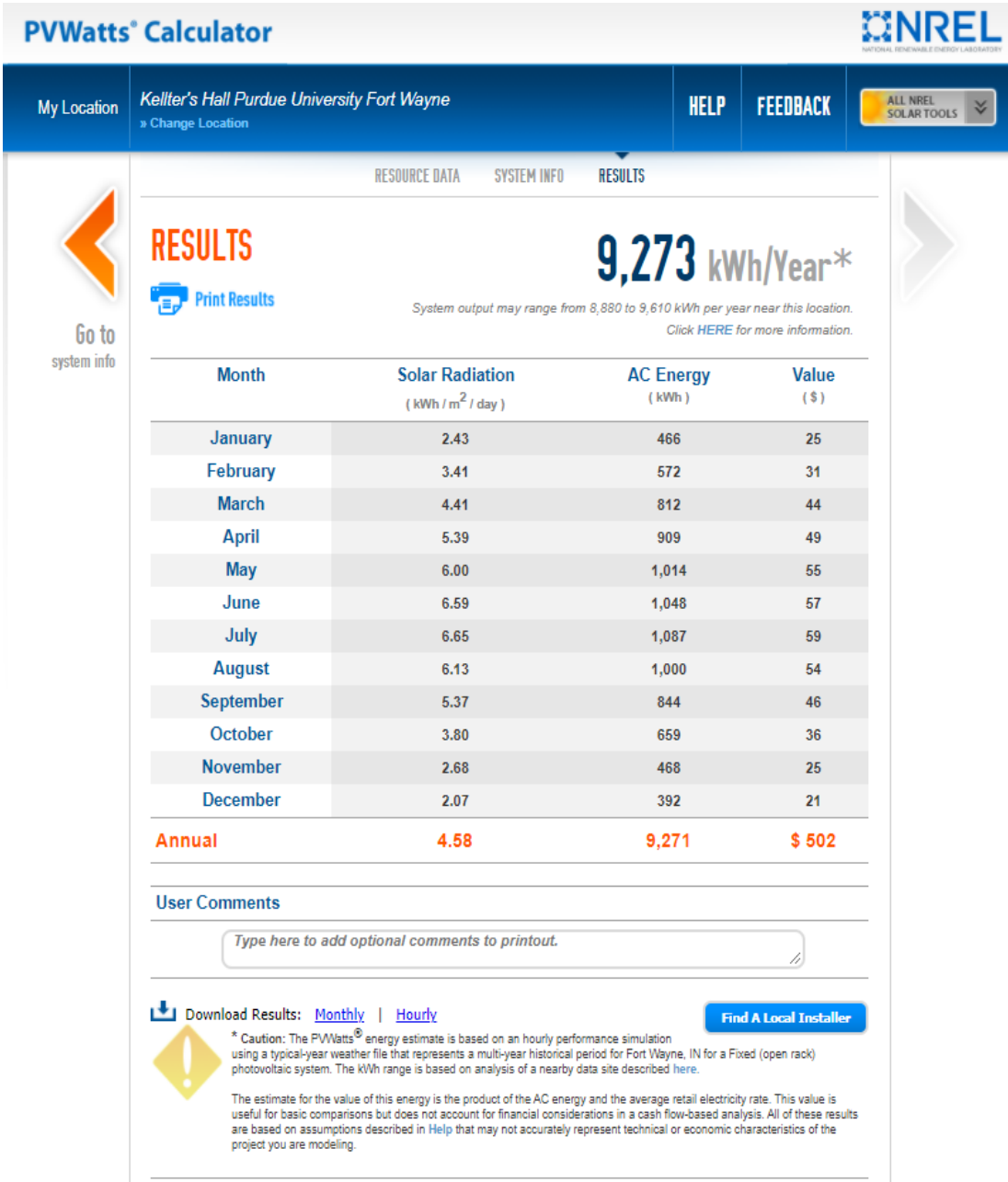


Figure C.3: PVWatts calculator, system results.

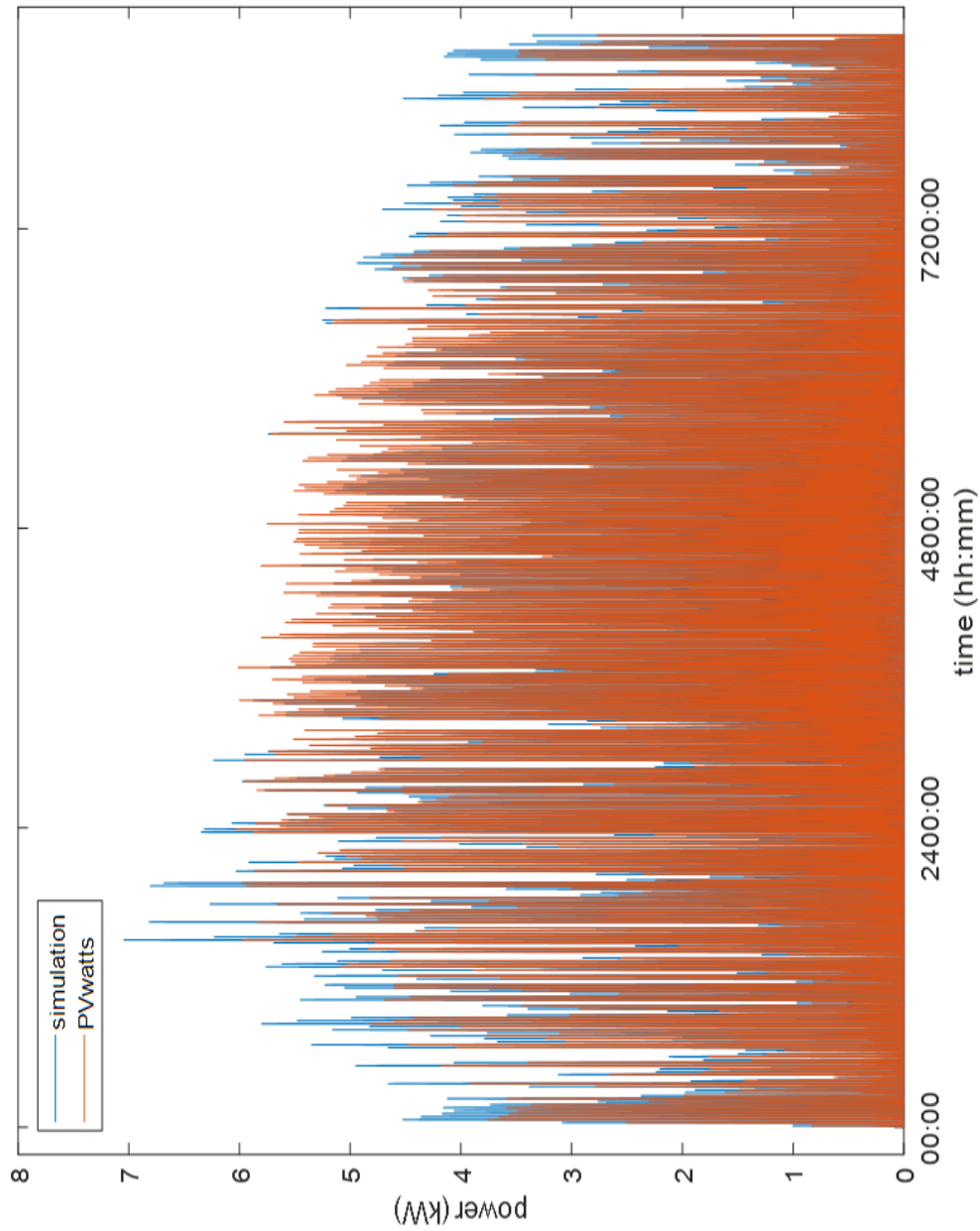


Figure C.4: Annual hourly model power output (simulation) compared to PVWatts calculator power output (PVWatts). Input weather data set based on TMY3, NREL (prospector), Purdue University Fort Wayne campus.

Table C.1: Sample of PVWatts calculator results of 7.6 kWp roof mounted PV array at Purdue University Fort Wayne campus. Input data TMY3.

Month	Plane of Array Irradiance (W/m ²)	DC array Output (kWh)	Value (\$)
1	75	490	25
2	95	599	31
3	137	849	44
4	162	950	49
5	186	1060	55
6	198	1095	57
7	206	1135	59
8	190	1045	54
9	161	881	46
10	118	690	36
11	80	491	25
12	64	413	21
Total	1672	9699	504

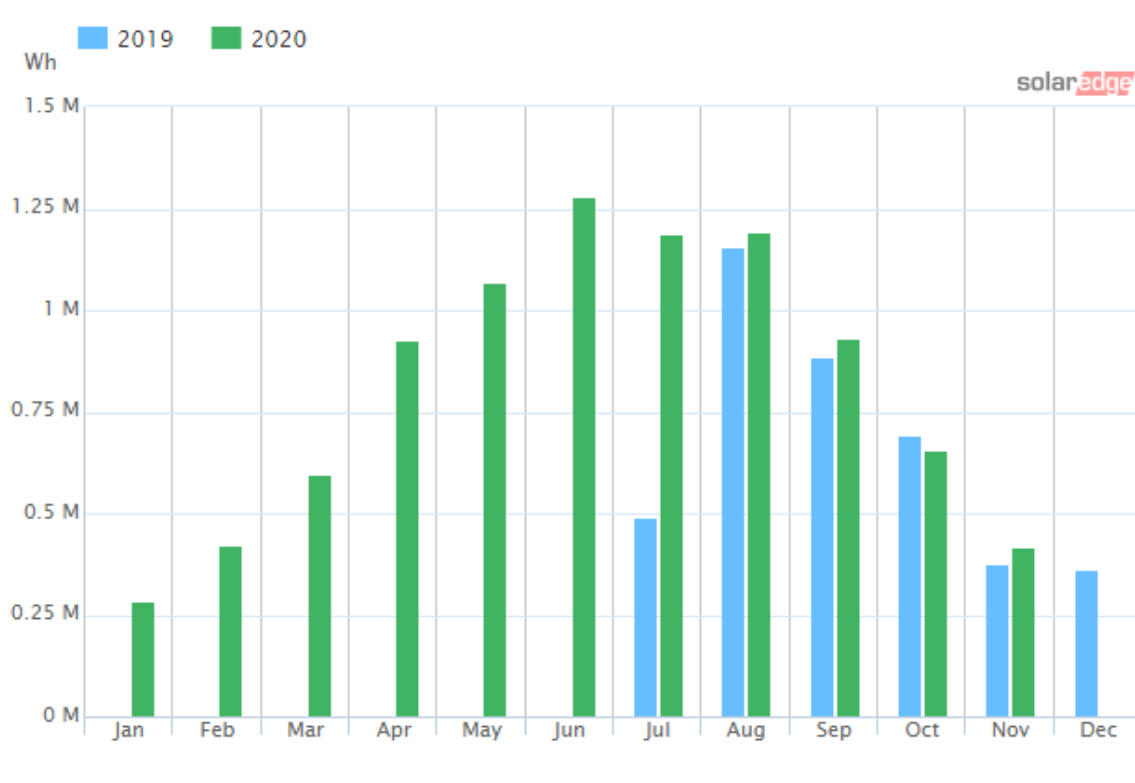


Figure C.5: Experimental recorded annual energy output of the 7.6 kWp roof mounted array at Kettler's Hall, Purdue University Fort Wayne. Data recorded in 2019 and 2020.

REFERENCES

1. Renewable Energy. (2020), <https://www.c2es.org/content/renewable-energy>
2. U.S. solar market insight. (2021), <https://www.seia.org/us-solar-market-insight>
3. Solar resource maps of world. (2021), <https://solargis.com/maps-and-gis-data/download/world>
4. Osmanbasic, E. (2019). *Challenges of making solar energy economical*.
<https://www.engineering.com/story/challenges-of-making-solar-energy-economical>
5. Modules, S. (1970). *What is inside a solar panel?*
<http://solarphotovoltaic.blogspot.com/2012/04/whats-inside-solar-panel.html>.
6. National Renewable Energy Lab. (2019). *Best Research-Cell Efficiency Chart*.
<https://www.nrel.gov/pv/cell-efficiency.html>.
7. Du, D., Darkwa, J., & Kokogiannakis, G. (2013). Thermal management systems for photovoltaic installations: A critical review. *Solar Energy*, 97 238-254.
8. Bahaidarah, H.M.S., Baloch, A.A.B., & Gandhidasan, P., Uniform cooling of photovoltaic panels: A review. *Renewable and Sustainable Energy Reviews*, 57, 1520-1544.
9. Popovici, C. G., Hudişteanu, S. V., Mateescu, T. D., & Cherecheş, N.-C. (2016). Efficiency improvement of photovoltaic panels by using air cooled heat sinks. *Energy Procedia*, 85, 425-432.
10. Alkhalidi, A., Khawaja, M. K., Kelany, A., & Ghaffar, A. (2019). Investigation of repurposed material utilization for environmental protection and reduction of overheat power losses in PV panels. *International Journal of Photoenergy*, 2019, 1-9.

11. Indira, S. S., Vaithilingam, C. A., Chong, K. K., Saidur, R., Faizal, M., Abubakar, S., & Paiman, S. (2020). A review on various configurations of hybrid concentrator photovoltaic and thermoelectric generator system. *Solar Energy*, 201, 122-148.
12. Nižetić, S., Čoko, D., Yadav, A., & Grubišić-Čabo, F. (2016). Water spray cooling technique applied on a photovoltaic panel: The performance response. *Energy Conversion and Management*, 108, 287-296.
13. Martis, M. S. (2006). *Validation of simulation-based models: A theoretical outlook*. Manipal Academy of Higher Education, Manipal, India.
14. Bouzguenda, M., Salmi, T., Gastli, A., & Masmoudi, A. (2012). Evaluating solar photovoltaic system performance using MATLAB. *2012 First International Conference on Renewable Energies and Vehicular Technology*.
15. Masters, G. M. (2004). *Renewable and Efficient Electric Power Systems*.
16. Mohammed, S. S., & Devaraj, D. (2014). Simulation and analysis of a standalone photovoltaic system with boost converter using MATLAB/Simulink. *2014 International Conference on Circuits, Power and Computing Technologies [ICCPCT-2014]*.
17. Anne, Labouret, Michel, Villoz. (2006), *Energie photovoltaïque*. Dunod 3ème.
18. Jürges, W. (1924). The heat transfer at a flat wall Der Wärmeübergang an einer ebenen Wand, *Beihefte zum Gesundh.-Ing.* 1:19.
19. Typical Meteorological Year (TMY). (2021). *NSDRB*. <https://nsrdb.nrel.gov/about/tmy.html>
20. Batra, D., & Davis, J. G. (1992). Conceptual data modelling in database design: similarities and differences between expert and novice designers. *International Journal of Man-machine Studies*, 37(1), 83-101

21. Carson, J. S. (1986). Convincing Users of Model's Validity is Challenging Aspect of Modeler's Job. *Industrial Engineering* 18 (6), 74-85
22. Ross, R.G., (1976). Interface design considerations for terrestrial solar cells modules, *Proceedings of the 12th IEEE photovoltaic specialist's conference*, Baton Rouge, LA, pp: 801- 806.
23. Faiman, D. (2008). Assessing the outdoor operating temperature of photovoltaic modules. *Progress in Photovoltaics: Research and Applications*, 16(4), 307-315.
24. Prilliman, M., Stein, J. S., Riley, D., & TamizhMani, G. (2020). Transient weighted moving average model of photovoltaic module back-surface temperature. *2020 47th IEEE Photovoltaic Specialists Conference (PVSC)*.
25. Dobos, A. P. (2014). *PVWatts version 5 manual (No. NREL/TP-6A20-62641)*. National Renewable Energy Lab. (NREL), Golden, CO (United States).
26. McAdams W.H. (1954). *Heat Transmission, 3rd ed.* McGraw-Hill, Tokyo, Japan.
27. Solaredge Power Optimizer increases energy output. SolarEdge Power Optimizer Increases Energy Output. (2021.). *SolarEdge*. <https://www.solaredge.com/us/products/power-optimizer>.
28. Mackley, R. D., Anderson, D. M., Thomle, J. N., and Strickland, C. E. (2015). *Technical and economic assessment of solar photovoltaic for groundwater extraction on the Hanford site*.
29. Fort Wayne, IN, electricity rates. (2021). *Electricity Local* <https://www.electricitylocal.com/states/indiana/fort-wayne/>.
30. San Diego, CA, electricity rates. (2021). *Electricity Local* <https://www.electricitylocal.com/states/california/san-diego/>.